Mathematics and Mechanics of Solids
XX(X):2–50

DOI: 10.1177/ToBeAssigned
www.sagepub.com/
SAGE

# Fractionalization of Forchheimer's correction to Darcy's law in porous media in large deformations

**Sachin Gunda[1], Alessandro Giammarini[2], Ariel Ramírez-Torres[3], Sundararajan Natarajan[1], Olga Barrera[4,5] and Alfio Grillo[2]**

**Abstract**

This work presents a theoretical and numerical study of the flow of the interstitial fluid that saturates the pore space of a biological tissue, principally aimed at modeling articular cartilage, and that is assumed to experience a dynamic regime different from the Darcian one, which is typically hypothesized in many biomechanical scenarios. The main issue of our research is the conjecture according to which, in the presence of a particular mechanical state of the porous matrix of the tissue under consideration, the fluid may exhibit two different types of deviation from Darcy's law. One is due to the need that may arise when accounting for the inertial forces characterizing the pore scale dynamics of the fluid. This aspect, in fact, can be resolved by turning to the so-called *Forchheimer correction* to Darcy's law, which amounts to introducing non-linearities in the relationship between the fluid filtration velocity and the dissipative forces describing the interactions between fluid and the solid matrix. The second source of discrepancies from classical Darcy's law emerges, for example, when pore scale disturbances to the flow, such as obstructions of the fluid path or clogging of the pores, result in a time delay in the relationship between drag forces and filtration velocity. Recently, models have been proposed in which such delay is described through constitutive laws featuring fractional integro-differential operators. Whereas, to the best of our knowledge, in the literature the above mentioned behaviors have been studied separately or in the limit of small deformations of the solid matrix, in this contribution we present a model of fluid flow in a deformable porous medium undergoing large deformation in which the fluid motion is governed by a fractional version of Forchheimer's correction. After reviewing Forchheimer's formulation of the flow in the context of finite deformations, we present a possible fractionalization of the Darcy-Forchheimer law, and we explain the numerical procedure adopted to solve the highly non-linear boundary value problem that results from the concomitant presence of the two deviations from the Darcian regime considered in our work. We complete our study by highlighting the way in which the fractional order of the model tunes the magnitude of the pore pressure and fluid filtration velocity.

**Keywords**

Flow in deformable porous media; Darcy's law; Forchheimer's correction; Media with memory; Integro-differential constitutive equations; Fractional Calculus; Fractional integrals and derivatives

## 1 Introduction

According to a rather consolidated modeling picture in the biomechanical literature [1], a biological tissue classified as *soft* and *hydrated* is regarded, at least, as a biphasic medium [2], constituted by a sufficiently compliant solid porous matrix and a fluid that participates in a variety of biophysical, biochemical, and mechanical processes, all essential for sustaining the tissue itself [1,3–13].

The characterization of the mechanical properties of the solid matrix of soft tissues, be they hydrated or not, has been the subject of several studies with increasing level of complexity: whereas the first, pioneering models looked at the essence of phenomenology, and, for their purposes, considered tissues (see, e.g., [7] for articular cartilage) homogeneous and isotropic, more recent works studied the consequences of inhomogeneity and anisotropy, especially in connection with the presence of reinforcing collagen fibers [14–21], often assumed to be statistically oriented [22–29].

Collagen fibers represent a very important chapter in the mechanical and hydraulic analysis of biological tissues. Indeed, besides exerting a structural action that contributes to the overall mechanical response of a given tissue, they influence considerably also the tendency of the tissue to enhance, or to inhibit, the circulation of fluid in its interior. At the macroscale, this property is referred to as *permeability*. For example, in the case of articular cartilage, Maroudas and Bullough [14] have hypothesized that the tissue's permeability depends on the distribution and orientation of the collagen fibers. Subsequent studies in this direction, conceived to examine Maroudas and Bullough's hypothesis [14] have been conducted, e.g., in [30,31], and set themselves in a line of research dedicated to the theoretical and numerical modeling of the biomechanics of fiber-reinforced, anisotropic tissues [17,27–29,32–41].

To the authors' knowledge, since Holmes and Mow's permeability model [7] for articular cartilage, the explicit coupling between this transport property and the tissue's deformation has been a leading topic in many other publications on the subject (see, e.g., [31–33,35,42]). In all these works, emphasis is put on the importance of understanding how the mechanics of the tissue combines with its permeability in order to provide acceptable descriptions of the fluid's behavior, especially in terms of its mechanical state. This is motivated by the fact that being able to predict, for example, the fluid pressure allows to estimate possible remarkable aspects of a tissue, like its global health [15,43,44].

Rather typical approaches having the purpose of studying the mechanics of soft and hydrated tissues, like articular cartilage, and, above all, of giving prominence to the coupling discussed above, are based on several formulations of poro-elasticity, in terms either of Biot's or of biphasic theory [1,27,30,31,33,35,45–47]. A common feature of the majority of these approaches is that they rely on the hypothesis that the flow of the

[1] Department of Mechanical Engineering, Indian Institute of Technology Madras, Chennai, Tamil Nadu, India.
[2] Dip. di Scienze Matematiche "G. L. Lagrange", Politecnico di Torino, Corso Duca degli Abruzzi 24, 10129, Torino, Italia.
[3] School of Mathematics & Statistics, Mathematics & Statistics Building, University Place, Glasgow, G12 8QQ, UK.
[4] School of Engineering, Computing and Mathematics, Oxford Brookes University, Headington, Oxford OX3 0BP, UK.
[5] Department of Engineering Science, University of Oxford, Parks Road, OX1 3PJ, Oxford, UK.

**Corresponding author:**
*Alfio Grillo, Dipartimento di Scienze Matematiche "G. L. Lagrange", Politecnico di Torino, Torino, 10129.
Email: alfio.grillo@polito.it

fluid obeys Darcy's law (see, e.g.,[1,33,48–50]), thereby presuming, in the most classical formulation, a linear relationship between the fluid filtration velocity and the pressure gradient realized in the tissue. More precisely, the filtration velocity is obtained by multiplying the tissue's permeability (which, in general, is a second-order tensor field) by the opposite of the pressure gradient. The resulting flow model has the advantage of being computationally cheap, because of the linearity of this relationship, and it is sufficient to capture the coupling between flow and deformation through a suitable definition of the permeability tensor (see, e.g.,[7]). In fact, this coupling is also capable of considering nonlinear deformations. In spite of this capability, however, in the literature there have also been attempts to elaborate flow models that account for non-Darcian behaviors of the fluid, like, for instance, those predicted by Forchheimer or Brinkman's corrections to Darcy's law (see, e.g.,[45,51,52]).

In the context of articular cartilage, in[45,52], the authors have hypothesized that, under certain loading conditions, as could be the case in compression tests in which the load is applied with a relatively high velocity, the mechanical behavior of the fluid is better approximated by the Darcy-Forchheimer model of the flow. In fact, adopting Forchheimer's correction means accounting for non-linear terms in the constitutive relationships between the filtration velocity and the drag forces that may generally result in slower flows and higher pressures than those predicted by Darcy's law. This, in turn, calls for the introduction of additional parameters to describe the flow, whose identification may depend on the structure of the porous medium[53], the model of permeability[30,33], and the experimental procedure employed to estimate the numerical values of the quantities at hand. In addition, it has been shown in[45] that resorting to the Darcy-Forchheimer law may be used to switch from a model of permeability to another one by attributing the resulting variations in the behavior of the fluid to the correction of the flow rather than to different assumptions on the permeability.

Another phenomenon that is not accounted for in the "classical" formulation of Darcy or Darcy-Forchheimer models is the anomalous "diffusion" of the fluid flow (see, e.g.,[54]). In particular, Darcy's law has proved to be non appropriate for fluid flow in high porosity media due to the influence of inertia, thermal, and convective terms and because of solid-fluid boundary effects that are not contemplated in Darcy's model[55].

Recently, a body of work has gone into collecting experimental evidence of anomalous "diffusion" (another type of non-Darcian behavior) for different classes of porous media, from tissues, such meniscal tissue[56], to rocks and porous building materials[57–61]. The predominant matter is the explicit time-dependence of the permeability (as opposed to the case of Darcy's model, in which the permeability varies in time through deformation and porosity), which results in a time-dependent flow rate due to the effect of fluid flow on the porous solid phase. Fluid flow has, indeed, an influence also on the morphology of the pores. Iaffaldano et al.[61] suggested that the permeability of sand depends on the solid particles moved by the fluid during the compaction process. Solid particles can contribute to closing pores (i.e., slowing diffusion) or can be arranged in a way that creates micro-channels, resulting in faster diffusion.

In[62], clogging of the pores and explicit time-dependence of the permeability of hydro-geological porous media are described by means of an integro-differential operator that keeps track of the time history of permeability. This study offers a very important point of departure for the introduction of Fractional Calculus in modeling flow in porous media, especially for describing deviations from Darcian transport, as is the case for subdiffusion or superdiffusion processes, both observable experimentally[54,63,64].

Confined compression tests in meniscal tissues have shown that anomalous transport phenomena are well captured by a fractional poroelastic models (e.g., of Biot-type) in which the pore pressure diffusion equation results from a modified version of Darcy's law involving fractional derivatives[56,65,66]. The permeability is then anomalous and the order of the derivative rules the fluid flow. Fittings of experimental data proved to be better than adopting classical Biot or biphasic models, and the fractional poroelastic model has been —for the first time— validated[65]. By using this fractional poroelastic model, it was possible to obtain information on the anisotropy and inhomogeneity both of the elasticity and of the permeability tensor of the meniscal tissue. However, the model is limited to small deformations.

Other studies[67,68] highlight the role of poroelasticity in the anomalous "diffusion" processes that can be observed on meniscus samples. In the literature, some investigations have been done to capture the relationship between the memory effects of the flow of interstitial fluid, which are due to the interactions between the fluid and the pore network, and the behavior of the solid phase. In particular, in[47] fractional Darcy's law was studied in the setting of small elastic strain, while, in[69], classical Darcy's law was coupled with a solid phase experiencing *"material hereditariness"*[70–73], i.e., dependence of the stress on the past history of strain, which was described by means of a fractional-order *"hereditariness"* model[74–77].

With respect to the review of literature done above, the novelty of our work resides in the search for memory effects associated with a *fractional Darcy-Forchheimer* model of flow in the framework of *finite deformations*. After presenting the constitute theory on which our study relies, we simulate an unconfined compression test, performed over a cylindrical specimen of a hypothetical tissue that has "borrowed" some properties from articular cartilage[15,18,31,44,78,79], but is assumed here to be homogeneous and isotropic. We speak of a "hypothetical tissue" because, for the time being, we do not have experimental values for the parameters defining the fractional operators adopted in the sequel. We choose articular cartilage because of the studies available in the literature that address explicitly memory effects in this tissue and employ Fractional Calculus (see e.g.[80,81], although the framework established therein is very much different from ours). In addition, we select the unconfined compression test since this is a rather standard experimental set-up and is able to provide information in a quite simple manner about the relationship between specimen deformation and fluid flow.

We emphasize that a generalization to an inhomogeneous and anisotropic medium, with statistical orientation of reinforcing collagen fibers, is not too demanding from the modeling point of view, since the literature in the field is quite rich[17,27–29,32–41], although it necessarily increases the computational burden.

Before proceeding, we clarify that, at the moment, we *are not* aiming at reproducing any experiment conducted on real tissues. Rather, we are presenting a study that is meant to indicate, through numerical simulations, new research directions in the field of Fractional Calculus applied to Biomechanics. In this sense, the numerical simulations presented in the sequel may provide guidance in devising experimental procedures aiming at quantifying the presence of possible memory effects in the flow of the interstitial fluid of articular cartilage. The model and the associated simulations, in fact, should act like a magnifying glass on the internal mechanics of the medium under investigation and of the non-local effects taking place in it. We believe that such information could be of aid in designing experiments on articular cartilage.

Our principal results are: (i) the formulation of a fractional constitutive equation that expresses the dissipative drag force stemming from the fluid-solid interactions as a functional of the fluid filtration velocity; and (ii) the numerical procedure developed to solve this equation together with the momentum and mass balance laws characterizing the nonlinear Darcy-Forchheimer model in finite deformations. The main outcomes of our simulations predict the influence of the fractionalization of Forchheimer's correction on pore pressure and magnitude of fluid filtration velocity.

## 2 Kinematics of biphasic mixtures

In this section, we briefly present the kinematics of solid-fluid mixtures in the framework delineated in[82,83], which has been already employed to describe articular cartilage[27,31,45,84]. The solid and the fluid phase are represented by two smooth material manifolds $\mathcal{M}_{\mathrm{s}}$ and $\mathcal{M}_{\mathrm{f}}$, and the embedding of the solid phase in the three dimensional Euclidean space $\mathscr{S}$ is called *reference placement* of the solid phase $\mathscr{B} \subset \mathscr{S}$.

Although the class of biological tissues taken as target may feature complicated internal structures, which generally comprise cells, extracellular matrix, and collagen fibers[2,14,17,20,28,29,31,33,35,39,41,78,85] (as is the case for articular cartilage), a simplified approach is followed in the sequel. This is done because, for a given target tissue, the focus of our work is not a detailed description of the tissue's structure. We are interested here in evaluating the influence that non-Darcian dynamics of the fluid phase may have on the tissue's overall mechanical behavior. In particular, to account for loading conditions that do not fully justify the hypothesis of negligibility of inertial forces, we consider Forchheimer's correction to Darcy's law[48,49,51,86–88]. Moreover, to account for dissipative flow features that, in the literature (see e.g[54,89–92]), have conducted to flow laws non-local in time, we propose a fractionalization of Forchheimer's correction. In particular, in the work of Magin et al.[93], a study on the anomalous NMR relaxation of bovine nasal cartilage is conducted by employing fractional models to describe the relaxation process of the overall tissue and of the matrix constituents. To this end, we suggest a relation between the fluid phase filtration velocity and the pressure gradient developed in the tissue that is highly non-linear, and is expressed through integro-differential operators of fractional type describing a possible non-locality in time in the constitutive representation of the drag forces as functionals of the fluid filtration velocity.

For each instant of time $t$ of the time window $\mathscr{I} \subset ]0, +\infty[$ in which we keep track of the evolution of the system, the motion $\chi(\cdot, t) : \mathscr{B} \to \mathscr{S}$ of the solid phase maps the reference placement $\mathscr{B}$ into the *current placement* $\chi(\mathscr{B}, t)$. In this work, we adhere to the description of the solid phase put forward in[45], in which the "points" of $\mathcal{M}_{\mathrm{s}}$ comprise both the cartilage matrix and the fibers and, thus, the two constituents of the solid phase share the same motion. Furthermore, for each $t \in \mathscr{I}$, the motion of the fluid is described by means of a one-parameter family of embeddings $\mathfrak{f}(\cdot, t) : \mathcal{M}_{\mathrm{f}} \to \mathscr{S}$ that attaches fluid particles $\mathfrak{X}_{\mathrm{f}} \in \mathcal{M}_{\mathrm{f}}$ to a points in the Euclidean space $\mathscr{S}$. The portion of $\mathscr{S}$ in which the solid and the fluid phases coexist is denoted by $\mathscr{B}_t := \chi(\mathscr{B}, t) \cap \mathfrak{f}(\mathcal{M}_{\mathrm{f}}, t)$ and constitute the solid-fluid mixture. Furthermore, for each time $t \in \mathscr{I}$, we assume that the inverse mappings in space $[\chi(\cdot, t)]^{-1} : \mathscr{B}_t \to \mathscr{B}$ is surjective with respect to the reference placement of the solid phase, so that for each point of the mixture there is a corresponding point in the reference placement of the solid phase.

Articular cartilage, described as a hydrated tissue, is seen at the macroscale as a mixture with a solid component and a fluid one. In particular, following[31,94], under the hypothesis that the heterogeneities at the fine scale do not affect the tissue at the considered length scale[86], we introduce an admissible representative element[86] and the fraction of relative volume which is occupied by the solid or by the fluid phase. These quantities are called, respectively, the solid volumetric fraction and the fluid volumetric fraction and are defined as $\phi_\alpha : \mathscr{B}_t \to ]0, 1[$, with $\alpha = \mathrm{s}, \mathrm{f}$.

For each point $x \in \mathscr{B}_t$ in the current placement and each point $X \in \mathscr{B}$ in the reference placement, we introduce the tangent spaces $T_x\mathscr{S}$ and $T_X\mathscr{B}$, and the dual spaces $T_x^*\mathscr{S}$ and $T_X^*\mathscr{B}$, respectively, as well as the tangent bundles $T\mathscr{S} := \bigsqcup_{x \in \mathscr{B}_t} T_x\mathscr{S}$ and $T\mathscr{B} := \bigsqcup_{X \in \mathscr{B}} T_X\mathscr{B}$. Similarly, we define the cotangent bundles $T^*\mathscr{S} := \bigsqcup_{x \in \mathscr{B}_t} T_x^*\mathscr{S}$ and $T^*\mathscr{B} := \bigsqcup_{X \in \mathscr{B}} T_X^*\mathscr{B}$.

The velocity of a solid particle passing at the time $t$ through the spatial point $x = \chi(X, t)$ is denoted by $\boldsymbol{v}_{\mathrm{s}}(x, t) = \dot{\chi}(X, t) \in T_x\mathscr{S}$, with the superimposed dot meaning partial differentiation with respect to time, while the velocity of a fluid particle passing through the same spatial point $x \in \mathscr{B}_t$ is obtained as $\boldsymbol{v}_{\mathrm{f}}(x,t) = \dot{\mathfrak{f}}(\mathfrak{X}_{\mathrm{f}},t) \in T_x\mathcal{S}$. The above defined velocities $\boldsymbol{v}_{\mathrm{s}}$ and $\boldsymbol{v}_{\mathrm{f}}$ are also known as *spatial* velocities, while the relative motion of the fluid with respect to the solid phase is described by the relative velocity as $\boldsymbol{w}_{\mathrm{fs}}(x,t) := \boldsymbol{v}_{\mathrm{f}}(x,t) - \boldsymbol{v}_{\mathrm{s}}(x,t)$. For the fluid phase, we also introduce the *filtration velocity* $\boldsymbol{q}(x,t) := \phi_{\mathrm{f}}(x,t)\boldsymbol{w}_{\mathrm{fs}}(x,t) \in T_x\mathcal{S}$, which represents the specific mass flux vector of fluid passing through $x \in \mathscr{B}_t$ at time $t$ (i.e., the mass flux vector normalized by the fluid true mass density $\varrho_{\mathrm{f}}$)[49].

Finally, we introduce the tangent map of the motion of the solid phase, $\boldsymbol{F}(X,t) = T\chi(X,t) \equiv D\chi(X,t)$, where $D\chi$ is the Jacobian tensor associated with $\chi$, known as the *deformation tensor* $\boldsymbol{F}(X,t) : T_X\mathscr{B} \to T_{\chi(X,t)}\mathcal{S}$, which transforms vectors of $T_X\mathscr{B}$ into vectors of $T_x\mathcal{S}$, with $x = \chi(X,t)$. In order for a motion to be admissible, the determinant of $\boldsymbol{F}$ is required to satisfy the condition $J(X,t) := \det\boldsymbol{F}(X,t) > 0$, for all $X \in \mathscr{B}$ and $t \in \mathscr{I}$, so that $\boldsymbol{F}$ is non-singular. Similarly, we define the inverse, the transpose, and the inverse transpose tensors of $\boldsymbol{F}$, that is, $\boldsymbol{F}^{-1}(x,t) : T_x\mathcal{S} \to T_X\mathscr{B}$, $\boldsymbol{F}^{\mathrm{T}}(x,t) : T_x^*\mathcal{S} \to T_X^*\mathscr{B}$, and $\boldsymbol{F}^{-\mathrm{T}}(X,t) : T_X^*\mathscr{B} \to T_x^*\mathcal{S}$, respectively, with $X = [\chi(\,\cdot\,,t)]^{-1}(x)$. As usual, the Cauchy-Green deformation tensor $\boldsymbol{C}(X,t) : T_X\mathscr{B} \to T_X^*\mathscr{B}$ is defined as $\boldsymbol{C}(X,t) = \boldsymbol{F}^{\mathrm{T}}(x,t)\boldsymbol{\eta}(x)\boldsymbol{F}(X,t)$, with $x = \chi(X,t)$, and $\boldsymbol{\eta}(x) : T_x\mathcal{S} \to T_x^*\mathcal{S}$ being the spatial metric tensor attached at the spatial point $x \in \mathcal{S}$[95]. When there is no room for confusion, also the less rigorous notations $\boldsymbol{C} = \boldsymbol{F}^{\mathrm{T}}.\boldsymbol{F} \equiv \boldsymbol{F}^{\mathrm{T}}\boldsymbol{\eta}\boldsymbol{F}$ will be employed, in which the dot "." is an abbreviation for the spatial metric tensor field $\boldsymbol{\eta}$.

## 3 Fundamental balance equations

In this section, we recall the fundamental balance equations for the modeling problem at hand, i.e., the balance of mass and the balance of linear momentum for both the solid and the fluid phase.

Our target tissue is viewed as a solid-fluid mixture, in which the solid phase comprises all the solid constituents of the tissue (in the present framework, these are essentially identified with the extracellular matrix and the structural components of the cells), while the fluid phase accounts for the interstitial fluid that flows through the pores.

As is often the case in the biomechanical modeling of soft hydrated tissues[1,31,33,45,52], both the solid and the fluid phase are regarded as incompressible (more specifically, we will assume that their true mass densities are constant), and their presence in the mixture under study is measured by their *volumetric fractions*, denoted by $\phi_{\mathrm{s}}$ and $\phi_{\mathrm{f}}$, respectively. Through these quantities, we define the *apparent mass densities* $\varrho_{\mathrm{s}}\phi_{\mathrm{s}}$ and $\varrho_{\mathrm{f}}\phi_{\mathrm{f}}$, with $\varrho_{\mathrm{s}}$ and $\varrho_{\mathrm{f}}$ being the true mass densities of the solid and the fluid. Hence, we write the balance of mass for each phase in the mixture's current placement $\mathscr{B}_t$ as[1,33,45,52]

$$\partial_t(\varrho_{\mathrm{s}}\phi_{\mathrm{s}}) + \mathrm{div}(\varrho_{\mathrm{s}}\phi_{\mathrm{s}}\boldsymbol{v}_{\mathrm{s}}) = 0 \quad \Rightarrow \quad \partial_t\phi_{\mathrm{s}} + \mathrm{div}(\phi_{\mathrm{s}}\boldsymbol{v}_{\mathrm{s}}) = 0, \qquad \text{in } \mathscr{B}_t, \tag{1a}$$

$$\partial_t(\varrho_{\mathrm{f}}\phi_{\mathrm{f}}) + \mathrm{div}(\varrho_{\mathrm{f}}\phi_{\mathrm{f}}\boldsymbol{v}_{\mathrm{f}}) = 0 \quad \Rightarrow \quad \partial_t\phi_{\mathrm{f}} + \mathrm{div}(\phi_{\mathrm{f}}\boldsymbol{v}_{\mathrm{f}}) = 0, \qquad \text{in } \mathscr{B}_t. \tag{1b}$$

The absence of terms on the right-hand side of Equations (1a) and (1b) means that, at the considered timescale, we see neither growth processes nor mass exchange between the constituents.

Since the mixture considered in our work is saturated, the condition $\phi_{\mathrm{s}} + \phi_{\mathrm{f}} = 1$ applies. Hence, the balance of mass for the solid phase and for the mixture as a whole, obtained by adding together Equations (1a) and (1b), can be rephrased as

$$\mathrm{D}_{\mathrm{s}}\phi_{\mathrm{s}} + \phi_{\mathrm{s}}\mathrm{div}\boldsymbol{v}_{\mathrm{s}} = 0, \qquad \text{in } \mathscr{B}_t, \tag{2a}$$

$$\mathrm{div}\boldsymbol{v}_{\mathrm{s}} + \mathrm{div}\boldsymbol{q} = 0, \qquad \text{in } \mathscr{B}_t, \tag{2b}$$

where the substantial derivative with respect to the motion of the solid phase has been introduced, i.e., $\mathrm{D}_{\mathrm{s}}\varsigma := \partial_t \varsigma + (\mathrm{grad}\varsigma)\boldsymbol{v}_{\mathrm{s}}$, for any differentiable field $\varsigma : \mathscr{B}_t \times \mathscr{I} \to \mathbb{S}$ valued in $\mathbb{S} \equiv \mathbb{R}$ or in higher-order vector or tensor spaces [13].

By composing Equations (2a) and (2b) with the pair of maps $(\chi, \mathcal{T}) : \mathscr{B} \times \mathscr{I} \to \mathscr{S} \times \mathscr{I}$, so that for any field $\varsigma$ it holds that $\varsigma_{\mathrm{L}} \equiv \varsigma \circ (\chi, \mathcal{T}) : \mathscr{B} \times \mathscr{I} \to \mathbb{S}$, $\mathrm{D}_{\mathrm{s}}\varsigma \circ (\chi, \mathcal{T}) = \dot{\varsigma}_{\mathrm{L}}$, and $J[\mathrm{div}\varsigma \circ (\chi, \mathcal{T})] = \mathrm{Div}(J\boldsymbol{F}^{-\mathrm{T}}\varsigma_{\mathrm{L}})$, the mass balance laws can be written with respect to the reference placement as

$$\dot{\Phi}_{\mathrm{s}} = 0, \qquad \text{in } \mathscr{B}, \tag{3a}$$

$$\dot{J} + \mathrm{Div}\boldsymbol{Q} = 0, \qquad \text{in } \mathscr{B}, \tag{3b}$$

where $\Phi_{\mathrm{s}}(X,t) := J(X,t)\phi_{\mathrm{s}}(x,t)$ and $\boldsymbol{Q}(X,t) := J(X,t)\boldsymbol{F}^{-1}(x,t)\boldsymbol{q}(x,t)$ are the solid phase *material volumetric fraction* and the *material filtration velocity*, defined through the pull-backs of $\phi_{\mathrm{s}}$ and $\boldsymbol{q}$, respectively [13,31,45], and $x = \chi(X,t)$. In the sequel, unless there is room for confusion, we shall omit the subscript "L" to indicate that a given quantity is written in "Lagrangian" formalism. For instance, the "Lagrangian" expression of the pore pressure will be $P := p \circ (\chi, \mathcal{T})$ rather than $p_{\mathrm{L}}$.

We emphasize that, in spite of the terminology "filtration velocity", $\boldsymbol{q}$ *is not* a true velocity. Rather, it is a *specific mass flux vector*, i.e., a mass flux vector defined by the multiplication of the velocity of the fluid relative to the solid, i.e., $\boldsymbol{w}_{\mathrm{fs}}$, by the volumetric fraction of the fluid $\phi_{\mathrm{f}}$. This way, the resulting expression equals the mass flux vector of the fluid relative to the solid, divided by the fluid's intrinsic volumetric mass density $\varrho_{\mathrm{f}}$. As remarked in [96], this is an important clarification, since it predicts how $\boldsymbol{q}$ transforms. Indeed, since $\boldsymbol{q}$ is a flux vector, it has to be identified with a *pseudo-vector* and, as such, its material counterpart, obtained by computing its backward Piola transformation, reads $\boldsymbol{Q}(X,t) = J(X,t)\boldsymbol{F}^{-1}(x,t)\boldsymbol{q}(x,t)$, with $x = \chi(X,t)$ [31,45,96,97].

Next, we introduce the balance of linear momentum in the current placement. Since, in the present framework, macroscopic inertial forces are assumed to be negligible from the outset, we write [30,45,52]

$$\begin{aligned} &\mathrm{div}\boldsymbol{\sigma}_{\mathrm{s}} + \boldsymbol{\pi}_{\mathrm{s}} + \varrho_{\mathrm{s}}\phi_{\mathrm{s}}\boldsymbol{g} = \boldsymbol{0}, & & \mathrm{div}(\boldsymbol{\sigma}_{\mathrm{s}} + \boldsymbol{\sigma}_{\mathrm{f}}) + (\varrho_{\mathrm{s}}\phi_{\mathrm{s}} + \varrho_{\mathrm{f}}\phi_{\mathrm{f}})\boldsymbol{g} = \boldsymbol{0}, \quad \text{in } \mathscr{B}_t, & (4a)\\ &\mathrm{div}\boldsymbol{\sigma}_{\mathrm{f}} + \boldsymbol{\pi}_{\mathrm{f}} + \varrho_{\mathrm{f}}\phi_{\mathrm{f}}\boldsymbol{g} = \boldsymbol{0}, & \Longrightarrow & \mathrm{div}\boldsymbol{\sigma}_{\mathrm{f}} + \boldsymbol{\pi}_{\mathrm{f}} + \varrho_{\mathrm{f}}\phi_{\mathrm{f}}\boldsymbol{g} = \boldsymbol{0}, \quad \text{in } \mathscr{B}_t, & (4b) \end{aligned}$$

where $\boldsymbol{\sigma}_{\mathrm{s}}$ and $\boldsymbol{\sigma}_{\mathrm{f}}$ are the Cauchy stress tensors of the solid and of the fluid phase, $\boldsymbol{\pi}_{\mathrm{s}}$ and $\boldsymbol{\pi}_{\mathrm{f}}$ are the force densities due to the exchanges of linear momentum between the phases, and $\boldsymbol{g}$ is the gravity acceleration co-vector. Note that, in the equations of the first column, each balance law is associated with a single phase, i.e., either with the solid or with the fluid phase. In the second column, instead, the second equation is identical to its homologous of the first column, while the first equation expresses the balance of linear momentum for the mixture as a whole. Indeed, it is obtained by adding together the balance laws associated with each single phase and by using the hypothesis of the mixture being closed with respect to linear momentum, i.e., $\boldsymbol{\pi}_{\mathrm{s}} + \boldsymbol{\pi}_{\mathrm{f}} = \boldsymbol{0}$.

Equations in the right column of (4a) and (4b) can also be reformulated in the reference placement as

$$\mathrm{Div}(\boldsymbol{T}_{\mathrm{s}} + \boldsymbol{T}_{\mathrm{f}}) + [\Phi_{\mathrm{s}}\varrho_{\mathrm{s}} + (J - \Phi_{\mathrm{s}})\varrho_{\mathrm{f}}]\boldsymbol{g} = \boldsymbol{0}, \tag{5a}$$

$$\mathrm{Div}\boldsymbol{T}_{\mathrm{f}} + \boldsymbol{F}^{-\mathrm{T}}\boldsymbol{\Pi}_{\mathrm{f}} + (J - \Phi_{\mathrm{s}})\varrho_{\mathrm{f}}\boldsymbol{g} = \boldsymbol{0}, \tag{5b}$$

where $\boldsymbol{T}_{\alpha}(X,t) := J(X,t)\boldsymbol{\sigma}_{\alpha}(x,t)\boldsymbol{F}^{-\mathrm{T}}(X,t)$, with $\alpha \in \{\mathrm{s},\mathrm{f}\}$, is the first Piola-Kirchhoff stress tensor associated with the $\alpha$th phase, $\boldsymbol{\Pi}_{\mathrm{f}}(X,t) = J(X,t)\boldsymbol{F}^{\mathrm{T}}(x,t)\boldsymbol{\pi}_{\mathrm{f}}(x,t) \in T^*_X\mathscr{B}$ is the pull-back of $\boldsymbol{\pi}_{\mathrm{f}}$ to the reference placement, and $x = \chi(X,t)$.

Since, according to Equation (3a), $\Phi_{\rm s}$ is constant in the time interval over which the system is observed, and it is determined univocally by the initial condition $\Phi_{\rm sR}$, we set $\Phi_{\rm s}(X,t) = \Phi_{\rm sR}(X)$, and we eliminate it from the set of unknowns featuring in the balance equations. This result, indeed, permits to write the volumetric fractions of the solid and of the fluid phase as $\phi_{\rm s}(\chi(X,t),t) = \Phi_{\rm sR}(X)/J(X,t)$ and $\phi_{\rm f}(\chi(X,t),t) = 1 - \Phi_{\rm sR}(X)/J(X,t)$. Therefore, Equations (2b), (4a), and (4b) feature 7 scalar equations in 21 unknowns: 3 for the components of the motion $\chi$; 3 for the components of the filtration velocity $\boldsymbol{q}$; 6 for the components of $\boldsymbol{\sigma}_{\rm s}$; 6 for the components of $\boldsymbol{\sigma}_{\rm f}$; and 3 for the components of $\boldsymbol{\pi}_{\rm f}$. To these unknowns, however, a Lagrange multiplier accompanying the incompressibility constraint has to be added, so that the full number of unknowns raises to 22. Consequently, to close the model, we need to supply the Cauchy stress tensors $\boldsymbol{\sigma}_{\rm s}$ and $\boldsymbol{\sigma}_{\rm f}$ as well as the force density $\boldsymbol{\pi}_{\rm f}$ constitutively, thereby introducing the missing 15 scalar equations. This way, the *remaining unknowns* to be determined are:

$$\chi, \quad \boldsymbol{q}, \quad p, \tag{6}$$

where $p$ is the pore pressure and represents the Lagrangian multiplier of the present theory.

# 4 General constitutive relations

It can be proved that, if the solid phase is hyperelastic and the macroscopic stress response of the fluid phase is not appreciably affected by the fluid viscosity, the Cauchy stress tensors are given by[1,30,31,33,45,48,50]

$$\boldsymbol{\sigma}_{\rm s} = -\phi_{\rm s} p \boldsymbol{\iota}^{\rm T} + \boldsymbol{\sigma}_{\rm sc}, \qquad \text{in } \mathscr{B}_t, \tag{7a}$$

$$\boldsymbol{\sigma}_{\rm f} = -\phi_{\rm f} p \boldsymbol{\iota}^{\rm T}, \qquad \text{in } \mathscr{B}_t, \tag{7b}$$

where $p$ is pore pressure, $\boldsymbol{\sigma}_{\rm sc}$ is the constitutive part of $\boldsymbol{\sigma}_{\rm s}$, and $\boldsymbol{\iota}$ is the identity tensor associated with $T\mathscr{S}$. Note that, in this work, the Cauchy stress tensors are taken as linear maps from $T^*\mathscr{S}$ into itself, i.e., $\boldsymbol{\sigma}_\alpha(x,t) : T^*_x\mathscr{S} \to T^*_x\mathscr{S}$, for all $x \in \mathscr{B}_t$, and, thus, the transpose of the identity tensor $\boldsymbol{\iota}$ is needed for consistency, since it applies that $\boldsymbol{\iota}^{\rm T}(x,t) : T^*_x\mathscr{S} \to T^*_x\mathscr{S}$, with $x \in \mathscr{B}_t$, and $\boldsymbol{\iota}^{\rm T}(x,t)\boldsymbol{\beta}(x,t) = \boldsymbol{\beta}(x,t)$, for every co-vector $\boldsymbol{\beta}(x,t) \in T^*_x\mathscr{S}$.

In view of the computational burden that will be introduced for describing the flow, for the purposes of our present study we assume that the solid phase is isotropic, homogeneous, and characterized by a Neo-Hookean hyperelastic strain energy density function $\Psi_{\rm s}(\boldsymbol{C})$[98], which, written per unit of volume of the reference placement, takes on the form

$$\Psi_{\rm s}(\boldsymbol{C}) = \tfrac{1}{2}\Phi_{\rm s}\mu_{\rm s}[I_1 - 3] - \tfrac{1}{2}\Phi_{\rm s}\mu_{\rm s}\,\log I_3 + \tfrac{1}{8}\Phi_{\rm s}\lambda_{\rm s}\,[\log I_3]^2, \tag{8}$$

where $\lambda_{\rm s}$ and $\mu_{\rm s}$ are Lamé's parameters, and $I_1$, $I_2$, and $I_3$ are the three principal invariants of the Green-Cauchy tensor $\boldsymbol{C}$, i.e.,

$$I_1 = {\rm tr}\boldsymbol{C}, \quad I_2 = \tfrac{1}{2}\{[{\rm tr}\boldsymbol{C}]^2 - {\rm tr}\boldsymbol{C}^2\}, \quad I_3 = \det \boldsymbol{C} = J^2. \tag{9}$$

Before going further, it is important to remark that there exist strain energy densities that are more appropriate than the Neo-Hookean one for tissues like articular cartilage. A rather typical example is the Holmes&Mow[7] strain energy density function, which has been extensively used and generalized in many works addressing the mechanics of articular cartilage in the biphasic context, especially when the fibers are included in order to make the model at least transversely isotropic[17,23,26–31,34–41,45,46].

By viewing $I_1$, $I_2$, and $I_3$ as functions of $\boldsymbol{C}$, and $\boldsymbol{C}$ as a function of $\boldsymbol{F}$, we can rewrite $\Psi_{\mathrm{s}}(\boldsymbol{C})$ as $\Psi_{\mathrm{s}}(\boldsymbol{C}) \equiv W_{\mathrm{s}}(\boldsymbol{F})$, and, thus, we determine $\boldsymbol{T}_{\mathrm{sc}}$ and $\boldsymbol{\sigma}_{\mathrm{sc}}$ as

$$\boldsymbol{T}_{\mathrm{sc}} = \frac{\partial W_{\mathrm{s}}}{\partial \boldsymbol{F}}(\boldsymbol{F}) = \boldsymbol{F}\left[2\frac{\partial \Psi_{\mathrm{s}}}{\partial \boldsymbol{C}}(\boldsymbol{C})\right] \quad \Rightarrow \quad \boldsymbol{\sigma}_{\mathrm{sc}}(x,t) = \frac{1}{J(X,t)}\left[\frac{\partial W_{\mathrm{s}}}{\partial \boldsymbol{F}}(\boldsymbol{F}(X,t))\right]\boldsymbol{F}^{\mathrm{T}}(x,t). \tag{10}$$

In the sequel, $\boldsymbol{T}_{\mathrm{sc}}$ will be referred to as *constitutive part of the first Piola-Kirchhoff stress tensor*. Its explicit expression of $\boldsymbol{T}_{\mathrm{sc}}$ will be supplied below, when discussing some numerical aspects of the problem at hand. Here, we simply notice that, since $\boldsymbol{T}_{\mathrm{sc}}$ is defined constitutively, $\boldsymbol{T}_{\mathrm{s}}$ is fully defined in terms of $\boldsymbol{T}_{\mathrm{sc}}$ and of the pore pressure $P := p \circ (\chi, \mathcal{T})$ (i.e., the pore pressure expressed as a function of the points of $\mathscr{B}$ and of time), and since $\boldsymbol{T}_{\mathrm{f}}$ depends only on $P$, then all the stresses featuring in the balance laws of interest are completely expressed in terms of the unknowns $\chi$ (through the deformation gradient tensor) and $P$. Moreover, since the same conclusions hold true also for the Cauchy stress tensors $\boldsymbol{\sigma}_{\mathrm{s}}$, $\boldsymbol{\sigma}_{\mathrm{sc}}$, and $\boldsymbol{\sigma}_{\mathrm{f}}$, the balance laws (4a) and (4b) can be recast in the form

$$\operatorname{div}(-p\boldsymbol{\iota}^{\mathrm{T}} + \boldsymbol{\sigma}_{\mathrm{sc}}) + (\varrho_{\mathrm{s}}\phi_{\mathrm{s}} + \varrho_{\mathrm{f}}\phi_{\mathrm{f}})\boldsymbol{g} = \boldsymbol{0}, \qquad \text{in } \mathscr{B}_t, \tag{11a}$$
$$-\phi_{\mathrm{f}}\operatorname{grad}p + \boldsymbol{\pi}_{\mathrm{fd}} + \varrho_{\mathrm{f}}\phi_{\mathrm{f}}\boldsymbol{g} = \boldsymbol{0}, \qquad \text{in } \mathscr{B}_t, \tag{11b}$$

with $\boldsymbol{\sigma}_{\mathrm{sc}}$ being given in Equation (10), and $\boldsymbol{\pi}_{\mathrm{fd}} := \boldsymbol{\pi}_{\mathrm{f}} - p\operatorname{grad}\phi_{\mathrm{f}}$ being referred to as the *dissipative part* of $\boldsymbol{\pi}_{\mathrm{f}}$ [1,13,48,50].

The stress tensor featuring in Equation (11a), i.e.,

$$\boldsymbol{\sigma}_{\mathrm{I}} := -p\boldsymbol{\iota}^{\mathrm{T}} + \boldsymbol{\sigma}_{\mathrm{sc}}, \tag{12}$$

represents the *internal part* [48] of the overall stress tensor of the solid-fluid mixture under investigation, that is, the stress tensor of the mixture exclusive of the dynamic contributions, which are negligible in the considered regime [30,48]. In fact, the structure of $\boldsymbol{\sigma}_{\mathrm{I}}$ yields the internal first and second Piola-Kirchhoff stress tensors $\boldsymbol{T}_{\mathrm{I}} = -JP\boldsymbol{F}^{-\mathrm{T}} + \boldsymbol{T}_{\mathrm{sc}}$, $\boldsymbol{S}_{\mathrm{I}} = -JP\boldsymbol{C}^{-1} + \boldsymbol{S}_{\mathrm{sc}}$, where $\boldsymbol{S}_{\mathrm{sc}}$ is defined as $\boldsymbol{S}_{\mathrm{sc}}(X,t) = J(X,t)\boldsymbol{F}^{-1}(x,t)\boldsymbol{\eta}^{-1}(x)\boldsymbol{\sigma}_{\mathrm{sc}}(x,t)\boldsymbol{F}^{-\mathrm{T}}(X,t)$, with $x = \chi(X,t)$. Moreover, since the solid phase is assumed to be hyperelastic, $\boldsymbol{S}_{\mathrm{I}}$ can be determined by differentiating an *augmented* strain energy density $\Psi_{\mathrm{s}}^{\mathrm{a}}$, obtained through the addition of the pressure term $-[J-1]P$ to $\Psi_{\mathrm{s}}(\boldsymbol{C})$, i.e.,

$$\Psi_{\mathrm{s}}^{\mathrm{a}}(\boldsymbol{C},P) := \Psi_{\mathrm{s}}(\boldsymbol{C}) - [J-1]P = \tfrac{1}{2}\Phi_{\mathrm{s}}\mu_{\mathrm{s}}[\operatorname{tr}\boldsymbol{C} - 3] - \Phi_{\mathrm{s}}\mu_{\mathrm{s}}\log J + \tfrac{1}{2}\Phi_{\mathrm{s}}\lambda_{\mathrm{s}}[\log J]^2 - [J-1]P, \tag{13a}$$
$$\boldsymbol{S}_{\mathrm{I}} = 2\frac{\partial \Psi_{\mathrm{s}}^{\mathrm{a}}}{\partial \boldsymbol{C}}(\boldsymbol{C},P) = -JP\boldsymbol{C}^{-1} + \boldsymbol{S}_{\mathrm{sc}} = -JP\boldsymbol{C}^{-1} + 2\frac{\partial \Psi_{\mathrm{s}}}{\partial \boldsymbol{C}}(\boldsymbol{C}). \tag{13b}$$

For future use, we also introduce the strain energy densities $W_{\mathrm{s}}(\boldsymbol{F}) \equiv \Psi_{\mathrm{s}}(\boldsymbol{C})$ and $W_{\mathrm{s}}^{\mathrm{a}}(\boldsymbol{F},P) \equiv \Psi_{\mathrm{s}}^{\mathrm{a}}(\boldsymbol{C},P)$.

There remains to determine $\boldsymbol{\pi}_{\mathrm{fd}}$ and, to do so, we proceed with the study of the dissipation inequality [13,33,45,48,50,99].

## 5 Constitutive representation of the dissipative forces

Under the hypotheses done so far, by assuming that the sole source of energetic loss is due to the momentum exchanged between the fluid and the solid phase, and adhering to the frameworks developed in [48,50], and, subsequently, in [13], it can be proven that the local form of the residual dissipation per unit of volume of $\mathscr{B}_t$ is given by

$$\mathfrak{D}^{(a)} = -\boldsymbol{\pi}_{\mathrm{fd}} \boldsymbol{w}_{\mathrm{fs}} = -\boldsymbol{\pi}_{\mathrm{fd}} \phi_{\mathrm{f}}^{-1} \boldsymbol{q} \geq 0. \tag{14}$$

Expressions similar to Equation (14) can be found in several publications (see e.g.[1,13,45,48,50]) and, thus, its full derivation will not be reported here. However, we recall that the superscript "(a)" in $\mathfrak{D}^{(a)}$ stands for "augmented", since, to obtain Equation (14), the constraint of incompressibility, imposed to each phase of the mixture, and reflected by the mass balance law (2b), is appended to the local form of the dissipation inequality, multiplied by the pore pressure $p$. This latter field, thus, acquires the meaning of the Lagrange multiplier[13,50] associated with the given constraint. For the advantages related with this procedure, the reader is referred to[50,100].

We recall that, throughout this work, all the force densities, and, thus, also $\boldsymbol{\pi}_{\mathrm{fd}}$, are identified as pseudo co-vectors, while all the velocities are defined as vectors. Hence, the juxtapositions $\boldsymbol{\pi}_{\mathrm{fd}} \boldsymbol{w}_{\mathrm{fs}}$ and $\boldsymbol{\pi}_{\mathrm{fd}} \boldsymbol{q}$ in Equation (14) are to be understood, in index notation, as $\boldsymbol{\pi}_{\mathrm{fd}} \boldsymbol{w}_{\mathrm{fs}} = [\boldsymbol{\pi}_{\mathrm{fd}}]_a [\boldsymbol{w}_{\mathrm{fs}}]^a$ and $\boldsymbol{\pi}_{\mathrm{fd}} \boldsymbol{q} = [\boldsymbol{\pi}_{\mathrm{fd}}]_a q^a$, where Einstein's convention of summation over repeated indices applies, unless stated otherwise.

We hypothesize that the dissipative force density $\boldsymbol{\pi}_{\mathrm{fd}}$ can be expressed constitutively, up to the sign, as the result of some suitably defined operator $O_{\boldsymbol{q}}$, applied to $\boldsymbol{q}$, and in which the subscript "$\boldsymbol{q}$" indicates that, in general, the operator may depend on $\boldsymbol{q}$ itself. Hence, we impose a relationship of the kind

$$\boldsymbol{\pi}_{\mathrm{fd}} \equiv -O_{\boldsymbol{q}} \boldsymbol{q}. \tag{15}$$

Such relationship is nonlinear in general, and, for consistency with Equation (14), it imposes that $O_{\boldsymbol{q}}$ complies with the dissipation inequality, so that the condition $\mathfrak{D}^{(a)} = [O_{\boldsymbol{q}} \boldsymbol{q}] \boldsymbol{q} \geq 0$ must be respected at all times and at all points of the region of space occupied by the mixture. Furthermore, by substituting the relationship (15) into the balance law (11b), we find the following operator equation in the unknown $\boldsymbol{q}$:

$$-O_{\boldsymbol{q}} \boldsymbol{q} = \phi_{\mathrm{f}} [\operatorname{grad} p - \varrho_{\mathrm{f}} \boldsymbol{g}]. \tag{16}$$

Among the various possible definitions of $O_{\boldsymbol{q}}$, each of which depends on the fluid that has to be modeled, we require $O_{\boldsymbol{q}}$ to be such that it vanishes identically for the null filtration velocity $\boldsymbol{q}_0 \equiv \boldsymbol{0}$, i.e.,

$$O_{\boldsymbol{q}} \boldsymbol{q} = O_{\boldsymbol{q}_0} \boldsymbol{q}_0 \equiv \boldsymbol{0}. \tag{17}$$

In addition, we require that the null vector field $\boldsymbol{q}_0 \equiv \boldsymbol{0}$ is the unique solution to the equation $O_{\boldsymbol{q}} \boldsymbol{q} = \boldsymbol{0}$. By doing so, when the pressure field solves $\operatorname{grad} p - \varrho_{\mathrm{f}} \boldsymbol{g} = \boldsymbol{0}$, so that also the left-hand side of Equation (16) vanishes, the solution is $\boldsymbol{q} = \boldsymbol{q}_0$. This requirement is important in view of the fact that a "modified" Caputo derivative will feature in the definition of the operator $O_{\boldsymbol{q}} \boldsymbol{q}$, thereby implying that a function $\boldsymbol{q}$ with non-vanishing initial value $\boldsymbol{q}(x, 0) \neq \boldsymbol{0}$ is, in general, a solution of the equation $O_{\boldsymbol{q}} \boldsymbol{q} = \boldsymbol{0}$ (see Equation (55)). Hence, to maintain the uniqueness of the solution $\boldsymbol{q}_0 \equiv \boldsymbol{0}$, we will always assume that $\boldsymbol{q}$ has null initial value.

The definition of $O_{\boldsymbol{q}} \boldsymbol{q}$ given above implies that also the right-hand side of Equation (16) vanishes for $\boldsymbol{q} = \boldsymbol{q}_0$, thereby recovering Stevin's law of the statics of fluids, i.e., $\operatorname{grad} p - \varrho_{\mathrm{f}} \boldsymbol{g} = \boldsymbol{0}$. Moreover, several other fluid behaviors are ruled out, like those characterized by non-null values of $\boldsymbol{\pi}_{\mathrm{fd}}$ for $\boldsymbol{q} = \boldsymbol{q}_0$. In the latter case, indeed, by denoting by $\boldsymbol{\pi}_{\mathrm{fd}}^{\mathrm{st}}$ the value of $\boldsymbol{\pi}_{\mathrm{fd}}$ in static conditions, the statics of the fluid under consideration is governed by the force balance $\boldsymbol{\pi}_{\mathrm{fd}}^{\mathrm{st}} - \phi_{\mathrm{f}} \operatorname{grad} p + \phi_{\mathrm{f}} \varrho_{\mathrm{f}} \boldsymbol{g} = \boldsymbol{0}$, which determines $\boldsymbol{\pi}_{\mathrm{fd}}^{\mathrm{st}}$ as $\boldsymbol{\pi}_{\mathrm{fd}}^{\mathrm{st}} = \phi_{\mathrm{f}}[\operatorname{grad} p - \varrho_{\mathrm{f}} \boldsymbol{g}]$[*] without constitutive prescriptions.

For the sake of clarity, before describing the operator $O_{\boldsymbol{q}}$ in detail for the case that characterizes the main novelty of this work, we briefly discuss the (classical) definitions of $O_{\boldsymbol{q}}$ that return Darcy's law and Forchheimer's correction to Darcy's law. In doing this, since gravity is not expected to play a relevant role for the problems that will be investigated in the sequel, we shall drop the buoyancy term $\varrho_{\mathrm{f}} \boldsymbol{g}$ for here on.

## 5.1 Darcy's law

Although Darcy's law is well-known, we find it useful to briefly review its origin and the range of its applicability in order to give context to the need for Forchheimer's correction and for its fractionalization.

Darcy's law is widely employed in the mechanics of porous media of environmental, industrial, and biological interest (see e.g. [1,33,49,50,87,101], to mention just a few) to describe, at the *macroscale*, the flow of a fluid through the pores of a given porous medium. Here, by "macroscale", it is meant the scale at which the porous medium and the fluid are viewed as a mixture. This can be achieved e.g. through asymptotic homogenization techniques [102–104] or volume averaging methods [49,87], thereby leading to Hybrid Mixture Theory [50]. Darcy's regime is satisfactory when the following two main hypotheses are met:

(i) The stress tensor of the fluid is well approximated by its so-called equilibrium part, so that any contribution due to the fluid viscosity is negligible and one can write the fluid's Cauchy stress tensor as $\boldsymbol{\sigma}_{\mathrm{f}} = -\phi_{\mathrm{f}} p \boldsymbol{\iota}^{\mathrm{T}}$.

(ii) Inertial forces are negligible both at the macroscale and at the microscale. At the macroscale, this assumption implies that no inertial effects are accounted for in the fluid's macroscopic momentum balance law, which reduces, thus, to Equation (11b). For what concerns the microscale, instead, the assumption of negligible inertial effects has two meanings. On the one hand, it requires that such effects are one or more orders of magnitude smaller than those of the other forces contributing to the flow, and, on the other hand, that the linear momentum exchanged between the fluid and the solid at their interface does not depend appreciably on the dynamic part of the overall mechanical stress (see e.g. [88]). In particular, this latter statement is reflected by the fact that, at the macroscale, and in the cases in which $\boldsymbol{\pi}_{\mathrm{fd}}$ can be expressed constitutively, one can prescribe $\boldsymbol{\pi}_{\mathrm{fd}}$ to be a linear function of $\boldsymbol{q}$ (see e.g. [1,49,50,87]), i.e.,

$$\boldsymbol{\pi}_{\mathrm{fd}} = \boldsymbol{\mathcal{G}}^{\boldsymbol{\pi}_{\mathrm{fd}}}(\boldsymbol{q}, \ldots) := -\boldsymbol{\mathcal{G}}^{\boldsymbol{r}}(\ldots)\boldsymbol{q} = -\boldsymbol{r}\boldsymbol{q}, \tag{18}$$

where $\boldsymbol{\mathcal{G}}^{\boldsymbol{\pi}_{\mathrm{fd}}}(\boldsymbol{q}, \ldots)$ is the constitute law expressing $\boldsymbol{\pi}_{\mathrm{fd}}$, $\boldsymbol{r}$ is a second-order tensor field, referred to as *resistivity tensor*, and $\boldsymbol{\mathcal{G}}^{\boldsymbol{r}}(\ldots)$ is its constitutive representation (here, the ellipses means that the considered constitute functions depend, in general, on variables that are left unspecified at the moment). In passing, we recall that there exist generalizations to Darcy's law that involve threshold phenomena, according to which, for example, relationships similar to Equation (18) can be written only when the norm of $\boldsymbol{\pi}_{\mathrm{fd}}$ exceeds a certain value (see e.g. [49]). However, these circumstances are out of the scopes of our present work.

[*]Note that this equation is different from Equation (11b) in that it applies in static conditions, whereas Equation (11b) holds true in dynamic regime, but in the limit of negligible inertial forces.

According to Equation (18), in the case of Darcy's law the identification $\mathcal{O}_{\boldsymbol{q}}\boldsymbol{q} \equiv \boldsymbol{r}\boldsymbol{q}$ applies, so that the operator $\mathcal{O}_{\boldsymbol{q}}$ is represented by $\boldsymbol{r}$ and is, thus, independent of $\boldsymbol{q}$. Furthermore, by substituting Equation (18) into the residual dissipation inequality (14), one obtains

$$\mathfrak{D}^{(\mathrm{a})} = -\boldsymbol{\pi}_{\mathrm{fd}}\,\phi_{\mathrm{f}}^{-1}\boldsymbol{q} = [\boldsymbol{r}\boldsymbol{q}]\phi_{\mathrm{f}}^{-1}\boldsymbol{q} = \phi_{\mathrm{f}}^{-1}\,\mathrm{tr}\{\boldsymbol{r}[\boldsymbol{q}\otimes\boldsymbol{q}]\} = \phi_{\mathrm{f}}^{-1}\,\mathrm{tr}\{\mathrm{sym}(\boldsymbol{r})[\boldsymbol{q}\otimes\boldsymbol{q}]\} \geq 0, \tag{19}$$

which requires the symmetric part of the resistivity tensor, $\mathrm{sym}(\boldsymbol{r})$, to be positive semi-definite. Typically, however, since one aims at obtaining an expression for $\boldsymbol{q}$ in closed form by substituting Equation (18) into the balance law (11b), and solving for $\boldsymbol{q}$, one assumes that $\mathrm{sym}(\boldsymbol{r})$ is positive definite and, often, it is also hypothesized from the outset that the resistivity tensor $\boldsymbol{r}$ is symmetric, so that the identity $\boldsymbol{r} \equiv \mathrm{sym}(\boldsymbol{r})$ is stated. Under these hypotheses, indeed, one achieves Darcy's law in the "popular" form

$$\boldsymbol{q} = -\frac{\boldsymbol{k}}{\mu}\mathrm{grad}\,p \equiv \boldsymbol{q}_{\mathrm{D}}, \qquad \boldsymbol{r} := \phi_{\mathrm{f}}\mu\boldsymbol{k}^{-1}, \tag{20}$$

where $\boldsymbol{k}$ is a second-order tensor field referred to as *permeability tensor*, $\mu$ is the fluid's viscosity, and $\boldsymbol{q}_{\mathrm{D}}$ stands for "Darcy's velocity".

With respect to the reference placement of the medium, Equation (20) transforms as

$$\boldsymbol{Q} = -\frac{\boldsymbol{K}}{\mu}\mathrm{Grad}\,P \equiv \boldsymbol{Q}_{\mathrm{D}}, \tag{21}$$

where $P$ is the pore pressure written as a function of the points $X$ of the reference placement and of time, i.e., $p(x,t) = P(X,t)$, while $\boldsymbol{K}$ is referred to as *material permeability tensor* and is related to $\boldsymbol{k}$ through the backward Piola transformation $\boldsymbol{K}(X,t) = J(X,t)\boldsymbol{F}^{-1}(x,t)\boldsymbol{k}(x,t)\boldsymbol{F}^{-\mathrm{T}}(X,t)$, with $x = \chi(X,t)$. Hence, the Darcian material filtration velocity $\boldsymbol{Q}_{\mathrm{D}}$ can be expressed in terms of the pore pressure and deformation gradient tensor.

Finally, having neglected the buoyancy terms in Equations (11a) and (11b), the equations to be solved in the case of validity of Darcy's regime can be summarized as

$$\mathrm{Div}(-JP\boldsymbol{F}^{-\mathrm{T}} + \boldsymbol{T}_{\mathrm{sc}}) = \boldsymbol{0}, \tag{22a}$$

$$\dot{J} = \mathrm{Div}\left[\frac{\boldsymbol{K}}{\mu}\mathrm{Grad}P\right], \tag{22b}$$

where $\boldsymbol{T}_{\mathrm{sc}} = \boldsymbol{F}\boldsymbol{S}_{\mathrm{sc}}$, with $\boldsymbol{S}_{\mathrm{sc}}$ being deducible from Equation (13b), is determined constitutively as shown in Equation (10), while the permeability tensor $\boldsymbol{K}$ is specified in Equation (43) below. Moreover, the material volumetric fractions $\Phi_{\mathrm{s}}$ and $\Phi_{\mathrm{f}}$, which feature in the definitions of $\boldsymbol{T}_{\mathrm{sc}}$ and $\boldsymbol{K}$, are $\Phi_{\mathrm{s}}(X,t) = J(X,t)\phi_{\mathrm{s}}(x,t) = \Phi_{\mathrm{sR}}(X)$ and $\Phi_{\mathrm{f}}(X,t) = J(X,t)\phi_{\mathrm{f}}(x,t)$, and $\Phi_{\mathrm{sR}}(X)$ is regarded as known. In the system of Equations (22a) and (22b), the unknowns are pressure $P$ and the motion $\chi$. The latter is accounted for by $\boldsymbol{F}$ and $J = \det\boldsymbol{F}$, and $\Phi_{\mathrm{f}}$ is expressed as $\Phi_{\mathrm{f}} = J - \Phi_{\mathrm{s}}$ by virtue of the backward Piola transformation of the saturation condition.

## *5.2 Forchheimer's correction*

Following [88], Forchheimer's correction to Darcy's law becomes necessary when the hypothesis (ii) of the section 5.1 is not satisfied. Indeed, as remarked in [88], the correction accounts for the inertial effects that characterize the pore scale dynamics of the fluid, and for those that take part to the momentum exchange between the fluid and the solid phase. In fact, it can be shown that (see e.g.[105]), at the macroscale, the consideration of the inertial effects mentioned above can be expressed in terms of a non-linear relationship between $\boldsymbol{\pi}_{\mathrm{fd}}$ and $\boldsymbol{q}$ of the type (see e.g.[45,52,88,99,106])

$$\boldsymbol{\pi}_{\mathrm{fd}} = \boldsymbol{\mathcal{G}}^{\boldsymbol{\pi}_{\mathrm{fd}}}(\boldsymbol{q}, \ldots) = \boldsymbol{\mathcal{G}}^{\boldsymbol{r}_{\mathrm{F}}}(\boldsymbol{q}, \ldots)\boldsymbol{q} = -\, \boldsymbol{r}_{\mathrm{F}}(\|\boldsymbol{q}\|)\boldsymbol{q}, \tag{23}$$

where $\boldsymbol{r}_{\mathrm{F}}(\|\boldsymbol{q}\|)$ can be thought of as a $\boldsymbol{q}$-dependent resistivity tensor. Note that, here and in the following, the subscript "F" stands for "Forchheimer", and is introduced in order to highlight that the current description differs from the Darcian one. In addition, as suggested by the identification $\boldsymbol{\mathcal{G}}^{\boldsymbol{r}_{\mathrm{F}}}(\boldsymbol{q}, \ldots) \equiv -\boldsymbol{r}_{\mathrm{F}}(\|\boldsymbol{q}\|)$, the resistivity tensor depends, in general, aside from $\|\boldsymbol{q}\|$, also on other parameters characterizing the flow, although we do not report them here explicitly for the sake of a lighter notation.

As reported in[45,52,88,99,106], the resistivity tensor $\boldsymbol{r}_{\mathrm{F}}(\|\boldsymbol{q}\|)$ can be defined as

$$\boldsymbol{r}_{\mathrm{F}}(\|\boldsymbol{q}\|) = \boldsymbol{r} + \|\boldsymbol{q}\|\boldsymbol{\mathfrak{a}}\boldsymbol{r} = \phi_{\mathrm{f}}\mu[\boldsymbol{k}^{-1} + \|\boldsymbol{q}\|\boldsymbol{\mathfrak{a}}\boldsymbol{k}^{-1}], \tag{24}$$

where $\boldsymbol{\mathfrak{a}}$, in general, is a second-order tensor field denominated *Forchheimer's coefficient*, having physical dimensions of the inverse of a characteristic velocity, and that is to be assigned constitutively (see Equation (37) below).

By comparing Equation (24) with the general definition (15), we obtain the identification

$$\mathcal{O}_{\boldsymbol{q}} \equiv \phi_{\mathrm{f}}\mu[\boldsymbol{k}^{-1} + \|\boldsymbol{q}\|\boldsymbol{\mathfrak{a}}\boldsymbol{k}^{-1}] = \phi_{\mathrm{f}}\mu\boldsymbol{k}^{-1}[\boldsymbol{\imath} + \|\boldsymbol{q}\|\boldsymbol{k}\boldsymbol{\mathfrak{a}}\boldsymbol{k}^{-1}]. \tag{25}$$

Moreover, by substituting Equation (25) into the constitutive representation (23) of $\boldsymbol{\pi}_{\mathrm{fd}}$, using the resulting expression into the force balance (16), and invoking the definition (20) of Darcy's velocity $\boldsymbol{q}_{\mathrm{D}}$, we find that $\boldsymbol{q}$ must satisfy the algebraic equation

$$\phi_{\mathrm{f}}\mu\boldsymbol{k}^{-1}[\boldsymbol{\imath} + \|\boldsymbol{q}\|\boldsymbol{k}\boldsymbol{\mathfrak{a}}\boldsymbol{k}^{-1}]\boldsymbol{q} = \phi_{\mathrm{f}}\mu\boldsymbol{k}^{-1}\boldsymbol{q}_{\mathrm{D}}, \tag{26}$$

which can be put in the equivalent form (see[45], in which a slightly different notation is employed)

$$[\boldsymbol{\imath} + \|\boldsymbol{q}\|\boldsymbol{k}\boldsymbol{\mathfrak{a}}\boldsymbol{k}^{-1}]\boldsymbol{q} = \boldsymbol{q}_{\mathrm{D}}. \tag{27}$$

The backward Piola transformation of Equation (27) produces[45]

$$[\boldsymbol{I} + \|\boldsymbol{Q}\|_{\boldsymbol{C}}\boldsymbol{K}\boldsymbol{\mathcal{A}}\boldsymbol{K}^{-1}]\boldsymbol{Q} = \boldsymbol{Q}_{\mathrm{D}}, \tag{28}$$

where $\boldsymbol{I}$ is the material identity tensor, $\|\boldsymbol{Q}\|_{\boldsymbol{C}} := J^{-1}\sqrt{[\boldsymbol{C} : (\boldsymbol{Q} \otimes \boldsymbol{Q})]}$ is the $\boldsymbol{C}$-norm of $\boldsymbol{Q}$, i.e., the norm of $\boldsymbol{Q}$ computed with respected to the deformed metric tensor induced by the right Cauchy-Green deformation tensor $\boldsymbol{C}$, while

$$\boldsymbol{\mathcal{A}}(X, t) := \boldsymbol{F}^{\mathrm{T}}(x, t)\boldsymbol{\mathfrak{a}}(x, t)\boldsymbol{F}^{-\mathrm{T}}(X, t) \tag{29}$$

is the backward Piola transform of Forchheimer's coefficient. Note that the norm $\|\boldsymbol{Q}\|_{\boldsymbol{C}}$ arises because of the identity $\|\boldsymbol{q}(x, t)\| = \|\boldsymbol{Q}(X, t)\|_{\boldsymbol{C}}$.

Finally, we notice that a rather suggestive reformulation of Equation (28) reads

$$\boldsymbol{R}_{\mathrm{F}}(\|\boldsymbol{Q}\|_{\boldsymbol{C}})\boldsymbol{Q} = \Phi_{\mathrm{f}}\mu\,\boldsymbol{K}^{-1}\boldsymbol{Q}_{\mathrm{D}}, \tag{30}$$

where we have introduced the material resistivity tensor

$$\boldsymbol{R}_{\mathrm{F}}(\|\boldsymbol{Q}\|_{\boldsymbol{C}}) := \Phi_{\mathrm{f}}\mu\boldsymbol{K}^{-1}\big[\boldsymbol{I} + \|\boldsymbol{Q}\|_{\boldsymbol{C}}\boldsymbol{K}\boldsymbol{\mathcal{A}}\boldsymbol{K}^{-1}\big], \tag{31}$$

related to $\boldsymbol{r}_{\mathrm{F}}(\|\boldsymbol{q}\|)$ through $\boldsymbol{R}_{\mathrm{F}}(\|\boldsymbol{Q}(X,t)\|_{\boldsymbol{C}(X,t)}) = \boldsymbol{F}^{\mathrm{T}}(x,t)[\boldsymbol{r}_{\mathrm{F}}(\|\boldsymbol{q}(x,t)\|)]\boldsymbol{F}(X,t)$, with $x = \chi(X,t)$.

The tensor function $\boldsymbol{R}_{\mathrm{F}}$ depends also on the deformation gradient tensor $\boldsymbol{F}$ through $\Phi_{\mathrm{f}}$ and $\boldsymbol{K}$, although we prefer not to emphasize this dependence here, both for notational convenience and for highlighting the fact that, since $\boldsymbol{R}_{\mathrm{F}}$ is the backward Piola transformation of $\boldsymbol{r}_{\mathrm{F}}$, it depends on the $\boldsymbol{C}$-norm of the material filtration velocity $\boldsymbol{Q}$.

*Remark 1.* Material resistivity tensor.
We find it useful to comment on the definition of the material resistivity tensor $\boldsymbol{R}_{\mathrm{F}}(\|\boldsymbol{Q}\|_{\boldsymbol{C}})$ given in Equation (31). To motivate this definition, we start from the momentum balance law (11b), in which we neglect gravity for the sake of simplicity, and we perform its pull-back to the system's reference placement, thereby obtaining

$$\begin{aligned} &J(X,t)\boldsymbol{F}^{\mathrm{T}}(x,t)\boldsymbol{\pi}_{\mathrm{fd}}(x,t) = J(X,t)\boldsymbol{F}^{\mathrm{T}}(x,t)\phi_{\mathrm{f}}(x,t)\mathrm{grad}p(x,t), \\ &\Rightarrow \quad \boldsymbol{\Pi}_{\mathrm{fd}} = \Phi_{\mathrm{f}}\,\mathrm{Grad}P, \end{aligned} \tag{32}$$

where the fully material dissipative force density $\boldsymbol{\Pi}_{\mathrm{fd}}$ is defined by $\boldsymbol{\Pi}_{\mathrm{fd}}(X,t) := J(X,t)\boldsymbol{F}^{\mathrm{T}}(x,t)\boldsymbol{\pi}_{\mathrm{fd}}(x,t)$. Next, we concentrate on the definition of $\boldsymbol{\Pi}_{\mathrm{fd}}$, and we substitute the constitute expression (23) into it, i.e.,

$$\boldsymbol{\Pi}_{\mathrm{fd}}(X,t) = -J(X,t)\boldsymbol{F}^{\mathrm{T}}(x,t)\boldsymbol{r}_{\mathrm{F}}(\|\boldsymbol{q}(x,t)\|)\boldsymbol{q}(x,t). \tag{33}$$

Then, by using the identity $\|\boldsymbol{q}(x,t)\| = \|\boldsymbol{Q}(X,t)\|_{\boldsymbol{C}(X,t)}$, and the relation linking $\boldsymbol{q}(x,t)$ with its material counterpart $\boldsymbol{Q}(X,t)$, i.e., $\boldsymbol{q}(x,t) = [J(X,t)]^{-1}\boldsymbol{F}(X,t)\boldsymbol{Q}(X,t)$, we find

$$\begin{aligned} \boldsymbol{\Pi}_{\mathrm{fd}}(X,t) &= -J(X,t)\boldsymbol{F}^{\mathrm{T}}(x,t)\boldsymbol{r}_{\mathrm{F}}(\|\boldsymbol{Q}(X,t)\|_{\boldsymbol{C}(X,t)})\frac{1}{J(X,t)}\boldsymbol{F}(X,t)\boldsymbol{Q}(X,t) \\ &= -\boldsymbol{F}^{\mathrm{T}}(x,t)\boldsymbol{r}_{\mathrm{F}}(\|\boldsymbol{Q}(X,t)\|_{\boldsymbol{C}(X,t)})\boldsymbol{F}(X,t)\boldsymbol{Q}(X,t) \\ &= -\boldsymbol{R}_{\mathrm{F}}(\|\boldsymbol{Q}(X,t)\|_{\boldsymbol{C}(X,t)})\boldsymbol{Q}(X,t), \end{aligned} \tag{34}$$

so that the identification $\boldsymbol{R}_{\mathrm{F}}(\|\boldsymbol{Q}(X,t)\|_{\boldsymbol{C}(X,t)}) := \boldsymbol{F}^{\mathrm{T}}(x,t)\boldsymbol{r}_{\mathrm{F}}(\|\boldsymbol{Q}(X,t)\|_{\boldsymbol{C}(X,t)})\boldsymbol{F}(X,t)$ can be made.

Although there exists some interest for the impact of Forchheimer's correction in porous media of biological relevance (see e.g.[45,51,52]), to the best of our knowledge the majority of the studies devoted to the identification of Forchheimer coefficient $\boldsymbol{\mathfrak{a}}$ come from hydrogeology[49] and petroleum engineering[107,108]. In fact, $\boldsymbol{\mathfrak{a}}$ is often expressed through (semi-)empirical laws. For instance, Wang et al.[109] provided an expression for $\boldsymbol{\mathfrak{a}}$ that, in our formalism, reads

$$\boldsymbol{\mathfrak{a}} := \varrho_{\mathrm{f}}\boldsymbol{\eta}\mu^{-1}\boldsymbol{k}\boldsymbol{\beta}, \tag{35}$$

where the tensor field $\boldsymbol{\beta}$ is said to be *non-Darcy coefficient*[109]. As done in[45], we take an empirical formula from Thauvin and Mohanty[53] and we adapt it to our purposes, thereby expressing $\boldsymbol{\beta}$ as

$$\boldsymbol{\beta} = c_0 \phi_{\mathrm{f}}^{c_1} [\boldsymbol{\eta}\boldsymbol{k}]^{c_2}, \tag{36}$$

in which $c_0$, $c_1$, and $c_2$ are empirical (real) constants, with $c_0$ having to be non-negative. Then, by substituting Equation (36) into Equation (35), and exploiting the positivity of all the eigenvalues of $\boldsymbol{k}$, we obtain

$$\boldsymbol{\mathfrak{a}} = c_0 \varrho_{\mathrm{f}} \phi_{\mathrm{f}}^{c_1} \mu^{-1} [\boldsymbol{\eta}\boldsymbol{k}]^{1+c_2}, \tag{37}$$

so that, by employing Equation (29), $\boldsymbol{\mathcal{A}}$ is defined by

$$\boldsymbol{\mathcal{A}}(X,t) = c_0 \varrho_{\mathrm{f}} \left[ \frac{\Phi_{\mathrm{f}}(X,t)}{J(X,t)} \right]^{c_1} \frac{1}{\mu} \boldsymbol{F}^{\mathrm{T}}(x,t) [\boldsymbol{\eta}(x)\boldsymbol{k}(x,t)]^{1+c_2} \boldsymbol{F}^{-\mathrm{T}}(X,t), \tag{38a}$$

$$\boldsymbol{\eta}(x)\boldsymbol{k}(x,t) = \frac{1}{J(X,t)} \boldsymbol{F}^{-\mathrm{T}}(X,t)\boldsymbol{C}(X,t)\boldsymbol{K}(X,t)\boldsymbol{F}^{\mathrm{T}}(x,t), \qquad \text{with } x = \chi(X,t). \tag{38b}$$

In this case, since it is in general not straightforward to express $\boldsymbol{Q}$ as a function of $\boldsymbol{Q}_{\mathrm{D}}$ in closed form, the model equations to be solved form the system

$$\mathrm{Div}(-JP\boldsymbol{F}^{-\mathrm{T}} + \boldsymbol{T}_{\mathrm{sc}}) = \boldsymbol{0}, \tag{39a}$$

$$\dot{J} + \mathrm{Div}\boldsymbol{Q} = 0, \tag{39b}$$

$$\left[\boldsymbol{I} + \|\boldsymbol{Q}\|_{\boldsymbol{C}} \boldsymbol{K}\boldsymbol{\mathcal{A}}\boldsymbol{K}^{-1}\right]\boldsymbol{Q} = \boldsymbol{Q}_{\mathrm{D}}, \tag{39c}$$

where the unknowns of the problem are the solid phase motion $\chi$, pore pressure $P$, and the material filtration velocity $\boldsymbol{Q}$. The stress tensor $\boldsymbol{T}_{\mathrm{sc}}$ and the material permeability $\boldsymbol{K}$ are assigned constitutively in Equations (10) and (43) (see below), while $\boldsymbol{\mathcal{A}}$ is determined through Equations (38a) and (38b).

A strong simplification of Equations (39a)–(39c) is achieved when the porous medium under consideration is assumed to be isotropic and, in particular, *"unconditionally isotropic"*[33]. In this case, indeed, the spatial permeability tensor $\boldsymbol{k}$ reduces to $\boldsymbol{k} = k_{\mathrm{iso}}\boldsymbol{\eta}^{-1}$, where $k_{\mathrm{iso}}$ is referred to as *scalar permeability*; the material permeability tensor becomes $\boldsymbol{K} = \kappa_{\mathrm{iso}}\boldsymbol{C}^{-1}$, with $\kappa_{\mathrm{iso}}(X,t) := J(X,t)k_{\mathrm{iso}}(x,t)$, and $x = \chi(X,t)$; the Forchheimer coefficient $\boldsymbol{\mathfrak{a}}$ reduces to $\boldsymbol{\mathfrak{a}} = c_0\varrho_{\mathrm{f}}\phi_{\mathrm{f}}^{c_1}\mu^{-1}k_{\mathrm{iso}}^{1+c_2}\boldsymbol{\imath}^{\mathrm{T}}$, and the material Forchheimer coefficient $\boldsymbol{\mathcal{A}}$ can be written as $\boldsymbol{\mathcal{A}} = \mathcal{A}_{\mathrm{iso}}\boldsymbol{I}^{\mathrm{T}}$, whereby it is fully represented by the scalar quantity

$$\mathcal{A}_{\mathrm{iso}} = c_0 \varrho_{\mathrm{f}} \left[ \frac{\Phi_{\mathrm{f}}}{J} \right]^{c_1} \frac{1}{\mu} \left[ \frac{\kappa_{\mathrm{iso}}}{J} \right]^{1+c_2}, \qquad \text{with } \Phi_{\mathrm{f}} > 0,\ k_{\mathrm{iso}} \geq 0, \text{ and } \mu > 0. \tag{40}$$

Then, by substituting this result into Equation (39c), and following a procedure similar to the one described in[45,52,106], we can express $\boldsymbol{Q}$ as a function of $\boldsymbol{Q}_{\mathrm{D}}$, i.e.,

$$\boldsymbol{Q} = \mathfrak{F}\boldsymbol{Q}_{\mathrm{D}} = -\frac{\mathfrak{F}\boldsymbol{K}}{\mu}\mathrm{Grad}P, \qquad \mathfrak{F} := \frac{2}{1 + \sqrt{1 + 4\mathcal{A}_{\mathrm{iso}}\|\boldsymbol{Q}_{\mathrm{D}}\|_{\boldsymbol{C}}}}, \tag{41}$$

where $\mathfrak{F}$ is referred to as *material friction factor*[45,52,106] (note that, in[45,52,106], Equation (41) is obtained in the spatial description and, thus, in the models presented therein the adjective *"material"* is not present).

A relevant consequence of Equation (41) is that, for an *"unconditionally isotropic"*[33] porous medium, $\boldsymbol{Q}$ can be understood as a reformulation of Darcy's law, in which the permeability is multiplicatively rescaled by means of $\mathfrak{F}$, which, in turn, depends again on the $\boldsymbol{C}$-norm of material Darcy's velocity $\|\boldsymbol{Q}_{\mathrm{D}}\|_{\boldsymbol{C}}$ as well as on $\kappa_{\mathrm{iso}}$, porosity, and the other flow parameters accounted for in the model. Therefore, under the hypothesis of *"unconditionally isotropic"* medium, Equations (39a)–(39c) condense as

$$\mathrm{Div}(-JP\boldsymbol{F}^{-\mathrm{T}} + \boldsymbol{T}_{\mathrm{sc}}) = \boldsymbol{0}, \tag{42a}$$

$$\dot{J} = \mathrm{Div}\left[\frac{\mathfrak{F}\boldsymbol{K}}{\mu}\mathrm{Grad}P\right], \tag{42b}$$

where $\mathfrak{F}$ and $\mathcal{A}_{\mathrm{iso}}$ are defined in Equations $(41)_{\mathrm{b}}$ and (40), respectively, and $\boldsymbol{K} = \kappa_{\mathrm{iso}}\boldsymbol{C}^{-1}$. In the sequel, we adopt an expression of $\kappa_{\mathrm{iso}}$ taken from Holmes&Mow[7], given by

$$\kappa_{\mathrm{iso}} = Jk_{\mathrm{ref}}\left[\frac{J-\Phi_{\mathrm{s}}}{1-\Phi_{\mathrm{s}}}\right]^{m_0}\exp\left(\frac{m_1}{2}[J^2-1]\right), \tag{43}$$

where $k_{\mathrm{ref}}$ is a reference permeability, while $m_0$ and $m_1$ are non-negative material parameters.

We conclude this section noticing that, as remarked in[45], setting $c_1 = -11/2$ and $c_2 = -1/2$ makes it possible to establish a proportionality relationship between the product $\mathcal{A}_{\mathrm{iso}}\|\boldsymbol{Q}_{\mathrm{D}}\|_{\boldsymbol{C}}$ and *Darcian Reynolds' number*[49]

$$\mathrm{Re}_{\mathrm{D}} := \frac{\varrho_{\mathrm{f}}}{\mu}\sqrt{\frac{\kappa_{\mathrm{iso}}}{\Phi_{\mathrm{f}}}}\,\|\boldsymbol{Q}_{\mathrm{D}}\|_{\boldsymbol{C}} = \frac{\varrho_{\mathrm{f}}}{\mu}\sqrt{\frac{\kappa_{\mathrm{iso}}}{J-\Phi_{\mathrm{s}}}}\,\|\boldsymbol{Q}_{\mathrm{D}}\|_{\boldsymbol{C}}, \tag{44}$$

so that we can write

$$\mathcal{A}_{\mathrm{iso}}\|\boldsymbol{Q}_{\mathrm{D}}\|_{\boldsymbol{C}} = c_0\left[\frac{\Phi_{\mathrm{f}}}{J}\right]^{-5}\mathrm{Re}_{\mathrm{D}} = c_0\left[\frac{J-\Phi_{\mathrm{s}}}{J}\right]^{-5}\mathrm{Re}_{\mathrm{D}}. \tag{45}$$

This result allows to express the friction factor $\mathfrak{F}$ as a function of $\mathrm{Re}_{\mathrm{D}}$, parameterized by $c_0$, only, i.e.,

$$\mathfrak{F} = \frac{2}{1+\sqrt{1+4c_0[\Phi_{\mathrm{f}}/J]^{-5}\mathrm{Re}_{\mathrm{D}}}}. \tag{46}$$

Clearly, for $c_0 = 0$, it holds that $\mathfrak{F} = 1$, which means $\boldsymbol{Q} = \boldsymbol{Q}_{\mathrm{D}}$, and, thus, that no Forchheimer's correction is accounted for.

Due to the lack of experimental results for biological porous media (at least, to the best of our knowledge), it is rather difficult to establish plausible values of $c_0$ (we recall, indeed, that, in spite of the hypothesis of isotropy, the tissue that has inspired this study is articular cartilage). To (partially) circumvent this difficulty, one can follow a path similar to the one outlined in[45], which introduces a *"trial friction factor"*[45], here denoted by $\mathfrak{F}_{\mathrm{trial}} \in\, ]0,1[$ , that allows to rewrite Equation (46) as

$$\mathfrak{F} = \frac{2}{1+\sqrt{1+4\frac{1-\mathfrak{F}_{\mathrm{trial}}}{\mathfrak{F}_{\mathrm{trial}}^2}\frac{[\Phi_{\mathrm{f}}/J]^{-5}}{[\Phi_{\mathrm{f0}}/J_0]^{-5}}\frac{\mathrm{Re}_{\mathrm{D}}}{\mathrm{Re}_{\mathrm{D0}}}}}, \tag{47}$$

(we have slightly modified the expression reported in[45]) where $J_0$, $\mathrm{Re}_{\mathrm{D}0}$, and $\Phi_{\mathrm{f}0}$ are reference constant values of the volume ratio $J$, of Darcian Reynolds' number $\mathrm{Re}_{\mathrm{D}}$, and of the fluid phase material volumetric fraction $\Phi_{\mathrm{f}}$, respectively. For example, in[45] these values are obtained by evaluating, at a given time and at a given point of the medium, the quantities $J$, $\mathrm{Re}_{\mathrm{D}}$, and $\Phi_{\mathrm{f}}$ under the hypothesis of *purely Darcian flow regime*, i.e., for $\boldsymbol{Q}$ set equal to $\boldsymbol{Q}_{\mathrm{D}}$. Note that Darcy's law is recovered in the limit $\mathfrak{F}_{\mathrm{trial}} \to 1^-$, while the flow is slowed down towards null filtration velocities for $\mathfrak{F}_{\mathrm{trial}} \to 0^+$.

In[45], an algorithm has been presented for the evaluation of the friction factor $\mathfrak{F}$, but we do not repeat it here, since this is out of the scopes of the present work. Rather, we recall that, similarly to the study presented in[45], the rationale behind the algorithmic determination of the friction factor is twofold. On the one hand, for consistency, the absolute value of the difference between $\mathfrak{F}_{\mathrm{trial}}$ and e.g. the maximum value of $\mathfrak{F}$, i.e., $\mathfrak{F}_{\max} := \max_{(X,t)\in\mathscr{B}\times[0,T]}\{\mathfrak{F}(X,t)\}$, should be less than a given threshold. On the other hand, since this reasoning applies, in principle, for any initial choice of $\mathfrak{F}_{\mathrm{trial}}$, an indication about the magnitude of this quantity may be supplied by the comparison of some physical quantities relevant for the flow computed by means of different models of permeability. For instance, given two permeability models for the same medium, one could determine the pressure relaxation curves for both models, estimate the differences between these curves, and *correct* —say— the first model by means of Forchheimer's correction, with a trial friction factor chosen in such a way that the *corrected* pressure relaxation curve is, in a certain norm, close enough to the one predicted by the second model.

## 5.3 Fractional Forchheimer's correction

From the point of view of mathematical modelling, this section is the heart of the present work since we propose here a fractionalization of the constitutive law (23), which we provide in the form

$$\boldsymbol{\pi}_{\mathrm{fd}}(t) := -\boldsymbol{r}_{\mathrm{F}}(\|\boldsymbol{q}(t)\|)\boldsymbol{q}(t) - \frac{\alpha\, t_{\mathrm{c}}^{\alpha}}{\Gamma(1-\alpha)} \int_{t_{\mathrm{in}}}^{t} \frac{\boldsymbol{r}_{\mathrm{F}}(\|\boldsymbol{q}(\tau)\|)}{(t-\tau)^{\alpha}}\, \mathcal{T}_{\mathrm{s}}\boldsymbol{q}(\tau)\mathrm{d}\tau, \tag{48}$$

where $\boldsymbol{r}_{\mathrm{F}}(\|\boldsymbol{q}(t)\|)$ is defined in Equation (24), $t_{\mathrm{c}}$ is a characteristic time scale of the flow, $\alpha \in \,]0,1[$ another characteristic parameter of the flow, and $\mathcal{T}_{\mathrm{s}}\boldsymbol{q}(\tau)$ denotes the *Truesdell rate* of $\boldsymbol{q}$, computed with respect to the velocity of the solid phase, and evaluated at time $\tau \in [t_{\mathrm{in}}, t]$. Note that, with the exception of $\alpha$, $t_{\mathrm{c}}$, and the independent variables $t$ and $\tau$, all the quantities featuring in Equation (48) have to be understood as functions of spatial points and time, although we report explicitly the sole dependence on time for the sake of a lighter notation. We emphasize that Equation (48), which, to the best of our knowledge, is novel and constitutes the starting point of the fractionalization of Forchheimer's correction, has been inspired by the works[47,54], in which similar models have been proposed to fractionalize Darcy's law.

We recall that, in the present context, the Truesdell rate of $\boldsymbol{q}$ can be computed as†

$$\mathcal{T}_{\mathrm{s}}\boldsymbol{q}(x,\tau) \equiv \frac{1}{J(\Xi(x,\tau),\tau)}\boldsymbol{F}(\Xi(x,\tau),\tau)\,\mathrm{D}_{\mathrm{s}}\{[J \circ (\Xi,\mathrm{t})]\boldsymbol{F}^{-1}\boldsymbol{q}\}(x,\tau), \tag{49}$$

†The right-hand side of Equation (51) is, in fact, *not* the *definition* of the Truesdell rate of $\boldsymbol{q}$, but just a simple way for computing it. A more rigorous way of writing it can be found e.g. in[110].

where $\mathrm{D}_\mathrm{s}$ is the substantial derivative with respect to the solid phase motion, while $\Xi$ and $\mathfrak{t}$ are auxiliary functions defined by the relations

$$\Xi : \mathscr{B}_t \times \mathscr{I} \to \mathscr{B}, \qquad (x,\tau) \mapsto \Xi(x,\tau) := [\chi(\,\cdot\,,\tau)]^{-1}(x) = X \in \mathscr{B}, \tag{50a}$$

$$\mathfrak{t} : \mathscr{B}_t \times \mathscr{I} \to \mathscr{I}, \qquad (x,\tau) \mapsto \mathfrak{t}(x,\tau) = \tau \in \mathscr{I}, \tag{50b}$$

and the composition of $J$ (or any other field over $\mathscr{B}\times\mathscr{I}$, just like $\boldsymbol{F}$ in Equation (51) below) with the pair of maps $(\Xi,\mathfrak{t})$ in required to express in rigorous formalism the reformulation of $J$ as a function of the points of $\mathscr{S}$ and time. Indeed, $[J\circ(\Xi,\mathfrak{t})](x,t) = J(\Xi(x,t),\mathfrak{t}(x,t)) = J(X,t)$.

In the spatial description, Equation (49) produces the result

$$\begin{aligned}
\mathscr{T}_\mathrm{s}\boldsymbol{q} &\equiv \frac{1}{J\circ(\Xi,\mathfrak{t})}[\boldsymbol{F}\circ(\Xi,\mathfrak{t})]\,\mathrm{D}_\mathrm{s}\{[J\circ(\Xi,\mathfrak{t})]\boldsymbol{F}^{-1}\boldsymbol{q}\} \\
&= [\operatorname{div}\boldsymbol{v}_\mathrm{s}]\boldsymbol{q} - [\operatorname{grad}\boldsymbol{v}_\mathrm{s}]\boldsymbol{q} + \mathrm{D}_\mathrm{s}\boldsymbol{q} \\
&= [\operatorname{div}\boldsymbol{v}_\mathrm{s}]\boldsymbol{q} - [\operatorname{grad}\boldsymbol{v}_\mathrm{s}]\boldsymbol{q} + [\operatorname{grad}\boldsymbol{q}]\boldsymbol{v}_\mathrm{s} + \partial_t\boldsymbol{q}.
\end{aligned} \tag{51}$$

However, since we are interested in the material description of the flow, we recall the definition of *material filtration velocity* $\boldsymbol{Q} = J[\boldsymbol{F}^{-1}\circ(\chi,\mathfrak{T})][\boldsymbol{q}\circ(\chi,\mathfrak{T})]$, in which the additional auxiliary map $\mathfrak{T} : \mathscr{B}\times\mathscr{I}\to\mathscr{I}$, such that $(X,\tau)\mapsto\mathfrak{T}(X,\tau) = \tau$, has been introduced to express $\boldsymbol{F}^{-1}$ and $\boldsymbol{q}$ as functions of time and of the points of $\mathscr{B}$, and we express $\mathscr{T}_\mathrm{s}\boldsymbol{q}$ as

$$\mathscr{T}_\mathrm{s}\boldsymbol{q}\circ(\chi,\mathfrak{T}) \equiv J^{-1}\boldsymbol{F}\,\overline{\{J[\boldsymbol{F}^{-1}\circ(\chi,\mathfrak{T})][\boldsymbol{q}\circ(\chi,\mathfrak{T})]\}}^{\boldsymbol{\cdot}} = J^{-1}\boldsymbol{F}\dot{\boldsymbol{Q}}. \tag{52}$$

Here, indeed, it holds again true that $[\boldsymbol{F}^{-1}\circ(\chi,\mathfrak{T})](X,\tau) = \boldsymbol{F}^{-1}(\chi(X,\tau),\mathfrak{T}(X,\tau)) = \boldsymbol{F}^{-1}(x,\tau)$ and $[\boldsymbol{q}\circ(\chi,\mathfrak{T})](X,\tau) = \boldsymbol{q}(\chi(X,\tau),\mathfrak{T}(X,\tau)) = \boldsymbol{q}(x,\tau)$.

By substituting Equation (48) into the force balance $-\phi_\mathrm{f}\operatorname{grad}p + \boldsymbol{\pi}_\mathrm{fd} = \boldsymbol{0}$, which replaces Equation (11b) after neglecting gravity, we obtain

$$\boldsymbol{r}_\mathrm{F}(\|\boldsymbol{q}(t)\|)\boldsymbol{q}(t) + \frac{\alpha\,t_\mathrm{c}^\alpha}{\Gamma(1-\alpha)}\int_{t_\mathrm{in}}^{t}\frac{\boldsymbol{r}_\mathrm{F}(\|\boldsymbol{q}(\tau)\|)}{(t-\tau)^\alpha}\mathscr{T}_\mathrm{s}\boldsymbol{q}(\tau)\mathrm{d}\tau = \phi_\mathrm{f}(t)\mu\,\boldsymbol{k}^{-1}(t)\boldsymbol{q}_\mathrm{D}(t), \tag{53}$$

which, by virtue of Equation (52), can be recast in the form

$$\begin{aligned}
&\boldsymbol{R}_\mathrm{F}(\|\boldsymbol{Q}(t)\|_{\boldsymbol{C}(t)})\boldsymbol{Q}(t) + \frac{\alpha\,t_\mathrm{c}^\alpha}{\Gamma(1-\alpha)}\int_{t_\mathrm{in}}^{t}\frac{J(t)}{J(\tau)}\frac{\boldsymbol{F}^\mathrm{T}(t)\boldsymbol{F}^{-\mathrm{T}}(\tau)\boldsymbol{R}_\mathrm{F}(\|\boldsymbol{Q}(\tau)\|_{\boldsymbol{C}(\tau)})}{(t-\tau)^\alpha}\dot{\boldsymbol{Q}}(\tau)\mathrm{d}\tau \\
&= \Phi_\mathrm{f}(t)\mu\,\boldsymbol{K}^{-1}(t)\boldsymbol{Q}_\mathrm{D}(t).
\end{aligned} \tag{54}$$

Before proceeding, the following two remarks are in order:

*Remark 2.* Equations (53) and (54) constitute a generalization of the fractional Cattaneo equation that, for the case of rigid media, is formulated in terms of the Caputo fractional derivative of order $\alpha$ of $\boldsymbol{q}$, since the Truesdell rate of $\boldsymbol{q}$ equals the time derivative of $\boldsymbol{q}$ (see Equation (51)). Indeed, if deformation were absent, if $\mathfrak{a}$ were identically null (Darcian case), and if the quantities $\phi_\mathrm{f}$, $\mu$, and $\boldsymbol{k} = k_\mathrm{iso}\boldsymbol{\eta}^{-1}$ were all constant in time, then Equation (53) would reduce to

$$\boldsymbol{q}(t) + \frac{\alpha\,t_\mathrm{c}^\alpha}{\Gamma(1-\alpha)}\int_{t_\mathrm{in}}^{t}\frac{\dot{\boldsymbol{q}}(\tau)}{(t-\tau)^\alpha}\mathrm{d}\tau = \boldsymbol{q}_\mathrm{D}(t). \tag{55}$$

Although many generalizations to Cattaneo's model can be found in the literature on Fractional Calculus, it should be emphasized that the majority of them works well in the regime of infinitesimal deformations[47,54,111,112]. Indeed, when the deformations have to be regarded as finite, relationships of the type provided in Equation (55) are not objective because of the presence of the time derivative of $\boldsymbol{q}$ featuring inside the integral. To avoid this problem, we take advantage of the property of $\boldsymbol{q}$ of being a pseudo-vector and, consequently, we have recourse to the most natural way to describe its time evolution, i.e., to its Truesdell rate[110,113]. Due to this choice, the backward Piola transformation of Equation (53) to the medium's reference placement yields Equation (54), which features the time derivative of the material filtration velocity $\boldsymbol{Q}$. In this case, because of the presence of the deformation, Cattaneo equation is not directly recovered under the sole assumptions that $\mathfrak{a}$ is null and that $\phi_{\mathrm{f}}$, $\mu$, and $\boldsymbol{k}$ are constant in time.

In the case of *"unconditionally isotropic"*[33] porous medium, the resistivity tensor given in Equation (31) reads

$$\boldsymbol{R}_{\mathrm{F}}(\|\boldsymbol{Q}\|_{\boldsymbol{C}}) = \frac{\Phi_{\mathrm{f}}\mu}{\kappa_{\mathrm{iso}}}[1 + \mathcal{A}_{\mathrm{iso}}\|\boldsymbol{Q}\|_{\boldsymbol{C}}]\boldsymbol{C} = \mathcal{R}_{\mathrm{F}}(\boldsymbol{F}, \boldsymbol{Q})\boldsymbol{C}, \tag{56}$$

where $\mathcal{A}_{\mathrm{iso}}$ is defined in Equation (40), and $\mathcal{R}_{\mathrm{F}}(\boldsymbol{F}, \boldsymbol{Q})$ is a *scalar resistivity coefficient* defined by

$$\mathcal{R}_{\mathrm{F}}(\boldsymbol{F}, \boldsymbol{Q}) := \frac{\Phi_{\mathrm{f}}\mu}{\kappa_{\mathrm{iso}}}[1 + \mathcal{A}_{\mathrm{iso}}\|\boldsymbol{Q}\|_{\boldsymbol{C}}]. \tag{57}$$

Therefore, after some algebraic passages, Equation (54) becomes

$$\begin{aligned}&\mathcal{R}_{\mathrm{F}}(\boldsymbol{F}(t), \boldsymbol{Q}(t))\boldsymbol{Q}(t) + \frac{\alpha\, t_{\mathrm{c}}^{\alpha}}{\Gamma(1-\alpha)} \int_{t_{\mathrm{in}}}^{t} \frac{J(t)}{J(\tau)} \frac{\mathcal{R}_{\mathrm{F}}(\boldsymbol{F}(\tau), \boldsymbol{Q}(\tau))}{(t-\tau)^{\alpha}} \boldsymbol{F}^{-1}(t)\boldsymbol{F}(\tau)\dot{\boldsymbol{Q}}(\tau)\mathrm{d}\tau \\ &= \mathcal{R}_{\mathrm{D}}(\boldsymbol{F}(t))\boldsymbol{Q}_{\mathrm{D}}(t),\end{aligned} \tag{58}$$

with $\mathcal{R}_{\mathrm{D}}(\boldsymbol{F}) := \Phi_{\mathrm{f}}\mu/\kappa_{\mathrm{iso}}$, and $\mathcal{R}_{\mathrm{D}}$ depending on $\boldsymbol{F}$ being through $\Phi_{\mathrm{f}}$ and $\kappa_{\mathrm{iso}}$.

In conclusion, for the fractional version of Forchheimer's correction analyzed in this section, the model equations to be solved are given by

$$\mathrm{Div}(-JP\boldsymbol{F}^{-\mathrm{T}} + \boldsymbol{T}_{\mathrm{sc}}) = \boldsymbol{0}, \tag{59a}$$

$$\dot{J} + \mathrm{Div}\boldsymbol{Q} = 0, \tag{59b}$$

$$\begin{aligned}&\mathcal{R}_{\mathrm{F}}(\boldsymbol{F}(t), \boldsymbol{Q}(t))\frac{1}{J(t)}\boldsymbol{F}(t)\boldsymbol{Q}(t) + \frac{\alpha\, t_{\mathrm{c}}^{\alpha}}{\Gamma(1-\alpha)} \int_{t_{\mathrm{in}}}^{t} \frac{\mathcal{R}_{\mathrm{F}}(\boldsymbol{F}(\tau), \boldsymbol{Q}(\tau))}{(t-\tau)^{\alpha}} \frac{1}{J(\tau)}\boldsymbol{F}(\tau)\dot{\boldsymbol{Q}}(\tau)\mathrm{d}\tau \\ &= \mathcal{R}_{\mathrm{D}}(\boldsymbol{F}(t))\frac{1}{J(t)}\boldsymbol{F}(t)\boldsymbol{Q}_{\mathrm{D}}(t).\end{aligned} \tag{59c}$$

Equations (59a)-(59c) are equivalent to a set of seven scalar equations in the seven unknowns represented by the three components of the solid phase motion $\chi$, pore pressure $P$ (which features both in the momentum balance law (59a) and in Darcy's velocity $\boldsymbol{Q}_{\mathrm{D}}$, as specified in Equation (21)), and the three components of filtration velocity $\boldsymbol{Q}$. Thus, to close the model, it suffices to assign the solid phase volumetric fraction in the reference placement, i.e., $\Phi_{\mathrm{s}}$, which is independent of time in the present study, and to prescribe constitutively the first Piola-Kirchhoff stress tensor of the solid phase, i.e., $\boldsymbol{T}_{\mathrm{sc}}$, the scalar permeability $\kappa_{\mathrm{iso}}$, and either the coefficient $c_0$ or the trial friction factor $f_{\mathrm{trial}}$.

## 6 Numerical implementation of the model equations

In this section, we introduce the most fundamental aspects of the determination of the numerical solution of the fractional Darcy-Forchheimer's model (59a)-(59c). We split our study into two parts: first, we concentrate on the discretization in time of Equation (59c) and, subsequently, we present the main introductory steps to the finite element implementation of the whole system (59a)-(59c).

### 6.1 Time discretization of the fractional Darcy-Forchheimer model

The starting point for the numerical implementation of Equation (58) is the identity

$$\frac{1}{\Gamma(1-\alpha)}\int_{t_{\mathrm{in}}}^{t}\frac{1}{(t-\tau)^{\alpha}}\boldsymbol{h}(\tau)\mathrm{d}\tau \underbrace{=}_{1-\alpha=\beta} \frac{1}{\Gamma(\beta)}\int_{t_{\mathrm{in}}}^{t}\frac{1}{(t-\tau)^{1-\beta}}\boldsymbol{h}(\tau)\mathrm{d}\tau, \tag{60}$$

which is valid for any scalar- or tensor-valued function $\boldsymbol{h}$ for which the considered integrals exist. By direct inspection of Equation (59c), the function $\boldsymbol{h}$ is identified with the expression

$$\boldsymbol{h}(\tau) \equiv \mathcal{R}_{\mathrm{F}}(\boldsymbol{F}(\tau),\boldsymbol{Q}(\tau))\frac{1}{J(\tau)}\boldsymbol{F}(\tau)\dot{\boldsymbol{Q}}(\tau), \tag{61}$$

with $\mathcal{R}_{\mathrm{F}}(\boldsymbol{F},\boldsymbol{Q})$ given in Equation (57).

The next step is the representation of the fractional operator featuring in Equation (59c) in the form suggested by Podlubny [114] for the numerical approximation of the Grünwald-Letnikov fractional derivative, which, for our purposes, we slightly modify as follows:

$$\begin{aligned}\frac{1}{\Gamma(\beta)}\int_{t_{\mathrm{in}}}^{t}(t-\tau)^{\beta-1}\boldsymbol{h}(\tau)\mathrm{d}\tau &= \lim_{N\to\infty}\left(\frac{t-t_{\mathrm{in}}}{N}\right)^{\beta}\sum_{n=0}^{N}\begin{bmatrix}\beta\\ n\end{bmatrix}\boldsymbol{h}\left(t-n\,\frac{t-t_{\mathrm{in}}}{N}\right)\\ &\approx \left(\frac{t-t_{\mathrm{in}}}{N_0}\right)^{\beta}\sum_{n=0}^{N_0}\begin{bmatrix}\beta\\ n\end{bmatrix}\boldsymbol{h}\left(t-n\,\frac{t-t_{\mathrm{in}}}{N_0}\right),\end{aligned} \tag{62}$$

where $\boldsymbol{h}$ is assumed to be continuous over the interval $[t_{\mathrm{in}},t]$, $N\in\mathbb{N}$ is the number of sub-intervals partitioning $t-t_{\mathrm{in}}$, $N_0\in\mathbb{N}$ is a sufficiently large value of $N$ above which the value of the sum in the limit does not change appreciably within a given tolerance, and the symbol

$$\begin{bmatrix}\beta\\ 0\end{bmatrix}=1 \qquad\text{and}\qquad \begin{bmatrix}\beta\\ n\end{bmatrix}=\frac{\prod_{i=1}^{n}(\beta+i-1)}{n!},\quad \text{for } n\geq 1, \tag{63}$$

generalizes the binomial factor to the case in which $\beta$ is not a natural number (see [114]).

To proceed, we discretize the time interval $[t_{\mathrm{in}},t_{\mathrm{fin}}]$ over which the system is observed by defining the time grid $\mathscr{T} := \{t_0,\dots,t_m,\dots,t_M\}\subseteq[t_{\mathrm{in}},t_{\mathrm{fin}}]$, so that $t_0\equiv t_{\mathrm{in}}$, $t_M\equiv t_{\mathrm{fin}}$, with $M\in\mathbb{N}$, $M\geq 1$, and $m=0,\dots,M$. We notice that, in our simulations, the value of $N_0$ that truncates the series defining the Riemann-Liouville fractional integral of $\boldsymbol{h}$, as specified in Equation (62), will be taken as a function of the instant of time at which the corresponding sum is evaluated. In particular, in this work, at each $t_m\in\mathscr{T}$, we define $\hat{N}_0(t_m)$ in such a way that the ratio $s_m := (t_m-t_0)/\hat{N}_0(t_m)$ is equal to the constant time step

$\Delta t$ used for updating the time dependence of the functions featuring in Equation (62). Then, we introduce the auxiliary notation

$$s_m = \frac{t_m - t_0}{\hat{N}_0(t_m)}, \qquad (s_m \equiv \Delta t \equiv t_m - t_{m-1} =: \Delta t_m, \text{in these simulations, for } m \geq 1 \text{ and } n \geq 1), \tag{64a}$$

$$\dot{\boldsymbol{Q}}_{\mathrm{app}}(t_m - ns_m) := \frac{\boldsymbol{Q}(t_m - n\, s_m) - \boldsymbol{Q}(t_{m-1} - n\, s_{m-1})}{\Delta t_m}, \qquad m \geq 1, \quad n = 0, \dots, \hat{N}_0(t_m), \tag{64b}$$

with $\Delta t_m := t_m - t_{m-1} > 0$ to indicate the integration step for the approximation of the integral in Equation (62), and to approximate the time derivative of $\boldsymbol{Q}$. Note that we need an approximation of $\dot{\boldsymbol{Q}}$, here supplied by $\dot{\boldsymbol{Q}}_{\mathrm{app}}$, in order to be able to handle numerically the time derivative defining $\boldsymbol{h}(\tau)$ in Equation (60).

For a given value of $n = 0, \dots, N_0 \equiv \hat{N}_0(t_m)$, we recast the approximated counterpart of the second term on the left-hand side of Equation (58) at $t = t_m$ as

$$\begin{aligned}
&\frac{\alpha\, t_{\mathrm{c}}^{\alpha}}{\Gamma(1-\alpha)} \int_{t_0}^{t_m} \frac{1}{(t_m - \tau)^{\alpha}} \frac{\mathcal{R}_{\mathrm{F}}(\boldsymbol{F}(\tau), \boldsymbol{Q}(\tau))}{J(\tau)} \boldsymbol{F}(\tau) \dot{\boldsymbol{Q}}(\tau) \mathrm{d}\tau \\
&\approx \alpha\, t_{\mathrm{c}}^{\alpha} s_m^{1-\alpha} \sum_{n=0}^{\hat{N}_0(t_m)} \begin{bmatrix} 1-\alpha \\ n \end{bmatrix} \frac{\mathcal{R}_{\mathrm{F}}(\boldsymbol{F}(t_m - ns_m), \boldsymbol{Q}(t_m - ns_m))}{J(t_m - ns_m)}\, \boldsymbol{F}(t_m - ns_m) \dot{\boldsymbol{Q}}_{\mathrm{app}}(t_m - ns_m) \\
&= \alpha\, t_{\mathrm{c}}^{\alpha} s_m^{1-\alpha} \frac{\mathcal{R}_{\mathrm{F}}(\boldsymbol{F}(t_m), \boldsymbol{Q}(t_m))}{J(t_m)}\, \boldsymbol{F}(t_m) \dot{\boldsymbol{Q}}_{\mathrm{app}}(t_m) \\
&\quad + \alpha\, t_{\mathrm{c}}^{\alpha} s_m^{1-\alpha} \sum_{n=1}^{\hat{N}_0(t_m)} \begin{bmatrix} 1-\alpha \\ n \end{bmatrix} \frac{\mathcal{R}_{\mathrm{F}}(\boldsymbol{F}(t_m - ns_m), \boldsymbol{Q}(t_m - ns_m))}{J(t_m - ns_m)}\, \boldsymbol{F}(t_m - ns_m) \dot{\boldsymbol{Q}}_{\mathrm{app}}(t_m - ns_m) \\
&=: \alpha\, t_{\mathrm{c}}^{\alpha} s_m^{1-\alpha} \frac{\mathcal{R}_{\mathrm{F}}(\boldsymbol{F}(t_m), \boldsymbol{Q}(t_m))}{J(t_m)}\, \boldsymbol{F}(t_m) \dot{\boldsymbol{Q}}_{\mathrm{app}}(t_m) + \alpha\, t_{\mathrm{c}}^{\alpha} \boldsymbol{\mathcal{F}}_{\alpha}(t_m),
\end{aligned} \tag{65}$$

where $1 \leq m \leq M$, and $\boldsymbol{\mathcal{F}}_{\alpha}(t_m)$ is defined by the sum

$$\boldsymbol{\mathcal{F}}_{\alpha}(t_m) := s_m^{1-\alpha} \sum_{n=1}^{\hat{N}_0(t_m)} \begin{bmatrix} 1-\alpha \\ n \end{bmatrix} \frac{\mathcal{R}_{\mathrm{F}}(\boldsymbol{F}(t_m - ns_m), \boldsymbol{Q}(t_m - ns_m))}{J(t_m - ns_m)}\, \boldsymbol{F}(t_m - ns_m) \dot{\boldsymbol{Q}}_{\mathrm{app}}(t_m - ns_m). \tag{66}$$

In conclusion, by collecting the results obtained so far, the time discretized form of Equation (58) reads:

$$\begin{aligned}
&\mathcal{R}_{\mathrm{F}}(\boldsymbol{F}(t_m), \boldsymbol{Q}(t_m)) \boldsymbol{Q}(t_m) + \alpha\, t_{\mathrm{c}}^{\alpha} s_m^{1-\alpha} \mathcal{R}_{\mathrm{F}}(\boldsymbol{F}(t_m), \boldsymbol{Q}(t_m))\, \dot{\boldsymbol{Q}}_{\mathrm{app}}(t_m) + \alpha\, t_{\mathrm{c}}^{\alpha} J(t_m) \boldsymbol{F}^{-1}(t_m) \boldsymbol{\mathcal{F}}_{\alpha}(t_m) \\
&= \mathcal{R}_{\mathrm{D}}(\boldsymbol{F}(t_m)) \boldsymbol{Q}_{\mathrm{D}}(t_m).
\end{aligned} \tag{67}$$

Moreover, to single out the unknown to be determined through the solution of Equation (67), i.e., $\boldsymbol{Q}(t_m)$, and in view of the linearization procedure that will be employed for the finite element simulations performed in the sequel, we take into account the expression of $\dot{\boldsymbol{Q}}_{\mathrm{app}}$ in Equation (64b), we highlight the dependence of $\boldsymbol{Q}_{\mathrm{D}}$ on $\boldsymbol{F}$ and $\mathrm{Grad}P$ by writing $\boldsymbol{Q}_{\mathrm{D}} = \boldsymbol{\mathcal{G}}^{\boldsymbol{Q}_{\mathrm{D}}}(\boldsymbol{F}, \mathrm{Grad}P)$, and we recast Equation (67) as

$$\boldsymbol{\mathcal{Z}}(\boldsymbol{F}_m, \mathrm{Grad}P_m, \boldsymbol{Q}_m) := \left(1 + \frac{\alpha t_{\mathrm{c}}^{\alpha} s_m^{1-\alpha}}{\Delta t_m}\right) \mathcal{R}_{\mathrm{F}}(\boldsymbol{F}_m, \boldsymbol{Q}_m) \boldsymbol{Q}_m - \frac{\alpha t_{\mathrm{c}}^{\alpha} s_m^{1-\alpha}}{\Delta t_m} \mathcal{R}_{\mathrm{F}}(\boldsymbol{F}_m, \boldsymbol{Q}_m) \boldsymbol{Q}_{m-1}$$

$$+\alpha t_{\mathrm{c}}^{\alpha} J_m \boldsymbol{F}_m^{-1} \boldsymbol{\mathcal{F}}_{\alpha}(t_m) - \mathcal{R}_{\mathrm{D}}(\boldsymbol{F}_m) \boldsymbol{\mathcal{G}}^{\boldsymbol{Q}_{\mathrm{D}}}(\boldsymbol{F}_m, \mathrm{Grad} P_m) = \boldsymbol{0}, \tag{68}$$

where, for any generic physical quantity $\Psi$, the notation $\Psi(t_m) \equiv \Psi_m$ has been employed to express that it is evaluated at time $t_m$ (the dependence on $X$ is omitted, but understood).

We remark that, by performing some lengthy algebraic manipulations, Equation (68) can be solved analytically for $\boldsymbol{Q}_m$ by turning it into a polynomial equation of grade four in $\boldsymbol{Q}_m$. This property descends from the dependence of $\mathcal{R}_{\mathrm{F}}(\boldsymbol{F}_m, \boldsymbol{Q}_m)$ on $\boldsymbol{Q}_m$ being through the $\boldsymbol{C}_m$-norm $||\boldsymbol{Q}_m||_{\boldsymbol{C}_m}$. However, although the four roots of an equation of this type can be computed analytically, it is very difficult to ascertain, for generic values of $\boldsymbol{F}_m$ and $\mathrm{Grad}P_m$, which solutions are physically admissible. Moreover, if more than one physically admissible solutions exist, the problem of non-uniqueness of the solution arises, and, even in the case in which the solution were unique, its analytical expression would be too complicated to study it in conjunction with the other two equations of the model. For all these reasons, we prefer to proceed with the search for a unique numeric solution, to be found through a Newton-Raphson method around a "good" initial guess. These considerations lead us to the adoption of the following procedure.

## 6.2 Linearization of the fractional Darcy-Forchheimer model

The discretized, fractional Darcy-Forchheimer equation (68) should be studied in conjunction with the discretized version of the balance laws (59a) and (59b), put in weak form in view of their finite element implementation. In this respect, we notice that we have conducted the numerical simulations of our work in ABAQUS®, partially writing our own code for solving Equations (59a), (59b) and (68), but not for the whole implementation. Thus, although we do not have complete control over the numerical procedures employed by the commercial software, some properties of Equations (59a), (59b), and (68) can be discussed, even without entering the details of their numerical analysis.

As anticipated above, we neglect gravity, and to render the weak forms of Equations (59a) and (59b) as simple as possible, we consider the case in which their associated boundary terms are identically zero. To comply with these conditions, we partition the boundary of $\mathscr{B}$, for the motion $\chi$, into the disjoint union of a traction-free part and Dirichlet part, and, for the pressure $P$, into the disjoint union of a flux-free part and, again, of a Dirichlet part. Then, within this setting, we take the procedure adopted in[97] for the purely Darcian, hyperelastic, and isotropic case, and extended in[115] for poroplasticity, and in[27] for anisotropic, fiber-reinforced porous media. In the sequel, we show the most fundamental steps of its generalization to our model, which, although being isotropic and hyperelastic, takes into account Forchheimer's correction to Darcy's law and the interactions between the fluid and the solid phase arising because of such correction.

To begin with, we consider a three-field formulation of the problem at hand, which involves Equation (68) and the time-discrete, weak forms of Equations (59a) and (59b). This leads to the system

$$A(\chi_m, P_m, \boldsymbol{Q}_m; \boldsymbol{V}_{\mathrm{v}}) := \int_{\mathscr{B}} \left\{ -J_m P_m \boldsymbol{F}_m^{-\mathrm{T}} + \boldsymbol{\mathcal{G}}^{\boldsymbol{T}_{\mathrm{sc}}}(\boldsymbol{F}_m) \right\} : \mathrm{Grad} \boldsymbol{V}_{\mathrm{v}} - \int_{\partial_{\mathrm{N}}^{\chi} \mathscr{B}} (\boldsymbol{T}_{\mathrm{Im}} \boldsymbol{N}) \boldsymbol{V}_{\mathrm{v}} = 0, \tag{69a}$$

$$B(\chi_m, P_m, \boldsymbol{Q}_m; P_{\mathrm{v}}) := -\int_{\mathscr{B}} \frac{J_m - J_{m-1}}{\Delta t_m} P_{\mathrm{v}} + \int_{\mathscr{B}} \boldsymbol{Q}_m \mathrm{Grad} P_{\mathrm{v}} - \int_{\partial_{\mathrm{N}}^{P} \mathscr{B}} (\boldsymbol{Q}_m \boldsymbol{N}) P_{\mathrm{v}} = 0, \tag{69b}$$

$$\begin{aligned} \boldsymbol{\mathcal{Z}}(\boldsymbol{F}_m, \mathrm{Grad}P_m, \boldsymbol{Q}_m) := {} & \left(1 + \frac{\alpha t_{\mathrm{c}}^{\alpha} s_m^{1-\alpha}}{\Delta t_m}\right) \mathcal{R}_{\mathrm{F}}(\boldsymbol{F}_m, \boldsymbol{Q}_m) \boldsymbol{Q}_m - \frac{\alpha t_{\mathrm{c}}^{\alpha} s_m^{1-\alpha}}{\Delta t_m} \mathcal{R}_{\mathrm{F}}(\boldsymbol{F}_m, \boldsymbol{Q}_m) \boldsymbol{Q}_{m-1} \\ & + \alpha t_{\mathrm{c}}^{\alpha} J_m \boldsymbol{F}_m^{-1} \boldsymbol{\mathcal{F}}_{\alpha}(t_m) - \mathcal{R}_{\mathrm{D}}(\boldsymbol{F}_m) \boldsymbol{\mathcal{G}}^{\boldsymbol{Q}_{\mathrm{D}}}(\boldsymbol{F}_m, \mathrm{Grad} P_m) = \boldsymbol{0}, \end{aligned} \tag{69c}$$

in the unknowns $\chi_m$, $P_m$, and $\boldsymbol{Q}_m$. To obtain Equations (69a) and (69b), we have introduced: the test functions $\boldsymbol{V}_{\mathrm{v}}$ and $P_{\mathrm{v}}$, identifiable with an arbitrary virtual velocity and an arbitrary virtual pressure, respectively; the constitutive representation $\boldsymbol{\mathcal{G}}^{\boldsymbol{T}_{\mathrm{sc}}}(\boldsymbol{F}_m) \equiv \boldsymbol{T}_{\mathrm{sc}}(t_m)$, at time $t_m$, of the first Piola-Kirchhoff stress tensor of the solid phase; the portions $\partial_{\mathrm{N}}^{\chi}\mathscr{B}$ and $\partial_{\mathrm{N}}^{P}\mathscr{B}$ of the boundary of $\mathscr{B}$, i.e., $\partial\mathscr{B}$, on which Neumann boundary conditions on the solid phase motion and on the pressure field are enforced, respectively; and the field of co-normals $\boldsymbol{N}$ associated with the boundary of $\mathscr{B}$. We remark that, although we have reported the boundary terms in Equations (69a) and (69b), these are identically null in our setting.

The system (69a)-(69c) is highly non-linear in the motion $\chi_m$ and in the filtration velocity $\boldsymbol{Q}_m$, and it will be solved by employing a linearization procedure. One possible way is to perform, for each time $t_m$, a Newton-Raphson method in a neighborhood of an initially *guessed* triple $(\chi_m^0, P_m^0, \boldsymbol{Q}_m^0)$, with unknown increments $(\delta\chi_m^1, \delta P_m^1, \delta\boldsymbol{Q}_m^1)$, and then, by iteration, to construct the sequence of triples

$$(\chi_m^k = \chi_m^{k-1} + \delta\chi_m^k, P_m^k = P_m^{k-1} + \delta P_m^k, \boldsymbol{Q}_m^k = \boldsymbol{Q}_m^{k-1} + \delta\boldsymbol{Q}_m^k), \quad \text{for } k \geq 1. \tag{70}$$

At each time $t_m$ and iteration $k \geq 1$, such a method requires the determination of the three increments $\delta\chi_m^k$, $\delta P_m^k$, and $\delta\boldsymbol{Q}_m^k$, for each of which it is necessary to provide a suitable spatial interpolation. However, rather than proceeding this way, we find it more convenient to follow a different path, as explained below.

*Two-field-approach by means of Dini's implicit function Theorem.* We notice that, for $m \geq 1$, there exists a non-empty open set $\Omega_m$ of triples

$$(\boldsymbol{F}_m, \mathrm{Grad}P_m, \boldsymbol{Q}_m) \in [T\mathscr{B}_t \otimes T^*\mathscr{B}] \times T^*\mathscr{B} \times T\mathscr{B}, \qquad \text{with } \boldsymbol{Q}_m \neq \boldsymbol{0}, \tag{71}$$

such that the function $\boldsymbol{\mathcal{Z}}$ defined by the right-hand side of Equation (69c) is of class $C^1(\Omega_m; T\mathscr{B})$. Then, we assume that there exists a non-empty subset of $\Omega_m$, hereafter denoted by $\Sigma_m \subset \Omega_m$, that consists of all the triples $(\boldsymbol{F}_m, \mathrm{Grad}P_m, \boldsymbol{Q}_m) \in \Omega_m$ that satisfy Equation (69c) as an identity, i.e., that constitute the intersection between $\Omega_m$ and the set of all the solutions of $\boldsymbol{\mathcal{Z}}(\boldsymbol{F}_m, \mathrm{Grad}P_m, \boldsymbol{Q}_m) = \boldsymbol{0}$, and for which the partial derivative of $\boldsymbol{\mathcal{Z}}$ with respect to $\boldsymbol{Q}_m$ is a non-singular second-order tensor. Hence, by setting $(\sharp) := (\boldsymbol{F}_m, \mathrm{Grad}P_m, \boldsymbol{Q}_m)$, it holds by hypothesis that $\det[\partial_{\boldsymbol{Q}_m}\boldsymbol{\mathcal{Z}}(\sharp)] \neq 0$ for all $(\boldsymbol{F}_m, \mathrm{Grad}P_m, \boldsymbol{Q}_m) \in \Sigma_m$, and $\partial_{\boldsymbol{Q}_m}\boldsymbol{\mathcal{Z}}(\sharp)$ is given by

$$\begin{aligned} \partial_{\boldsymbol{Q}_m}\boldsymbol{\mathcal{Z}}(\sharp) &= \mathcal{R}_{\mathrm{F}}(\boldsymbol{F}_m, \boldsymbol{Q}_m)\left[1 + \frac{\alpha t_{\mathrm{c}}^{\alpha} s_m^{1-\alpha}}{\Delta t_m}\right]\boldsymbol{I} + \left\{\boldsymbol{Q}_m + \frac{\alpha t_{\mathrm{c}}^{\alpha} s_m^{1-\alpha}}{\Delta t_m}[\boldsymbol{Q}_m - \boldsymbol{Q}_{m-1}]\right\} \otimes \frac{\partial\mathcal{R}_{\mathrm{F}}}{\partial\boldsymbol{Q}_m}(\boldsymbol{F}_m, \boldsymbol{Q}_m) \\ &= \mathcal{R}_{\mathrm{F}}(\boldsymbol{F}_m, \boldsymbol{Q}_m)\left[1 + \frac{\alpha t_{\mathrm{c}}^{\alpha} s_m}{s_m^{\alpha}\Delta t_m}\right]\boldsymbol{I} + \frac{\Phi_{\mathrm{f}m}\mu}{\kappa_{\mathrm{iso}m}}\mathcal{A}_{\mathrm{iso}m}\left\{\boldsymbol{Q}_m + \frac{\alpha t_{\mathrm{c}}^{\alpha} s_m}{s_m^{\alpha}\Delta t_m}[\boldsymbol{Q}_m - \boldsymbol{Q}_{m-1}]\right\} \otimes \frac{J_m^{-2}\boldsymbol{C}_m\boldsymbol{Q}_m}{\|\boldsymbol{Q}_m\|_{\boldsymbol{C}_m}}, \end{aligned} \tag{72}$$

where $\Phi_{\mathrm{f}m} \equiv J_m - \Phi_{\mathrm{sR}}$ is the pull-back of the fluid phase volumetric fraction evaluated at time $t_m$, while $\kappa_{\mathrm{iso}m}$ and $\mathcal{A}_{\mathrm{iso}m}$ denote $\kappa_{\mathrm{iso}}$ and $\mathcal{A}_{\mathrm{iso}}$ at time $t_m$.

In fact, all the properties of $\boldsymbol{\mathcal{Z}}$ and of $\partial_{\boldsymbol{Q}_m}\boldsymbol{\mathcal{Z}}$ enunciated so far constitute the hypotheses of Dini's Implicit Function Theorem for vector-valued functions of multiple arguments. Therefore, by selecting one triple $(\bar{\sharp}) \equiv (\bar{\boldsymbol{F}}_m, \mathrm{Grad}\bar{P}_m, \bar{\boldsymbol{Q}}_m) \in \Sigma_m$ (for which, thus, $\boldsymbol{\mathcal{Z}}(\bar{\sharp}) = \boldsymbol{0}$, and $\det[\partial_{\boldsymbol{Q}_m}\boldsymbol{\mathcal{Z}}(\bar{\sharp})] \neq 0$), there exists a neighborhood $\mathscr{V}(\bar{\boldsymbol{F}}_m, \mathrm{Grad}\bar{P}_m, \bar{\boldsymbol{Q}}_m) \subset \Omega_m$ of such triple such that, for the elements of the intersection $\mathscr{V}(\bar{\boldsymbol{F}}_m, \mathrm{Grad}\bar{P}_m, \bar{\boldsymbol{Q}}_m) \cap \Sigma_m \neq \emptyset$ it is possible to express $\boldsymbol{Q}_m$ as a function of $\boldsymbol{F}_m$ and $\mathrm{Grad}\, P_m$ for some neighborhood $\mathscr{U}(\bar{\boldsymbol{F}}_m, \mathrm{Grad}\bar{P}_m) \subset [T\mathscr{B}_t \otimes T^*\mathscr{B}] \times T^*\mathscr{B}$ of the pair $(\bar{\boldsymbol{F}}_m, \mathrm{Grad}\bar{P}_m)$. By denoting this vector-valued function by

$$\boldsymbol{\mathcal{G}}^{\boldsymbol{Q}_m} : \mathscr{U}(\bar{\boldsymbol{F}}_m, \mathrm{Grad}\bar{P}_m) \to T\mathscr{B}, \qquad (\boldsymbol{F}_m, \mathrm{Grad}\, P_m) \mapsto \boldsymbol{\mathcal{G}}^{\boldsymbol{Q}_m}(\boldsymbol{F}_m, \mathrm{Grad}\, P_m) = \boldsymbol{Q}_m, \tag{73}$$

Equation (69c) is identically satisfied by replacing $\boldsymbol{Q}_m$ with $\boldsymbol{\mathcal{G}}^{\boldsymbol{Q}_m}(\boldsymbol{F}_m, \mathrm{Grad}\, P_m)$, thereby obtaining

$$\hat{\boldsymbol{\mathcal{Z}}}(\boldsymbol{F}_m, \mathrm{Grad} P_m) \equiv \boldsymbol{\mathcal{Z}}(\boldsymbol{F}_m, \mathrm{Grad} P_m, \boldsymbol{\mathcal{G}}^{\boldsymbol{Q}_m}(\boldsymbol{F}_m, \mathrm{Grad}\, P_m)) = \boldsymbol{0}, \tag{74}$$

for all $(\boldsymbol{F}_m, \mathrm{Grad}\, P_m) \in \mathscr{U}(\bar{\boldsymbol{F}}_m, \mathrm{Grad}\bar{P}_m)$. Hence, the just defined function $\hat{\boldsymbol{\mathcal{Z}}} : \mathscr{U}(\bar{\boldsymbol{F}}_m, \mathrm{Grad}\bar{P}_m) \to T\mathscr{B}$ is constant in the neighborhood $\mathscr{U}(\bar{\boldsymbol{F}}_m, \mathrm{Grad}\bar{P}_m)$ and, since it also of class $C^1$ therein, it has vanishing differential. In fact, upon setting $\boldsymbol{Y}_m := \mathrm{Grad} P_m$ and $(\natural) := (\boldsymbol{F}_m, \mathrm{Grad} P_m) \equiv (\boldsymbol{F}_m, \boldsymbol{Y}_m) \in \mathscr{U}(\bar{\boldsymbol{F}}_m, \mathrm{Grad}\bar{P}_m)$, from the condition of annihilation of the differential of $\hat{\boldsymbol{\mathcal{Z}}}$ along any pair of admissible increments $(\delta\boldsymbol{F}_m, \delta\boldsymbol{Y}_m)$, we find:

$$\begin{aligned}
\mathrm{d}\hat{\boldsymbol{\mathcal{Z}}}(\natural)(\delta\boldsymbol{F}_m, \delta\boldsymbol{Y}_m) =& [\partial_{\boldsymbol{F}_m}\hat{\boldsymbol{\mathcal{Z}}}(\natural)] : \delta\boldsymbol{F}_m + [\partial_{\boldsymbol{Y}_m}\hat{\boldsymbol{\mathcal{Z}}}(\natural)]\delta\boldsymbol{Y}_m \\
=& [\partial_{\boldsymbol{F}_m}\boldsymbol{\mathcal{Z}}(\sharp)] : \delta\boldsymbol{F}_m + [\partial_{\boldsymbol{Y}_m}\boldsymbol{\mathcal{Z}}(\sharp)]\delta\boldsymbol{Y}_m \\
&+ [\partial_{\boldsymbol{Q}_m}\boldsymbol{\mathcal{Z}}(\sharp)][\partial_{\boldsymbol{F}_m}\boldsymbol{\mathcal{G}}^{\boldsymbol{Q}_m}(\natural)] : \delta\boldsymbol{F}_m + [\partial_{\boldsymbol{Q}_m}\boldsymbol{\mathcal{Z}}(\sharp)][\partial_{\boldsymbol{Y}_m}\boldsymbol{\mathcal{G}}^{\boldsymbol{Q}_m}(\natural)]\delta\boldsymbol{Y}_m \\
=& \left\{\partial_{\boldsymbol{F}_m}\boldsymbol{\mathcal{Z}}(\sharp) + [\partial_{\boldsymbol{Q}_m}\boldsymbol{\mathcal{Z}}(\sharp)][\partial_{\boldsymbol{F}_m}\boldsymbol{\mathcal{G}}^{\boldsymbol{Q}_m}(\natural)]\right\} : \delta\boldsymbol{F}_m \\
&+ \left\{\partial_{\boldsymbol{Y}_m}\boldsymbol{\mathcal{Z}}(\sharp) + [\partial_{\boldsymbol{Q}_m}\boldsymbol{\mathcal{Z}}(\sharp)][\partial_{\boldsymbol{Y}_m}\boldsymbol{\mathcal{G}}^{\boldsymbol{Q}_m}(\natural)]\right\}\delta\boldsymbol{Y}_m = 0.
\end{aligned} \tag{75}$$

Accordingly, the coefficients of $\delta\boldsymbol{F}_m$ and $\delta\boldsymbol{Y}_m$ must vanish independently from one another, i.e.,

$$\partial_{\boldsymbol{F}_m}\boldsymbol{\mathcal{Z}}(\sharp) + [\partial_{\boldsymbol{Q}_m}\boldsymbol{\mathcal{Z}}(\sharp)][\partial_{\boldsymbol{F}_m}\boldsymbol{\mathcal{G}}^{\boldsymbol{Q}_m}(\natural)] = \boldsymbol{O} \quad\Rightarrow\quad \partial_{\boldsymbol{F}_m}\boldsymbol{\mathcal{G}}^{\boldsymbol{Q}_m}(\natural) = -[\partial_{\boldsymbol{Q}_m}\boldsymbol{\mathcal{Z}}(\sharp)]^{-1}\partial_{\boldsymbol{F}_m}\boldsymbol{\mathcal{Z}}(\sharp), \tag{76a}$$

$$\partial_{\boldsymbol{Y}_m}\boldsymbol{\mathcal{Z}}(\sharp) + [\partial_{\boldsymbol{Q}_m}\boldsymbol{\mathcal{Z}}(\sharp)][\partial_{\boldsymbol{Y}_m}\boldsymbol{\mathcal{G}}^{\boldsymbol{Q}_m}(\natural)] = \boldsymbol{0} \quad\Rightarrow\quad \partial_{\boldsymbol{Y}_m}\boldsymbol{\mathcal{G}}^{\boldsymbol{Q}_m}(\natural) = -[\partial_{\boldsymbol{Q}_m}\boldsymbol{\mathcal{Z}}(\sharp)]^{-1}\partial_{\boldsymbol{Y}_m}\boldsymbol{\mathcal{Z}}(\sharp), \tag{76b}$$

where $\boldsymbol{O}$ is the null element in the space of third-order tensors.

The result reported in Equation (73) permits to rephrase the system (69a)-(69c) as a system consisting of its first two equations only, i.e.[27,97,115],

$$\hat{A}(\chi_m, P_m; \boldsymbol{V}_\mathrm{v}) := \int_{\mathscr{B}} \left\{ -J_m P_m \boldsymbol{F}_m^{-\mathrm{T}} + \boldsymbol{\mathcal{G}}^{\boldsymbol{T}_\mathrm{sc}}(\boldsymbol{F}_m)\right\} : \mathrm{Grad}\boldsymbol{V}_\mathrm{v} = 0, \tag{77a}$$

$$\hat{B}(\chi_m, P_m; P_\mathrm{v}) := -\int_{\mathscr{B}} \frac{J_m - J_{m-1}}{\Delta t_m} P_\mathrm{v} + \int_{\mathscr{B}} \boldsymbol{\mathcal{G}}^{\boldsymbol{Q}_m}(\boldsymbol{F}_m, \mathrm{Grad} P_m)\mathrm{Grad} P_\mathrm{v} = 0, \tag{77b}$$

where the functionals $\hat{A}$ and $\hat{B}$ are highly non-linear both in $\chi_m$ and in $P_m$.

*Remark 3.* It is important to remark that the function $\boldsymbol{\mathcal{G}}^{\boldsymbol{Q}_m}$, although it exists, is not determined explicitly, since its determination would constitute a very demanding task. However, it is not necessary to find it in closed form. This is because we are going to solve Equations (77a) and (77b) through a Newton-Raphson linearization procedure, which, to determine the unknown increments of $\chi_m$ and $P_m$ at each iteration, only requires the knowledge of the partial derivatives of $\boldsymbol{\mathcal{G}}^{\boldsymbol{Q}_m}$ at the values of $\boldsymbol{F}_m$ and $\mathrm{Grad}\, P_m$ obtained at the preceding iteration. In this respect, we emphasize that, since an expression of $\boldsymbol{\mathcal{G}}^{\boldsymbol{Q}_m}$ as a function of $\boldsymbol{F}_m$ and $\mathrm{Grad}\, P_m$ is not available, the writing $\hat{B}(\chi_m, P_m; P_\mathrm{v})$ has to be regarded as merely formal. More specifically, it has to be understood as $\hat{B}(\chi_m, P_m; P_\mathrm{v}) \equiv B(\chi_m, P_m, \boldsymbol{Q}_m; P_\mathrm{v})$, in which $\chi_m$ and $P_m$ are the solutions to Equations (77a) and (77b), obtained by means of the procedure just mentioned, while $\boldsymbol{Q}_m$ will be determined separately through an additional Newton-Raphson method applied to Equation (69c), once $\boldsymbol{F}_m$ and $\mathrm{Grad}\, P_m$ are known.

*Newton-Raphson method applied to Equations (77a) and (77b).* To sketch the linearization procedure adopted to solve Equations (77a) and (77b), we set $k \geq 1$, with $k \in \mathbb{N}$, and we introduce both for $\chi_m$ and for $P_m$ the values inherited from the $(k-1)$th iteration, i.e., $\chi_m^{k-1}$ and $P_m^{k-1}$, which are regarded as known, and the *unknown* increments $\delta\chi_m^k$ and $\delta P_m^k$. Hence, we write[27,97,115]

$$\chi_m^k := \chi_m^{k-1} + \delta\chi_m^k \qquad \Rightarrow \qquad \delta \boldsymbol{F}_m^k = \mathrm{Grad}\delta\chi_m^k, \tag{78a}$$

$$P_m^k := P_m^{k-1} + \delta P_m^k \qquad \Rightarrow \qquad \delta \mathrm{Grad} P_m^k = \mathrm{Grad}\delta P_m^k. \tag{78b}$$

Then, to shorten the notation, we define $\mathsf{u}_m^{k-1} := (\chi_m^{k-1}, P_m^{k-1})$ and the *approximated* functionals

$$\hat{A}_{\mathrm{app}}(\delta\chi_m^k, \delta P_m^k; \boldsymbol{V}_{\mathrm{v}}) := \hat{A}(\mathsf{u}_m^{k-1}; \boldsymbol{V}_{\mathrm{v}}) + \mathcal{D}_\chi \hat{A}(\mathsf{u}_m^{k-1}; \boldsymbol{V}_{\mathrm{v}})[\delta\chi_m^k] + \mathcal{D}_P \hat{A}(\mathsf{u}_m^{k-1}; \boldsymbol{V}_{\mathrm{v}})[\delta P_m^k], \tag{79a}$$

$$\hat{B}_{\mathrm{app}}(\delta\chi_m^k, \delta P_m^k; P_{\mathrm{v}}) := \hat{B}(\mathsf{u}_m^{k-1}; P_{\mathrm{v}}) + \mathcal{D}_\chi \hat{B}(\mathsf{u}_m^{k-1}; P_{\mathrm{v}})[\delta\chi_m^k] + \mathcal{D}_P \hat{B}(\mathsf{u}_m^{k-1}; P_{\mathrm{v}})[\delta P_m^k], \tag{79b}$$

where for a generic functional $\hat{L} \in \{\hat{A}, \hat{B}\}$ and a generic virtual field $\psi_{\mathrm{v}} \in \{\boldsymbol{V}_{\mathrm{v}}, P_{\mathrm{v}}\}$, $\mathcal{D}_\chi \hat{L}(\mathsf{u}_m^{k-1}; \psi_{\mathrm{v}})[\delta\chi_m^k]$ and $\mathcal{D}_P \hat{L}(\mathsf{u}_m^{k-1}; \psi_{\mathrm{v}})[\delta P_m^k]$ denote the Gâteaux derivatives of $\hat{L}$ with respect to the motion and pressure, evaluated at $(\mathsf{u}_m^{k-1}, \psi_{\mathrm{v}})$, and computed along the increments $\delta\chi_m^k$ and $\delta P_m^k$, respectively.

Upon enforcing the conditions $\hat{A}_{\mathrm{app}}(\delta\chi_m^k, \delta P_m^k; \boldsymbol{V}_{\mathrm{v}}) = 0$ and $\hat{B}_{\mathrm{app}}(\delta\chi_m^k, \delta P_m^k; P_{\mathrm{v}}) = 0$, the equations determining the increments $\delta\chi_m^k$ and $\delta P_m^k$ at each time $t_m$ and $k$th iteration of Newton's method, for $k \geq 1$, are given by[97,115,116]

$$\mathcal{D}_\chi \hat{A}(\mathsf{u}_m^{k-1}; \boldsymbol{V}_{\mathrm{v}})[\delta\chi_m^k] + \mathcal{D}_P \hat{A}(\mathsf{u}_m^{k-1}; \boldsymbol{V}_{\mathrm{v}})[\delta P_m^k] = -\hat{A}(\mathsf{u}_m^{k-1}; \boldsymbol{V}_{\mathrm{v}}), \tag{80a}$$

$$\mathcal{D}_\chi \hat{B}(\mathsf{u}_m^{k-1}; P_{\mathrm{v}})[\delta\chi_m^k] + \mathcal{D}_P \hat{B}(\mathsf{u}_m^{k-1}; P_{\mathrm{v}})[\delta P_m^k] = -\hat{B}(\mathsf{u}_m^{k-1}; P_{\mathrm{v}}). \tag{80b}$$

As is standard in linearization methods, the iterations stop for some positive integer $k_* \geq 1$ such that, for all $k \geq k_*$, the absolute values $|\hat{A}(\chi_m^k, P_m^k; \boldsymbol{V}_{\mathrm{v}})|$ and $|\hat{B}(\chi_m^k, P_m^k; P_{\mathrm{v}})|$ are smaller than a given tolerance.

Finally, there remains to determine the explicit expressions of the Gâteaux derivatives reported in Equations (80a) and (80b). In fact, the Gâteaux derivatives featuring in Equation (80a) are rather standard, and especially the one evaluated along $\delta\chi_m^k$ can be found in textbooks (see e.g.[98,117]). However, in order to make our work self-contained, we show all the terms of Equations (80a) and (80b). To begin with, we notice that, due to the hypothesis of incompressibility of the solid and fluid phase, the stress tensor featuring in Equation (77a), which we write at time $t_m$ and $k$th iteration as

$$\boldsymbol{T}_{\mathrm{I}m}^k := -J_m^k P_m^k [\boldsymbol{F}_m^k]^{-\mathrm{T}} + \boldsymbol{\mathcal{G}}^{\boldsymbol{T}_{\mathrm{sc}}}(\boldsymbol{F}_m^k), \tag{81}$$

can be obtained by employing the augmented energy density $W_{\mathrm{s}}^{\mathrm{a}}(\boldsymbol{F}_m, P_m) \equiv \Psi_{\mathrm{s}}^{\mathrm{a}}(\boldsymbol{C}_m, P_m)$, with $\Psi_{\mathrm{s}}^{\mathrm{a}}$ given in Equation (13a). Hence, upon writing

$$W_{\mathrm{s}}^{\mathrm{a}}(\boldsymbol{F}_m, P_m) = \tfrac{1}{2}\Phi_{\mathrm{sR}}\mu_{\mathrm{s}}[\mathrm{tr}\boldsymbol{C}_m - 3] - \Phi_{\mathrm{sR}}\mu_{\mathrm{s}} \log J_m + \tfrac{1}{2}\Phi_{\mathrm{sR}}\lambda_{\mathrm{s}}[\log J_m]^2 - [J_m - 1]P_m, \tag{82}$$

where we have highlighted the dependence on $\boldsymbol{F}_m$ (through $\boldsymbol{C}_m$ and $J_m$ on the right-hand side) and $P_m$, it holds that

$$\boldsymbol{T}_{\mathrm{I}m}^k \equiv \boldsymbol{\mathcal{G}}^{\boldsymbol{T}_{\mathrm{I}}}(\boldsymbol{F}_m^k, P_m^k)$$

$$= \frac{\partial W_{\mathrm{s}}^{\mathrm{a}}}{\partial \boldsymbol{F}_m}(\boldsymbol{F}_m^k, P_m^k) = \underbrace{\Phi_{\mathrm{sR}}\mu_{\mathrm{s}}\boldsymbol{\eta}\boldsymbol{F}_m^k\boldsymbol{G}^{-1} - \Phi_{\mathrm{sR}}\mu_{\mathrm{s}}[\boldsymbol{F}_m^k]^{-\mathrm{T}} + \Phi_{\mathrm{sR}}\lambda_{\mathrm{s}}[\log J_m^k][\boldsymbol{F}_m^k]^{-\mathrm{T}}}_{\equiv \boldsymbol{\mathcal{G}}^{\boldsymbol{T}_{\mathrm{sc}}}(\boldsymbol{F}_m)} - J_m^k P_m^k[\boldsymbol{F}_m^k]^{-\mathrm{T}}, \tag{83}$$

where $\boldsymbol{G}$ is the material metric tensor. Accordingly, the Gâteaux derivatives $\mathcal{D}_\chi \hat{A}(\mathsf{u}_m^{k-1}; \boldsymbol{V}_{\mathrm{v}})[\delta\chi_m^k]$ and $\mathcal{D}_P \hat{A}(\mathsf{u}_m^{k-1}; \boldsymbol{V}_{\mathrm{v}})[\delta P_m^k]$ are given by

$$\mathcal{D}_\chi \hat{A}(\mathsf{u}_m^{k-1}; \boldsymbol{V}_{\mathrm{v}})[\delta\chi_m^k] = \int_{\mathscr{B}} \left[\frac{\partial^2 W_{\mathrm{s}}^{\mathrm{a}}}{\partial \boldsymbol{F}_m^2}(\boldsymbol{F}_m^{k-1}, P_m^{k-1}) : \mathrm{Grad}\,\delta\chi_m^k\right] : \mathrm{Grad}\boldsymbol{V}_{\mathrm{v}} =: [C_{\chi\chi}]_m^{k-1}(\delta\chi_m^k, \boldsymbol{V}_{\mathrm{v}}), \tag{84a}$$

$$\mathcal{D}_P \hat{A}(\mathsf{u}_m^{k-1}; \boldsymbol{V}_{\mathrm{v}})[\delta P_m^k] = \int_{\mathscr{B}} \left[\frac{\partial^2 W_{\mathrm{s}}^{\mathrm{a}}}{\partial \boldsymbol{F}_m \partial P_m}(\boldsymbol{F}_m^{k-1}, P_m^{k-1})\delta P_m^k\right] : \mathrm{Grad}\boldsymbol{V}_{\mathrm{v}} =: [C_{\chi P}]_m^{k-1}(\delta P_m^k, \boldsymbol{V}_{\mathrm{v}}), \tag{84b}$$

where the notation $[C_{\chi\chi}]_m^{k-1}(\delta\chi_m^k, \boldsymbol{V}_{\mathrm{v}})$ and $[C_{\chi P}]_m^{k-1}(\delta P_m^k, \boldsymbol{V}_{\mathrm{v}})$ is meant to highlight the influence of the motion on itself and the one of the pore pressure on the motion, respectively.

We recognize that the second derivative of $W_{\mathrm{s}}^{\mathrm{a}}$ with respect to $\boldsymbol{F}_m$, hereafter denoted by $\mathbb{A}_{\mathrm{I}m}^{k-1}$, is the (augmented) *algorithmic first elasticity tensor*[117] of the mixture as a whole, while the mixed derivative of $W_{\mathrm{s}}^{\mathrm{a}}$ with respect to $\boldsymbol{F}_m$ and $P_m$ is representative of the presence of the pore pressure, intended as a Lagrange multiplier of the present theory, in the expression of the mixture's internal stress tensor. In explicit form, these derivatives read

$$\frac{\partial^2 W_{\mathrm{s}}^{\mathrm{a}}}{\partial \boldsymbol{F}_m^2}(\boldsymbol{F}_m^{k-1}, P_m^{k-1}) \equiv \mathbb{A}_{\mathrm{I}m}^{k-1} = \boldsymbol{\eta} \,\underline{\otimes}\, \boldsymbol{S}_{\mathrm{I}m}^{k-1} + [\boldsymbol{\eta}\boldsymbol{F}_m^{k-1}]\mathbb{C}_{\mathrm{I}m}^{k-1} : [(\boldsymbol{\eta}\boldsymbol{F}_m^{k-1})^{\mathrm{T}} \,\underline{\otimes}\, \boldsymbol{I}^{\mathrm{T}}], \tag{85a}$$

$$\frac{\partial^2 W_{\mathrm{s}}^{\mathrm{a}}}{\partial \boldsymbol{F}_m \partial P_m}(\boldsymbol{F}_m^{k-1}, P_m^{k-1}) = -J_m^{k-1}[\boldsymbol{F}_m^{k-1}]^{-\mathrm{T}}. \tag{85b}$$

where $\boldsymbol{S}_{\mathrm{I}m}^{k-1} = [\boldsymbol{F}_m^{k-1}]^{-1}\boldsymbol{\eta}^{-1}\boldsymbol{T}_{\mathrm{I}m}^{k-1}$ is the internal part of the mixture's second Piola-Kirchhoff stress tensor, and $\mathbb{C}_{\mathrm{I}m}^{k-1}$ is the elasticity tensor associated with it (i.e., $\mathbb{C}_{\mathrm{I}m}^{k-1}$ consists of the sum of the true elasticity tensor of the solid phase and of the pressure contribution stemming from the hypothesis of incompressibility)

$$\mathbb{C}_{\mathrm{I}m}^{k-1} = 4\frac{\partial^2 \Psi_{\mathrm{s}}^{\mathrm{a}}}{\partial \boldsymbol{C}_m^2}(\boldsymbol{C}_m^{k-1}, P_m^{k-1}). \tag{86a}$$

Note that, in writing the last term of Equation (85a), the minor symmetry of $\mathbb{C}_{\mathrm{I}m}^{k-1}$ in its last pair of indices has been used. More explicitly, for the considered $W_{\mathrm{s}}^{\mathrm{a}}$, the first elasticity tensor is given by

$$\begin{aligned} \mathbb{A}_{\mathrm{I}m}^{k-1} =& \Phi_{\mathrm{sR}}\mu_{\mathrm{s}}\boldsymbol{\eta} \,\underline{\otimes}\, \boldsymbol{G}^{-1} + (\Phi_{\mathrm{sR}}\mu_{\mathrm{s}} - \Phi_{\mathrm{sR}}\lambda_{\mathrm{s}}\log J_m^{k-1} + J_m^{k-1}P_m^{k-1})[\boldsymbol{F}_m^{k-1}]^{-\mathrm{T}} \,\overline{\otimes}\, [\boldsymbol{F}_m^{k-1}]^{-1} \\ &+ (\Phi_{\mathrm{sR}}\lambda_{\mathrm{s}} - J_m^{k-1}P_m^{k-1})[\boldsymbol{F}_m^{k-1}]^{-\mathrm{T}} \otimes [\boldsymbol{F}_m^{k-1}]^{-\mathrm{T}}. \end{aligned} \tag{87}$$

*Remark 4.* In order to comply with the user interface of the "UMAT" subroutine in ABAQUS®, the Gâteaux derivative $\mathcal{D}_\chi \hat{A}(\mathsf{u}_m^{k-1}; \boldsymbol{V}_{\mathrm{v}})[\delta\chi_m^k]$ in Equation (84a) is rephrased in such a way that its integrand is calculated with respect to the symmetrized increment of the deformation rate, defined as $\delta\boldsymbol{d}_m^k := \mathrm{sym}\big(\boldsymbol{\eta}(\mathrm{Grad}\,\delta\chi_m^k)[\boldsymbol{F}_m^{k-1}]^{-1}\big)$, to the updated symmetrized "spatial" gradient of the Eulerian counterpart of $\boldsymbol{V}_{\mathrm{v}}$, which we write as $\boldsymbol{d}_{\mathrm{v}m}^k := \mathrm{sym}\big(\boldsymbol{\eta}(\mathrm{Grad}\,\boldsymbol{V}_{\mathrm{v}})[\boldsymbol{F}_m^{k-1}]^{-1}\big)$, to the increment of the deformation rate $\delta \boldsymbol{l}_m^k := (\mathrm{Grad}\, \delta\chi_m^k)[\boldsymbol{F}_m^{k-1}]^{-1}$, and to the "spatial" gradient of the Eulerian counterpart of $\boldsymbol{V}_{\mathrm{v}}$, which is $\boldsymbol{l}_{\mathrm{v}m}^k := (\mathrm{Grad}\, \boldsymbol{V}_{\mathrm{v}})[\boldsymbol{F}_m^{k-1}]^{-1}$. To this end, we define the push-forward of the elasticity tensor $\mathbb{C}_{\mathrm{I}m}^{k-1}$ featuring in Equation (85a), i.e.,

$$[\mathbbm{c}_{\mathrm{I}m}^{k-1}]^{spqr} := \frac{1}{J_m^{k-1}}[\mathbb{C}_{\mathrm{I}m}^{k-1}]^{SPQR}[\boldsymbol{F}_m^{k-1}]^s{}_S[\boldsymbol{F}_m^{k-1}]^p{}_P[\boldsymbol{F}_m^{k-1}]^q{}_Q[\boldsymbol{F}_m^{k-1}]^r{}_R, \tag{88}$$

and we write the second Piola-Kirchhoff stress tensor as $\boldsymbol{S}_{\mathrm{I}m}^{k-1} = J_m^{k-1}[\boldsymbol{F}_m^{k-1}]^{-1}\boldsymbol{\sigma}_{\mathrm{I}m}^{k-1}[\boldsymbol{F}_m^{k-1}]^{-\mathrm{T}}$. Hence, after some calculations, the *algorithmic elasticity tensor* required by the "UMAT" subroutine is given as[117]

$$\mathbbm{a}_m^{k-1} := \mathbbm{c}_{\mathrm{I}m}^{k-1} + \tfrac{1}{2}\big(\boldsymbol{\eta}^{-1}\underline{\otimes}\,\boldsymbol{\sigma}_{\mathrm{I}m}^{k-1} + \boldsymbol{\eta}^{-1}\overline{\otimes}\,\boldsymbol{\sigma}_{\mathrm{I}m}^{k-1} + \boldsymbol{\sigma}_{\mathrm{I}m}^{k-1}\underline{\otimes}\,\boldsymbol{\eta}^{-1} + \boldsymbol{\sigma}_{\mathrm{I}m}^{k-1}\overline{\otimes}\,\boldsymbol{\eta}^{-1}\big), \tag{89}$$

whereas Equation (84a) can be reformulated by expressing $\mathbb{A}_{\mathrm{I}m}^{k-1}$ in terms of the quantities $J_m^{k-1}\mathbbm{c}_{\mathrm{I}m}^{k-1}$ and $J_m^{k-1}\boldsymbol{\sigma}_{\mathrm{I}m}$ (see section 4.6.1 of the Theory Manual of ABAQUS®[118]) as

$$\begin{aligned}[C_{\chi\chi}]_m^{k-1}(\delta\chi_m^k, \boldsymbol{V}_{\mathrm{v}}) &= \int_{\mathscr{B}} \delta\boldsymbol{d}_m^k : [J_m^{k-1}\mathbbm{c}_{\mathrm{I}m}^{k-1}] : \boldsymbol{d}_{\mathrm{v}m}^k + \int_{\mathscr{B}} J_m^{k-1}\boldsymbol{\sigma}_{\mathrm{I}m}^{k-1} : [(\delta\boldsymbol{l}_m^k)^{\mathrm{T}}\boldsymbol{\eta}\boldsymbol{l}_{\mathrm{v}m}^k] \\ &=: [\hat{C}_{\boldsymbol{dd}}]_m^{k-1}(\delta\boldsymbol{d}_m^k, \boldsymbol{d}_{\mathrm{v}m}^k) + [\hat{C}_{\boldsymbol{ll}}]_m^{k-1}(\delta\boldsymbol{l}_m^k, \boldsymbol{l}_{\mathrm{v}m}^k).\end{aligned} \tag{90}$$

Analogously, we can rewrite $[C_{\chi P}]_m^{k-1}(\delta\chi_m^k, \boldsymbol{V}_{\mathrm{v}})$ in the equivalent form

$$[C_{\chi P}]_m^{k-1}(\delta P_m^k, \boldsymbol{V}_{\mathrm{v}}) = -\int_{\mathscr{B}} \delta P_m^k\, [J_m^{k-1}\boldsymbol{\eta}^{-1}] : \boldsymbol{d}_{\mathrm{v}m}^k =: [\hat{C}_{\boldsymbol{d}P}]_m^{k-1}(\delta P_m^k, \boldsymbol{d}_{\mathrm{v}m}^k). \tag{91}$$

We compute now the Gâteaux derivatives $\mathcal{D}_\chi \hat{B}(\mathsf{u}_m^{k-1}; P_{\mathrm{v}})[\delta\chi_m^k]$ and $\mathcal{D}_P \hat{B}(\mathsf{u}_m^{k-1}; P_{\mathrm{v}})[\delta P_m^k]$, which constitute the part of the numerical procedure at hand containing the novelty of this work. To perform these calculations, we employ, indeed, the time-discrete form of the fractional relationship (67) between the (material) filtration velocity and the pressure gradient. This leads to

$$\begin{aligned}\mathcal{D}_\chi \hat{B}(\mathsf{u}_m^{k-1}; P_{\mathrm{v}})[\delta\chi_m^k] = &-\int_{\mathscr{B}} \frac{1}{\Delta t_m} J_m^{k-1}\{[\boldsymbol{F}_m^{k-1}]^{-\mathrm{T}} : [\mathrm{Grad}\,\delta\chi_m^k]\}P_{\mathrm{v}} \\ &+ \int_{\mathscr{B}} \left[\frac{\partial \boldsymbol{\mathcal{G}}^{\boldsymbol{Q}_m}}{\partial \boldsymbol{F}_m}(\boldsymbol{F}_m^{k-1}, \mathrm{Grad}\, P_m^{k-1}) : \mathrm{Grad}\,\delta\chi_m^k\right]\mathrm{Grad}P_{\mathrm{v}},\end{aligned} \tag{92a}$$

$$\mathcal{D}_P \hat{B}(\mathsf{u}_m^{k-1}; P_{\mathrm{v}})[\delta P_m^k] = \int_{\mathscr{B}} \left[\frac{\partial \boldsymbol{\mathcal{G}}^{\boldsymbol{Q}_m}}{\partial \mathrm{Grad}P_m}(\boldsymbol{F}_m^{k-1}, \mathrm{Grad}P_m^{k-1})\mathrm{Grad}\,\delta P_m^k\right]\mathrm{Grad}P_{\mathrm{v}}. \tag{92b}$$

We remark that, although an explicit expression of the function $\boldsymbol{\mathcal{G}}^{\boldsymbol{Q}_m}$ is not available, and since it is only necessary to know the partial derivatives $\partial_{\boldsymbol{F}_m}\boldsymbol{\mathcal{G}}^{\boldsymbol{Q}_m}(\boldsymbol{F}_m^{k-1}, \mathrm{Grad}\, P_m^{k-1})$ and $\partial_{\mathrm{Grad}P_m}\boldsymbol{\mathcal{G}}^{\boldsymbol{Q}_m}(\boldsymbol{F}_m^{k-1}, \mathrm{Grad}\, P_m^{k-1})$, which are both evaluated at the $(k-1)$th Newton iteration, and are, thus, known, Dini's implicit function theorem permits to determine these derivatives exactly through Equations (76a) and (76b). Therefore, Equations (92a) and (92b) become

$$\mathcal{D}_\chi \hat{B}(\mathsf{u}_m^{k-1}; P_{\mathrm{v}})[\delta\chi_m^k] \equiv [C_{P\chi}]_m^{k-1}(\delta\chi_m^k, P_{\mathrm{v}})$$

$$
\begin{aligned}
&= -\int_{\mathscr{B}} \frac{1}{\Delta t_m} J_m^{k-1} \{ [\boldsymbol{F}_m^{k-1}]^{-\mathrm{T}} : [\mathrm{Grad}\, \delta\chi_m^k] \} P_{\mathrm{v}} \\
&\quad - \int_{\mathscr{B}} \left\{ \left[ \frac{\partial \boldsymbol{\mathcal{Z}}}{\partial \boldsymbol{Q}_m}(\sharp_m^{k-1}) \right]^{-1} \left[ \frac{\partial \boldsymbol{\mathcal{Z}}}{\partial \boldsymbol{F}_m}(\sharp_m^{k-1}) \right] : \mathrm{Grad}\, \delta\chi_m^k \right\} \mathrm{Grad} P_{\mathrm{v}}, \qquad (93a)
\end{aligned}
$$

$$
\begin{aligned}
\mathcal{D}_P \hat{B}(\mathsf{u}_m^{k-1}; P_{\mathrm{v}})[\delta P_m^k] &\equiv [C_{PP}]_m^{k-1}(\delta P_m^k, P_{\mathrm{v}}) \\
&= -\int_{\mathscr{B}} \left\{ \left[ \frac{\partial \boldsymbol{\mathcal{Z}}}{\partial \boldsymbol{Q}_m}(\sharp_m^{k-1}) \right]^{-1} \left[ \frac{\partial \boldsymbol{\mathcal{Z}}}{\partial \mathrm{Grad} P_m}(\sharp_m^{k-1}) \right] \mathrm{Grad}\, \delta P_m^k \right\} \mathrm{Grad} P_{\mathrm{v}}, \qquad (93b)
\end{aligned}
$$

where $\partial_{\boldsymbol{Q}_m} \boldsymbol{\mathcal{Z}}$ has been determined in Equation (72), while the derivatives of $\boldsymbol{\mathcal{Z}}$ with respect to $\boldsymbol{F}_m$ and $\mathrm{Grad}\, P_m$ are given by

$$
\begin{aligned}
\frac{\partial \boldsymbol{\mathcal{Z}}}{\partial \boldsymbol{F}_m}(\sharp_m^{k-1}) &= \left( 1 + \frac{\alpha t_{\mathrm{c}}^{\alpha} s_m^{1-\alpha}}{\Delta t_m} \right) \left[ \boldsymbol{Q}_m^{k-1} \otimes \frac{\partial \mathcal{R}_{\mathrm{F}}}{\partial \boldsymbol{F}_m}(\boldsymbol{F}_m^{k-1}, \boldsymbol{Q}_m^{k-1}) \right] - \frac{\alpha t_{\mathrm{c}}^{\alpha} s_m^{1-\alpha}}{\Delta t_m} \boldsymbol{Q}_{m-1} \otimes \frac{\partial \mathcal{R}_{\mathrm{F}}}{\partial \boldsymbol{F}_m}(\boldsymbol{F}_m^{k-1}, \boldsymbol{Q}_m^{k-1}) \\
&\quad + \alpha t_{\mathrm{c}}^{\alpha} J_m^{k-1} [\boldsymbol{F}_m^{k-1}]^{-1} \boldsymbol{\mathcal{F}}_{\alpha}(t_m) \otimes [\boldsymbol{F}_m^{k-1}]^{-\mathrm{T}} - \alpha t_{\mathrm{c}}^{\alpha} J_m^{k-1} [\boldsymbol{F}_m^{k-1}]^{-1} \otimes \{ [\boldsymbol{F}_m^{k-1}]^{-1} \boldsymbol{\mathcal{F}}_{\alpha}(t_m) \} \\
&\quad - \boldsymbol{\mathcal{G}}^{\boldsymbol{Q}_{\mathrm{D}}}(\boldsymbol{F}_m^{k-1}, \mathrm{Grad}\, P_m^{k-1}) \otimes \frac{\partial \mathcal{R}_{\mathrm{D}}}{\partial \boldsymbol{F}_m}(\boldsymbol{F}_m^{k-1}) - \mathcal{R}_{\mathrm{D}}(\boldsymbol{F}_m^{k-1}) \frac{\partial \boldsymbol{\mathcal{G}}^{\boldsymbol{Q}_{\mathrm{D}}}}{\partial \boldsymbol{F}_m}(\boldsymbol{F}_m^{k-1}, \mathrm{Grad} P_m^{k-1}), \qquad (94a) \\
\frac{\partial \boldsymbol{\mathcal{Z}}}{\partial \mathrm{Grad} P_m}(\sharp_m^{k-1}) &= -\mathcal{R}_{\mathrm{D}}(\boldsymbol{F}_m^{k-1}) \frac{\partial \boldsymbol{\mathcal{G}}^{\boldsymbol{Q}_{\mathrm{D}}}}{\partial \mathrm{Grad} P_m}(\boldsymbol{F}_m^{k-1}, \mathrm{Grad} P_m^{k-1}) = (J_m^{k-1} - \Phi_{\mathrm{sR}}) [\boldsymbol{C}_m^{k-1}]^{-1}, \qquad (94b)
\end{aligned}
$$

and, again, the notation $[C_{P\chi}]_m^{k-1}(\delta\chi_m^k, P_{\mathrm{v}})$ and $[C_{PP}]_m^{k-1}(\delta P_m^k, P_{\mathrm{v}})$ puts in evidence the influence of the pore pressure on the motion and the self-influence of the pore pressure. For completeness, we supply also the expressions of the derivatives of $\mathcal{R}_{\mathrm{F}}$, $\mathcal{R}_{\mathrm{D}}$, and $\boldsymbol{\mathcal{G}}^{\boldsymbol{Q}_{\mathrm{D}}}$ with respect to $\boldsymbol{F}_m$. To this end, we write $\kappa_{\mathrm{iso}}$ and $\mathcal{A}_{\mathrm{iso}}$ as functions of $J_m$, i.e., we set $\kappa_{\mathrm{iso}} \equiv \hat{\kappa}_{\mathrm{iso}}(J_m)$ and $\mathcal{A}_{\mathrm{iso}} \equiv \hat{\mathcal{A}}_{\mathrm{iso}}(J_m)$, and we express $||\boldsymbol{Q}_m||_{\boldsymbol{C}_m}$ as a function of $\boldsymbol{F}_m$, i.e., $||\boldsymbol{Q}_m||_{\boldsymbol{C}_m} \equiv \hat{\mathfrak{Q}}(\boldsymbol{F}_m)$. Then, we obtain:

$$
\begin{aligned}
\frac{\partial \mathcal{R}_{\mathrm{D}}}{\partial \boldsymbol{F}_m}(\boldsymbol{F}_m^{k-1}) &= \mathcal{R}_{\mathrm{D}}(\boldsymbol{F}_m^{k-1}) \left[ \frac{J_m^{k-1}}{J_m^{k-1} - \Phi_{\mathrm{sR}}} - \frac{J_m^{k-1}}{\hat{\kappa}_{\mathrm{iso}}(J_m^{k-1})} \frac{\partial \hat{\kappa}_{\mathrm{iso}}}{\partial J_m}(J_m^{k-1}) \right] [\boldsymbol{F}_m^{k-1}]^{-\mathrm{T}}, \qquad (95a) \\
\frac{\partial \hat{\mathfrak{Q}}}{\partial \boldsymbol{F}_m}(\boldsymbol{F}_m^{k-1}) &= -||\boldsymbol{Q}_m^{k-1}||_{\boldsymbol{C}_m^{k-1}} [\boldsymbol{F}_m^{k-1}]^{-\mathrm{T}} + \frac{1}{J_m^{k-1} ||\boldsymbol{Q}_m^{k-1}||_{\boldsymbol{C}_m^{k-1}}} \frac{\boldsymbol{\eta} \boldsymbol{F}_m^{k-1} \boldsymbol{Q}_m^{k-1}}{J_m^{k-1}} \otimes \boldsymbol{Q}_m^{k-1}, \qquad (95b) \\
\frac{\partial \mathcal{R}_{\mathrm{F}}}{\partial \boldsymbol{F}_m}(\boldsymbol{F}_m^{k-1}, \boldsymbol{Q}_m^{k-1}) &= \frac{\partial \mathcal{R}_{\mathrm{D}}}{\partial \boldsymbol{F}_m}(\boldsymbol{F}_m^{k-1}) [1 + \hat{\mathcal{A}}_{\mathrm{iso}}(J_m^{k-1}) ||\boldsymbol{Q}_m^{k-1}||_{\boldsymbol{C}_m^{k-1}}] \\
&\quad + \mathcal{R}_{\mathrm{D}}(\boldsymbol{F}_m^{k-1}) \left\{ \frac{\partial \hat{\mathcal{A}}_{\mathrm{iso}}}{\partial J_m}(J_m^{k-1}) J_m^{k-1} ||\boldsymbol{Q}_m^{k-1}||_{\boldsymbol{C}_m^{k-1}} [\boldsymbol{F}_m^{k-1}]^{-\mathrm{T}} \right. \\
&\quad \left. + \hat{\mathcal{A}}_{\mathrm{iso}}(J_m^{k-1}) \frac{\partial \hat{\mathfrak{Q}}}{\partial \boldsymbol{F}_m}(\boldsymbol{F}_m^{k-1}) \right\}, \qquad (95c) \\
\frac{\partial \boldsymbol{\mathcal{G}}^{\boldsymbol{Q}_{\mathrm{D}}}}{\partial \boldsymbol{F}_m}(\boldsymbol{F}_m^{k-1}, \mathrm{Grad}\, P_m^{k-1}) &= \frac{J_m^{k-1}}{\hat{\kappa}_{\mathrm{iso}}(J_m^{k-1})} \frac{\partial \hat{\kappa}_{\mathrm{iso}}}{\partial J_m}(J_m^{k-1}) \boldsymbol{Q}_{\mathrm{D}m}^{k-1} \otimes [\boldsymbol{F}_m^{k-1}]^{-\mathrm{T}} \\
&\quad - [\boldsymbol{F}_m^{k-1}]^{-1} \otimes \boldsymbol{Q}_{\mathrm{D}m}^{k-1} - [\boldsymbol{C}_m^{k-1}]^{-1} \underline{\otimes} \boldsymbol{\eta} \boldsymbol{F}_m^{k-1} \boldsymbol{Q}_{\mathrm{D}m}^{k-1}. \qquad (95d)
\end{aligned}
$$

Finally, we notice that the definitions supplied in Equations (84a) and (93b) allow to rewrite Equation (80a) in the more suggestive form

$$[C_{\chi\chi}]^{k-1}_m(\delta\chi^k_m, \boldsymbol{V}_{\rm v}) + [C_{\chi P}]^{k-1}_m(\delta P^k_m, \boldsymbol{V}_{\rm v}) = -\hat{A}(\mathsf{u}^{k-1}_m; \boldsymbol{V}_{\rm v}), \tag{96a}$$

$$[C_{P\chi}]^{k-1}_m(\delta\chi^k_m, P_{\rm v}) + [C_{PP}]^{k-1}_m(\delta P^k_m, P_{\rm v}) = -\hat{B}(\mathsf{u}^{k-1}_m; P_{\rm v}), \tag{96b}$$

with $[C_{\chi P}]^{k-1}_m(\cdot\,,\cdot)$ and $[C_{P\chi}]^{k-1}_m(\cdot\,,\cdot)$ being related through the identity[27,97]

$$\begin{aligned}[C_{P\chi}]^{k-1}_m(\delta\chi^k_m, P_{\rm v}) =& \frac{1}{\Delta t_m}[C_{\chi P}]^{k-1}_m(P_{\rm v}, \delta\chi^k_m) \\ & - \int_{\mathscr{B}} \left\{ \left[ \frac{\partial \boldsymbol{\mathcal{Z}}}{\partial \boldsymbol{Q}_m}(\sharp^{k-1}_m) \right]^{-1} \left[ \frac{\partial \boldsymbol{\mathcal{Z}}}{\partial \boldsymbol{F}_m}(\sharp^{k-1}_m) \right] : \mathrm{Grad}\delta\chi^k_m \right\} \mathrm{Grad} P_{\rm v}.\end{aligned} \tag{97}$$

Equations (96a) and (96b) are a "prelude" to their associated algebraic form, which is achieved by introducing the finite element discretization of the problem at hand and the interpolation functions for the unknown increments $\delta\chi^k_m$ and $\delta P^k_m$ as well as for the virtual fields $\boldsymbol{V}_{\rm v}$ and $P_{\rm v}$. In fact, each summand on the right-hand side of Equations (96a) and (96b) gives rise to a specific block of the matrix of the coefficients of the system of algebraic equations associated with Equations (80a) and (80b).

It is important to emphasize that, while Equation (96a) is essentially the same as the one studied in[27,97,115], the main differences between these previous studies and our work are condensed in Equation (96b). The first difference is given by the second term of the functional $[C_{P\chi}]^{k-1}_m(\cdot, \cdot)$, which collects all the modifications to the Darcian model that are associated both with Forchheimer's correction and with its fractionalization (it can be proven, in this respect, that Darcy's model is retrieved by setting $\alpha = 0$ and $\mathscr{A}_{\rm iso} = 0$ identically). This term, in fact, describes a coupling between pressure and deformation that, because of the Jacobian $\partial\boldsymbol{\mathcal{Z}}/\partial\boldsymbol{Q}_m$ and of the derivative $\partial\boldsymbol{\mathcal{Z}}/\partial\boldsymbol{F}_m$, is much more intricate than the Darcian one, and, in addition, it takes into account the non-locality in time of the model under investigation through $\boldsymbol{\mathcal{F}}_\alpha(t_m)$. The second difference with the Darcian model addressed in[27,97,115] is related to the definition of the functional $[C_{PP}]^{k-1}_m(\cdot\,,\cdot)$, which, again, keeps track of the non-locality in time and of all the interactions between the flow and the deformation through the inverse of the Jacobian $\partial\boldsymbol{\mathcal{Z}}/\partial\boldsymbol{Q}_m$ (cf. Equation (72)).

In spite of the differences just discussed, for the purpose of implementation in ABAQUS®, and, in particular, due to the limitation of "UMAT" and "UMATHT" subroutines present in the adopted software, in the numerical tests performed in this work, we neglect the second integral defining $[C_{P\chi}]^{k-1}_m(\delta\chi^k_m, P_{\rm v})$ on the far right-hand side of Equations (93a) and (97). Hence, for the forthcoming simulations, we substitute the terms $[C_{P\chi}]^{k-1}_m(\delta\chi^k_m, P_{\rm v})$ and in Equation (96b) with its approximated counterpart

$$\begin{aligned}[C^{\rm app}_{P\chi}]^{k-1}_m(\delta\chi^k_m, P_{\rm v}) &:= -\int_{\mathscr{B}} \frac{1}{\Delta t_m} J^{k-1}_m \{[\boldsymbol{F}^{k-1}_m]^{-\rm T} : [\mathrm{Grad}\,\delta\chi^k_m]\} P_{\rm v} \\ &= -\int_{\mathscr{B}} \frac{1}{\Delta t_m} J^{k-1}_m \mathrm{tr}[\boldsymbol{\eta}^{-1}\delta\boldsymbol{d}^k_m] P_{\rm v} \\ &=: [\hat{C}^{\rm app}_{P\boldsymbol{d}}]^{k-1}_m(\delta\boldsymbol{d}^k_m, P_{\rm v}),\end{aligned} \tag{98}$$

and we solve the approximated system

$$[C_{\chi\chi}]^{k-1}_m(\delta\chi^k_m, \boldsymbol{V}_{\rm v}) + [C_{\chi P}]^{k-1}_m(\delta P^k_m, \boldsymbol{V}_{\rm v}) = -\hat{A}(\mathsf{u}^{k-1}_m; \boldsymbol{V}_{\rm v}), \tag{99a}$$

$$[C^{\rm app}_{P\chi}]^{k-1}_m(\delta\chi^k_m, P_{\rm v}) + [C_{PP}]^{k-1}_m(\delta P^k_m, P_{\rm v}) = -\hat{B}(\mathsf{u}^{k-1}_m; P_{\rm v}). \tag{99b}$$

Note that, analogously to Equation (99b), also the term $[C_{PP}]^{k-1}_m(\delta P^k_m, P_{\rm v})$ can be recast in the equivalent form

$$\begin{aligned}[C_{PP}]^{k-1}_m(\delta P^k_m, P_{\rm v}) &= -\int_{\mathscr{B}} \{(\mathrm{Grad}\delta P^k_m)[\boldsymbol{F}^{k-1}_m]^{-1}\}[J^{k-1}_m \mathfrak{B}^{k-1}_m]\{(\mathrm{Grad}P_{\rm v})[\boldsymbol{F}^{k-1}_m]^{-1}\} \\ &=: [\hat{C}_{PP}]^{k-1}_m(\delta p^k_m, p_{\rm v}),\end{aligned} \tag{100}$$

where $p_{\rm v} := P_{\rm v} \circ (\Xi, \mathfrak{t})$ is the spatial counterpart of the virtual pressure field $p^k_m := P^k_m \circ (\Xi, \mathfrak{t})$, and we have set

$$\mathfrak{B}^{k-1}_m := \frac{1}{J^{k-1}_m}\boldsymbol{F}^{k-1}_m\left[\frac{\partial \boldsymbol{\mathcal{Z}}}{\partial \boldsymbol{Q}_m}(\sharp^{k-1}_m)\right]^{-1}\left[\frac{\partial \boldsymbol{\mathcal{Z}}}{\partial \mathrm{Grad}P_m}(\sharp^{k-1}_m)\right][\boldsymbol{F}^{k-1}_m]^{\rm T}. \tag{101}$$

Clearly, this way of proceeding has the drawback that not all the interactions introduced by our model are equally considered in the algorithm employed. However, the algorithm makes it still possible to account for those deviations from Darcy's regime that the fractional version of Forchheimer's correction studied in our work unfolds in the term $[C_{PP}]^{k-1}_m(\delta P^k_m, P_{\rm v})$ through $\mathfrak{B}^{k-1}_m$ and in the residue $\hat{B}(\mathsf{u}^{k-1}_m; P_{\rm v})$.

Finally, by solving Equations (99a) and (99b) for $\delta\chi^k_m$ and $\delta P^k_m$, reconstructing the motion and fluid pressure at the $k$th iteration as $\chi^k_m = \chi^{k-1}_m + \delta\chi^k_m$ and $P^k_m = P^{k-1}_m + \delta P^k_m$, and computing the functionals $\hat{A}(\mathsf{u}^k_m, \boldsymbol{V}_{\rm v})$ and $\hat{B}(\mathsf{u}^k_m, P_{\rm v})$, the pair $(\chi_m, P_m)$ that solves Equations (77a) and (77b) is found, as anticipated above, when, for some $k_* \in \mathbb{N}$, the absolute values $|\hat{A}(\mathsf{u}^k_m, \boldsymbol{V}_{\rm v})|$ and $|\hat{B}(\mathsf{u}^k_m, P_{\rm v})| \equiv |B(\chi^k_m, P^k_m, \boldsymbol{Q}^k_m; P_{\rm v})|$ remain smaller than a given threshold for all $k > k_*$.

There is, however, a last step of the algorithm employed here that has to be commented. Indeed, to solve Equations (99a) and (99b), it is necessary to know the residue

$$\hat{B}(\mathsf{u}^{k-1}_m; P_{\rm v}) \equiv \hat{B}(\chi^{k-1}_m, P^{k-1}_m; P_{\rm v}) = B(\chi^{k-1}_m, P^{k-1}_m, \boldsymbol{Q}^{k-1}_m; P_{\rm v}), \qquad k \geq 1. \tag{102}$$

Yet, this quantity is unknown for all $k \geq 2$, because $\boldsymbol{Q}^{k-1}_m$ has still to be determined. On the other hand, $\boldsymbol{Q}^{k-1}_m$ is known only for $k = 1$, since $\boldsymbol{Q}^0_m$ is either guessed or computed by solving Equation (69c) through another Newton-Raphson procedure (see next paragraph). Hence, since $\chi^0_m$ and $P^0_m$ are supplied by the initial guess, also the residue $B(\chi^0_m, P^0_m, \boldsymbol{Q}^0_m; P_{\rm v})$ is entirely defined. In conclusion, the filtration velocity $\boldsymbol{Q}^{k-1}_m$ must be computed at each $k \geq 2$. This is done by applying, again, the Newton-Raphson method shown in the next paragraph, and, with this procedure, also $\boldsymbol{Q}^k_m$ is obtained. Therefore, the filtration velocity $\boldsymbol{Q}_m$ at time $t_m$ can be approximated with the value of $\boldsymbol{Q}^k_m$ for $k > k_*$, with $k_* \in \mathbb{N}$ being such that $|\boldsymbol{\mathcal{Z}}(\boldsymbol{F}^k_m, \mathrm{Grad}\, P^k_m, \boldsymbol{Q}^k_m)|$ is smaller than a given threshold for all $k > k_*$.

*Determination of $\boldsymbol{Q}_m$.* The separate determination of $\boldsymbol{Q}_m$ is necessary for computing the residues $\hat{B}(\chi^{k-1}_m, P^{k-1}_m; P_{\rm v}) \equiv B(\chi^{k-1}_m, P^{k-1}_m, \boldsymbol{Q}^{k-1}_m; P_{\rm v})$, for all $k \geq 2$. For $k = 1$, instead, the residue $B(\chi^0_m, P^0_m, \boldsymbol{Q}^0_m; P_{\rm v})$ is entirely defined by the initial triple $(\chi^0_m, P^0_m, \boldsymbol{Q}^0_m)$. In this work, to simplify the computational burden, we have opted to prescribe $\boldsymbol{Q}^0_m$ arbitrarily through an "educated guess", since this does not affect considerably the convergence to the value of $\boldsymbol{Q}_m$ that solves approximately Equation (69c).

To compute the residue $\hat{B}(\chi^{k-1}_m, P^{k-1}_m; P_{\rm v}) \equiv B(\chi^{k-1}_m, P^{k-1}_m, \boldsymbol{Q}^{k-1}_m; P_{\rm v})$, for all $k \geq 2$, we determine $\boldsymbol{Q}^{k-1}_m$ as follows. First, for each $k \geq 2$, we write $\boldsymbol{Q}^{k-1}_m$ as $\boldsymbol{Q}^{k-1,l}_m := \boldsymbol{Q}^{k-1,l-1}_m + \delta\boldsymbol{Q}^{k-1,l}_m$. Here, $l \geq 1$,

$l \in \mathbb{N}$, is the counter of the Newton-Raphson procedure *"nested"*[119] in the $k$th iteration of the outer procedure, employed to calculate $\chi_m^k$ and $P_m^k$, while $\delta \boldsymbol{Q}_m^{k-1,l}$ is the increment of the filtration velocity at the $l$th iteration nested in the $(k-1)$th iteration of the outer scheme. We notice that, for $l = 1$, the quantity $\boldsymbol{Q}_m^{k-1,0}$ is a guessed value of the filtration velocity that can be taken equal to $\boldsymbol{Q}_m^{k-2}$. Then, we approximate the function $\boldsymbol{\mathcal{Z}}$ with its Taylor polynomial of the first grade in $\delta \boldsymbol{Q}_m^{k-1,l}$, thereby writing

$$\begin{aligned} &\boldsymbol{\mathcal{Z}}_{\text{app}}(\boldsymbol{F}_m^{k-1}, \text{Grad}\, P_m^{k-1}, \boldsymbol{Q}_m^{k-1,l-1} + \delta\boldsymbol{Q}_m^{k-1,l}) \\ &:= \boldsymbol{\mathcal{Z}}(\boldsymbol{F}_m^{k-1}, \text{Grad}\, P_m^{k-1}, \boldsymbol{Q}_m^{k-1,l-1}) + \left[\frac{\partial \boldsymbol{\mathcal{Z}}}{\partial \boldsymbol{Q}_m}(\boldsymbol{F}_m^{k-1}, \text{Grad}\, P_m^{k-1}, \boldsymbol{Q}_m^{k-1,l-1})\right]\delta\boldsymbol{Q}_m^{k-1,l}, \quad l \geq 1. \end{aligned} \tag{103}$$

Next, by setting $\boldsymbol{\mathcal{Z}}_{\text{app}}(\boldsymbol{F}_m^{k-1}, \text{Grad}\, P_m^{k-1}, \boldsymbol{Q}_m^{k-1,l-1} + \delta\boldsymbol{Q}_m^{k-1,l}) = \boldsymbol{0}$ for $l \geq 1$, $\delta\boldsymbol{Q}_m^{k-1,l}$ is obtained as

$$\delta\boldsymbol{Q}_m^{k-1,l} = -\left[\frac{\partial \boldsymbol{\mathcal{Z}}}{\partial \boldsymbol{Q}_m}(\boldsymbol{F}_m^{k-1}, \text{Grad}\, P_m^{k-1}, \boldsymbol{Q}_m^{k-1,l-1})\right]^{-1} \boldsymbol{\mathcal{Z}}(\boldsymbol{F}_m^{k-1}, \text{Grad}\, P_m^{k-1}, \boldsymbol{Q}_m^{k-1,l-1}), \quad l \geq 1. \tag{104}$$

and $\boldsymbol{Q}_m^{k-1,l}$ can be reconstructed according to its definition. As usual, the iterations stop when, for some $l_*(k) \in \mathbb{N}$, the absolute value $|\boldsymbol{\mathcal{Z}}(\boldsymbol{F}_m^{k-1}, \text{Grad}\, P_m^{k-1}, \boldsymbol{Q}_m^{k-1,l})|$ remains smaller than a given tolerance for all $l > l_*(k)$. Accordingly, $\boldsymbol{Q}_m^{k-1}$ is formally identified with the limit $\boldsymbol{Q}_m^{k-1} := \lim_{l\to+\infty} \boldsymbol{Q}_m^{k-1,l}$. This permits to calculate the residue $\hat{B}(\chi_m^{k-1}, P_m^{k-1}, P_{\text{v}}) \equiv B(\chi_m^{k-1}, P_m^{k-1}, \boldsymbol{Q}_m^{k-1}; P_{\text{v}})$ as

$$B(\chi_m^{k-1}, P_m^{k-1}, \boldsymbol{Q}_m^{k-1}; P_{\text{v}}) = -\int_{\mathscr{B}} \frac{J_m^{k-1} - J_{m-1}}{\Delta t_m} P_{\text{v}} + \int_{\mathscr{B}} \boldsymbol{Q}_m^{k-1} \text{Grad}\, P_{\text{v}}. \tag{105}$$

To conclude this paragraph, we notice that $\boldsymbol{Q}_m^k$ is calculated with the same scheme employed for $\boldsymbol{Q}_m^{k-1}$, after determining the pair $(\boldsymbol{F}_m^k, \text{Grad}\, P_m^k)$ by solving Equations (99a) and (99b), so that the quantity $|\boldsymbol{\mathcal{Z}}(\boldsymbol{F}_m^k, \text{Grad}\, P_m^k, \boldsymbol{Q}_m^k)|$ remains smaller than a given threshold. We also remark that, at a given time $t_m$, the stopping criterion for the aforementioned scheme is the convergence within a certain tolerance of $(\chi_m^k, P_m^k)$, which is assured for $k > k_*$. However, one more nested Newton-Raphson procedure is required to calculate $\boldsymbol{Q}_m$. In fact, after determining the approximated solution $(\chi_m^k, P_m^k) \equiv (\chi_m, P_m)$ of Equations (77a) and (77b), the value $\boldsymbol{Q}_m^k = \lim_{l\to+\infty} \boldsymbol{Q}_m^{k,l}$ is formally found by calling the nested Newton-Raphson method, and $\boldsymbol{Q}_m$ is found as $\boldsymbol{Q}_m^k \equiv \boldsymbol{Q}_m$, for $k > k_*$.

## 7 Summary of the model and benchmark tests

In this section, we describe the initial and boundary value problem (IBVP) employed for our numerical experiments, which will be conducted in ABAQUS® by following the numerical procedure explained in section *"Numerical implementation of the model equations"*.

Our simulations refer to the mathematical model conceived in the previous sections, which aims at describing a class of biological tissues characterized, on the one hand, by non-negligible pore scale inertial effects of the fluid and, on the other hand, by a complex microstructure of the pore network that gives rise to flow laws modeled as non-local in time[47,54,63,64]. For the purpose of studying this kind of media, we concentrate on simulating Equations (59a)-(59c), so that it is possible to highlight how the overall behavior of the system under evaluation is influenced by the fractional constitutive law of $\boldsymbol{Q}$ specified in Equation (58). In this respect, we notice that the standard Darcy-Forchheimer model, represented by

Equations (42a) and (42b), can be recovered from the fractional one by setting $\alpha = 0$, while standard Darcy's model can be obtained by setting $c_0 = 0$ and $\alpha = 0$ in Equation (37).

In the following simulations, we replicate the setup of an experimentally relevant uni-axial compression test in which, before the application of the load, a cylindrical sample of the hypothetical tissue under study is put in a compression chamber, situated in the inner part of the experimental apparatus. Inside the chamber, the sample is positioned between two impermeable plates, made of steel or, more generally, of a material that does not allow for adhesion bonds with the sample itself. Moreover, in the inner chamber, an apparatus circulates warm water that maintains the sample in isothermal conditions. Then, the experiment is conducted in control of displacement: the movement of the upper plate is controlled, and it exerts a prescribed compression on the tissue. At the end of the compression phase, which is when the maximum prescribed displacement is reached, the load is kept constant in order to study the relaxation of the biological tissue.

We perform the simulation of the just described unconfined compression test by solving Equations (59a)-(59c) for a cylindrical specimen of tissue over the time interval $[t_{\rm in}, t_{\rm fin}] \equiv [0, t_{\rm fin}]$. The specimen has initial radius $R = 1.5\,\mathrm{mm}$ and initial height $H = 1\,\mathrm{mm}$, as shown in Fig 1. Since we do not simulate the plates, boundary conditions are applied directly on the specimen's boundary, which coincides with the boundary of its reference placement, $\partial\mathscr{B}$, and can be partitioned as $\partial\mathscr{B} = \Gamma_{\rm U} \cup \Gamma_{\rm L} \cup \Gamma_{\rm B}$, with $\Gamma_{\rm U}$, $\Gamma_{\rm L}$, and $\Gamma_{\rm B}$ being the specimen's upper, lateral, and bottom surface, respectively. We recall that, since the constitutive framework has been set, the system (59a)-(59c) constitutes seven scalar equations in the seven unknowns given by the three components of the motion $\chi$, pore pressure $P$, and the three components of the material filtration velocity $\boldsymbol{Q}$.

To assign the boundary conditions, we introduce a reference frame, associated with $\mathscr{B}$, and having origin at the center $X_{\rm O}$ of $\Gamma_{\rm B}$, and axes directed along the unit vectors of the triad $\mathscr{E}_{\rm O} := \{\boldsymbol{E}_1, \boldsymbol{E}_2, \boldsymbol{E}_3\} \subset T_{X_{\rm O}}\mathscr{B}$, in which $\boldsymbol{E}_3$ identifies the axial direction of the specimen, while $\boldsymbol{E}_1$ and $\boldsymbol{E}_2$ span the transversal plane. We also introduce the co-normals $\boldsymbol{N}_{\rm U}$, $\boldsymbol{N}_{\rm L}$, and $\boldsymbol{N}_{\rm B}$ to $\Gamma_{\rm U}$, $\Gamma_{\rm L}$, and $\Gamma_{\rm B}$, and we notice that $\boldsymbol{N}_{\rm U}$ and $\boldsymbol{N}_{\rm B}$ are parallel and anti-parallel to the co-vector $\boldsymbol{E}^3$ of the co-vector basis dual to $\mathscr{E}_{\rm O}$. Hence, for every time $t \in [0, t_{\rm fin}]$, the following boundary conditions represent the experimental setup illustrated above:

$$\chi^3(X,t) = \chi^3_{\rm U}(X,t), \qquad [\boldsymbol{T}_{\rm I}\boldsymbol{N}_{\rm U}]\boldsymbol{E}_1 = 0, \qquad [\boldsymbol{T}_{\rm I}\boldsymbol{N}_{\rm U}]\boldsymbol{E}_2 = 0, \qquad \text{on } \Gamma_{\rm U}, \tag{106a}$$

$$\boldsymbol{Q}\boldsymbol{N}_{\rm U} = 0, \qquad \text{on } \Gamma_{\rm U}, \tag{106b}$$

$$\boldsymbol{T}_{\rm I}\boldsymbol{N}_{\rm L} = \boldsymbol{0}, \qquad \text{on } \Gamma_{\rm L}, \tag{106c}$$

$$P = 0, \qquad \text{on } \Gamma_{\rm L}, \tag{106d}$$

$$\chi(X,t) = \chi_{\rm B}(X,t), \qquad \text{on } \Gamma_{\rm B}, \tag{106e}$$

$$\boldsymbol{Q}\boldsymbol{N}_{\rm B} = 0, \qquad \text{on } \Gamma_{\rm B}, \tag{106f}$$

where $\chi^3_{\rm U}(X,t)$ is the time-dependent loading function, defined by[31,45,120,121]

$$\chi^3_{\rm U}(X,t) \equiv \chi^3(X^1, X^2, H, t) := \begin{cases} H - u_{\rm T}\dfrac{t}{t_{\rm ramp}}, & t \in\, ]0, t_{\rm ramp}], \\ H - u_{\rm T}, & t \in\, ]t_{\rm ramp}, t_{\rm fin}], \end{cases} \tag{107}$$

while, with a slight abuse of notation, $\chi_{\mathrm{B}}(X,t)$ is given by $\chi_{\mathrm{B}}(X,t) = (X^1, X^2, 0)$ for all $t \in [0, t_{\mathrm{fin}}]$, and for all pairs $(X^1, X^2)$ belonging to cross section of the specimen at $X^3 = 0$. These prescriptions represent the fact that a prescribed axial compression is applied onto the upper surface of the specimen, while its bottom surface is clamped. The absolute value of the applied axial displacement $|\chi^3(X,t) - \chi^3_{\mathrm{U}}(X,t)|$ increases in time until it reaches the maximum $u_{\mathrm{T}} = 0.2\,\mathrm{mm}$ at $t = t_{\mathrm{ramp}} = 20\,\mathrm{s}$ and, afterwards, it is kept constant until the final time of the simulated experiment $t = t_{\mathrm{fin}} = 50\,\mathrm{s}$.

The second and third conditions in Equation (106a) indicate that no tangential tractions are applied on $\Gamma_{\mathrm{U}}$. In addition, Equations (106c) and (106d) mean that the lateral surface of the specimen $\Gamma_{\mathrm{L}}$ is traction-free and that the pore pressure is atmospheric. Finally, Equations (106b) and (106f) show that the upper and lower surfaces are both insulated, so that no fluid flow may occur through them. The fluid, however, is free to escape through the lateral surfaces of the specimen during compression.

A schematic representation of the cylindrical specimen and of the boundary conditions discussed above is shown in Fig 1.

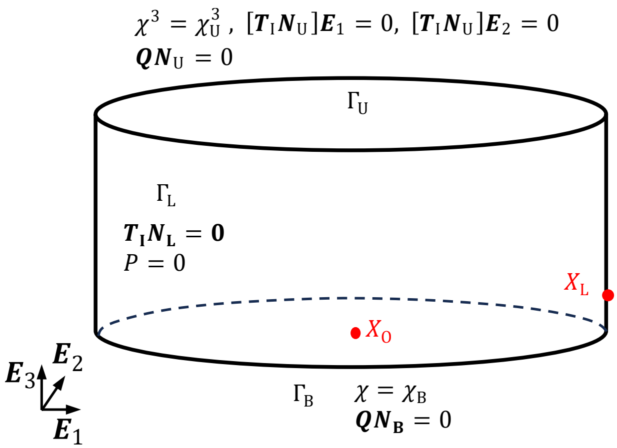


**Figure 1.** Geometry and boundary conditions for unconfined compression test

The prescribed initial conditions for the IBVP are

$$\chi(X,0) = \chi_{\mathrm{in}}(X), \qquad \text{in } \mathscr{B}, \tag{108a}$$
$$P(X,0) = 0, \qquad \text{in } \mathscr{B}, \tag{108b}$$
$$\boldsymbol{Q}(X,0) = \boldsymbol{0}, \qquad \text{in } \mathscr{B}, \tag{108c}$$

where, again, with a slight abuse of notation, we set $\chi_{\mathrm{in}}(X) = (X^1, X^2, X^3)$ for all the inner point of $\mathscr{B}$. We remark that, at the initial time $t = t_{\mathrm{in}} = 0\,\mathrm{s}$, Equations (59a)-(59c) are identically satisfied, whereas, for $t \in ]0, t_{\mathrm{fin}}]$, it is necessary to have $\boldsymbol{Q}(X,t) \neq \boldsymbol{0}$ in order to meet the hypotheses of Dini's Theorem, as explained in subsection *"Linearization of the fractional Darcy-Forchheimer model"*. Hence, for coding purposes, to avoid the explicit separation of the case $t = 0\,\mathrm{s}$ from the case $t \in ]0, t_{\mathrm{fin}}]$, the initial condition for the filtration velocity $\boldsymbol{Q}$ is taken near the machine precision.

Under the initial and boundary conditions (106a)-(106e) and (108a)-(108c), we study the evolution of the system for different values of the fractional order $\alpha$, and of the characteristic time $t_{\mathrm{c}}$ in order to observe

| Parameter | Symbol | Numerical value | Unit of measure | Reference |
|---|---|---|---|---|
| Initial radius | $R$ | 1.5 | mm | - |
| Initial height | $H$ | 1.0 | mm | - |
| Referential solidity | $\Phi_{\mathrm{s}}$ | 0.2 | - | 52 |
| Reference permeability | $k_{\mathrm{ref}}$ | $1.88 \cdot 10^{-11}$ | $\mathrm{mm}^2$ | 45 |
| Material parameter | $m_0$ | 0.0848 | - | 122 |
| Material parameter | $m_1$ | 4.6380 | - | 122 |
| First Lamé's constant | $\lambda_{\mathrm{s}}$ | $5.55 \cdot 10^5$ | Pa | 31 |
| Second Lamé's constant | $\mu_{\mathrm{s}}$ | $2.22 \cdot 10^5$ | Pa | 31 |
| Density fluid phase | $\varrho_{\mathrm{f}}$ | $1 \cdot 10^3$ | $\mathrm{kg/m}^3$ | 52 |
| Fluid viscosity | $\mu$ | $1 \cdot 10^{-9}$ | $\mathrm{MPa \cdot s}$ | - |
| Forchheimer's parameter | $c_0$ | $1.44 \cdot 10^9$ | - | - |
| Forchheimer's parameter | $c_1$ | -5.5 | - | 45 |
| Forchheimer's parameter | $c_2$ | -0.5 | - | 45 |

**Table 1.** Values of the material parameters used for the numerical simulations.

the evolution of the flux, of the deformation, and of the stress field over time. In particular, we perform two sets of simulations: for the first one, we assign the characteristic time $t_{\mathrm{c}} = 50\,\mathrm{s}$ and we let $\alpha$ vary as $\alpha \in \{0.0, 0.2, 0.4, 0.6, 0.8, 1.0\}$, and, for $\alpha = 0.0$, we recover the non-fractional Darcy-Forchheimer model; for the second set, we take $\alpha = 0.4$, and we assign the characteristic time as $t_{\mathrm{c}} \in \{1\,\mathrm{s}, 50\,\mathrm{s}, 500\,\mathrm{s}\}$. With these test cases, we aim to observe the effects of the two new material constants, $\alpha$ and $t_{\mathrm{c}}$, related to the fractional model, on the behavior of the biphasic medium as a whole. The values of the material parameters adopted in the model are reported in Table 1.

The model is solved in ABAQUS® by having recourse to the subroutine "UMAT" for implementing Equation (59a), to the subroutine "UMATHT" for implementing (59b), and by selecting the option *"Fully coupled thermal-stress analysis"* in order to solve simultaneously for the deformation and the pore pressure. The latter option is selected to insert the terms $[C^{\mathrm{app}}_{P\chi}]$ and $[C_{\chi P}]$, which introduce the coupling between the deformation and the pore pressure in the linearization of the fractional Forchheimer model. We remark that the "UMATHT" subroutine, although originally meant for energy conservation, is used for implementing the mass conservation equation (59b) by using the similarity between these equations[66] (see Appendix A for detailed information).

For the simulations, C3D8T elements are used, which are 3D brick elements with three displacements and one pore pressure degree of freedom. Each element has eight integration points. The model has 23800 elements and 26535 nodes. A backward time integration scheme is adopted, with constant time increment of $\Delta t = 1\,s$.

## 8 Results and discussion

In this section, we present and discuss the numerical simulations of the compression tests described in the previous section. Emphasis will be placed on commenting the memory effects introduced by fractional Forchheimer's correction (59c). Our aim is to contextualize the effects introduced by the fractional law through the comparison of the numerical simulations performed under the assumption either of Darcy's law or of non-fractional Darcy-Forchheimer's law. We will focus on the description of the filtration velocity and on its coupling with the deformation of the solid phase, through the visualization of the system's evolution. In this respect, we recall that the filtration velocity is, by definition, the product of the fluid phase volumetric fraction which, because of the hypothesis of saturation, coincides with the porosity, and the velocity of the fluid relative to the solid. Therefore, for a specimen under compression, the filtration velocity of the fluid is not a mere consequence of its kinematic relative to the solid, since there exists also a direct feedback of the deformation on the fluid volumetric fraction. Indeed, under compression, it decreases until the compaction limit, which, in turn, places a lower bound on the volumetric deformation itself. As noticed, e.g., in[30], the natural condition $\Phi_{\mathrm{f}}(X,t) = J(X,t) - \Phi_{\mathrm{s}}(X) \geq 0$ yields the *"unilateral constraint"* $J(X,t) \geq \Phi_{\mathrm{s}}(X)$ at all points $X \in \mathscr{B}$ and at all times.

We remark that the simulated specimen consists of a hypothetical tissue, which, as anticipated above, could refer, with some modeling adjustments, to articular cartilage, since it features a complex microstructure that can manifest itself though memory effects[80,81].

## *8.1 Flow through the lateral surface of the specimen*

The magnitude of the filtration velocity is attained on a locus of points that, due to the axial symmetry of the problem under study, coincides with the circle defined by lower edge, i.e., $\mathscr{C}_{\mathrm{BL}} := \overline{\Gamma}_{\mathrm{B}} \cap \overline{\Gamma}_{\mathrm{L}}$, where the superimposed bar denotes the topological closure of the set to which it is applied. However, since the conditions on the motion imposed on the Dirichlet nodes of the mesh lying on $\Gamma_{\mathrm{B}}$ have led to small numerical artifacts in the computation of the filtration velocity, we study the evolution of the magnitude of this quantity in a relatively small, stripe-shaped subset of $\Gamma_{\mathrm{L}}$, containing $\mathscr{C}_{\mathrm{BL}}$. In particular, in this subset, we select the point of coordinates $X_{\mathrm{L}} = (1.5,\ 0\,, 0.14) \in \Gamma_{\mathrm{L}}$ (dimensions are given in millimetres), and we observe the evolution of the magnitude of the filtration velocity at this point, i.e., of $\|\boldsymbol{q}(X_{\mathrm{L}},t)\|$, for for different values of $\alpha$ and $t_{\mathrm{c}}$.

By computing $\|\boldsymbol{q}(X_{\mathrm{L}},t)\|$ for various values of $\alpha$ (see Figure 2), we notice that the behavior of the filtration velocity depends noticeably on the fractional order $\alpha$, whereas the value of the characteristic time scales the trend imposed by $\alpha$. In fact, both in the Darcy model and in the Darcy-Forchheimer model, the maximum of $\|\boldsymbol{q}(X_{\mathrm{L}},t)\|$ is registered at time $t = t_{\mathrm{ramp}}$ (see Figure 3). Yet, for the fractional Forchheimer model, the maximum of $\|\boldsymbol{q}(X_{\mathrm{L}},t)\|$ is observed at times larger than $t_{\mathrm{ramp}}$. Moreover, by setting $t_{\max}(\alpha) := \operatorname{argmax}_{t\in[0,t_{\mathrm{fin}}]}\{\|\boldsymbol{q}_{\alpha}(X_{\mathrm{L}},t)\|\}$, where $\boldsymbol{q}_{\alpha}$ indicates the filtration velocity computed for a given fractional order $\alpha$, we notice that $t_{\max}(\alpha)$ increases with $\alpha$. As a consequence of this behavior, we also observe a widening of the time interval over which $\|\boldsymbol{q}(X_{\mathrm{L}},t)\|$ grows monotonically in time. This result constitutes a delay in the attainment of $q_{\max} := \max_{t\in[0,t_{\mathrm{fin}}]}\{\|\boldsymbol{q}_{\alpha}(X_{\mathrm{L}},t)\|\}$, and is an expected feature of the model. Its physical interpretation could be related to the complexity of the microstructure, which manifests itself, for instance, through the tortuosity of the pore network, or to some inertial effects of the fluid taking place at the pore scale.

Because of the presence of Forchheimer's coefficient, $\|\boldsymbol{q}(X_{\mathrm{L}},t)\|$ is smaller than the one computed with the equivalent Darcy model (i.e., same setting and same parameters, but $\alpha = 0$ and $c_0 = 0$), while it is comparable with the one predicted by the non-fractional Darcy-Forchheimer model, although some important differences characterize the shapes of the curves in the two cases (see Figure 2).

Although there are studies in the literature in which the nonlinear effects associated with standard Forchheimer's model have been interpreted as a correction to the "true" permeability[45], the physics of the process described by the model presented in our work is different, and such conclusions can be limiting.

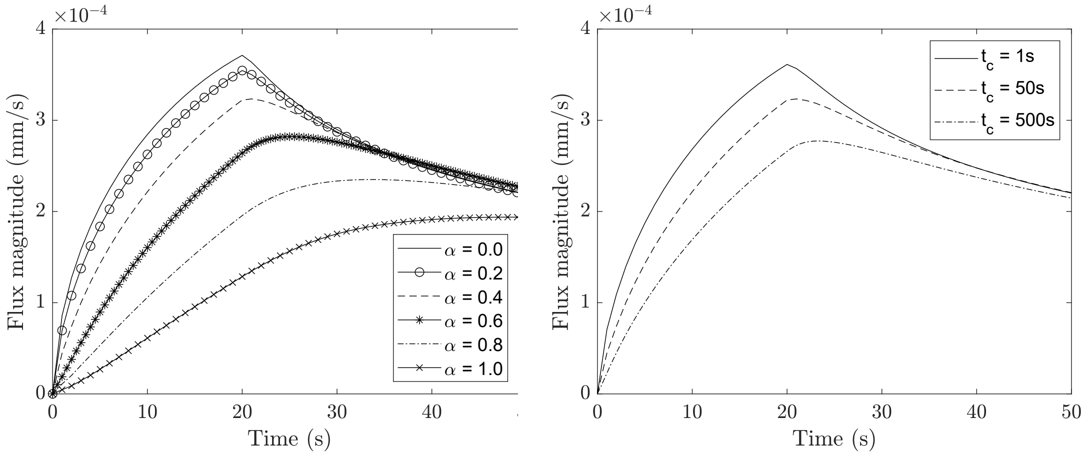


**(a)** Influence of $\alpha$ **(b)** Influence of $t_c$

**Figure 2.** Time evolution of the Euclidean norm $\|\boldsymbol{q}(X_\mathrm{L}, t)\|$ of the filtration velocity ("flux magnitude" in the figures), evaluated at the node corresponding to the point $X_\mathrm{L} = (1.5,\, 0\,, 0.14) \in \Gamma_\mathrm{L}$, for $\alpha = 0$ (i.e., standard Darcy-Forchheimer case) and for varying $\alpha \in \{0.2, 0.4, 0.6, 0.8, 1.0\}$ with $t_\mathrm{c} = 50s$. (left panel), and for $t_\mathrm{c} \in \{1\,\mathrm{s}, 50\,\mathrm{s}, 500\,\mathrm{s}\}$ with $\alpha = 0.4$ (right panel)

.

Indeed, the analogy with the correction of the permeability is evident only as long as we limit ourselves to a specific time frame in which the recent history of the filtration velocity is monotonically increasing or decreasing. In fact, if we study $\|\boldsymbol{q}(X_\mathrm{L}, t)\|$ for $t \in ]0, T_\mathrm{ramp}]$, we notice that the flow's history in the time integral will affect the determination of the flux itself in a predicable way. During the loading ramp, the efflux will grow because of the increasing compression, and it is already known that the time derivative of the filtration velocity inside the integral of Equation (59c) is positive, so that it exerts an antagonistic action with respect to equivalent Darcy's velocity. In this case, the filtration velocity $\boldsymbol{q}$ will be lower than the one in the corresponding standard Darcy-Forchheimer model, i.e., under the same boundary and initial conditions. Similarly, if we were to analyze the fluid outflow at the boundary for $t \;\in ]t_*, t_\mathrm{fin}]$, with $t_*$ sufficiently larger than $t_\mathrm{ramp}$, since the efflux decreases in time, the effect of the time integral would have a sympathetic effect with respect to the equivalent Darcy velocity, thereby producing results that would be associated with higher permeability. This would mean that, depending on the history of the fluid flow, the tissue would be more or less permeable.

Finally, it can be observed that, for the reasons delineated above, the increase in the fractional order implies that the flux magnitude relaxes more slowly towards the stationary state, as it is seen in Figure 3.

## *8.2 Fractional effects in the central region*

Next, we move on to analyze the dynamics of the interstitial fluid in the central region of the specimen. As shown in Figure 4c, in the center $X_\mathrm{O}$ of the bottom surface $\Gamma_\mathrm{B}$, the fractional Forchheimer correction induces values of the pore pressure that are even higher than those attained with the non-fractional

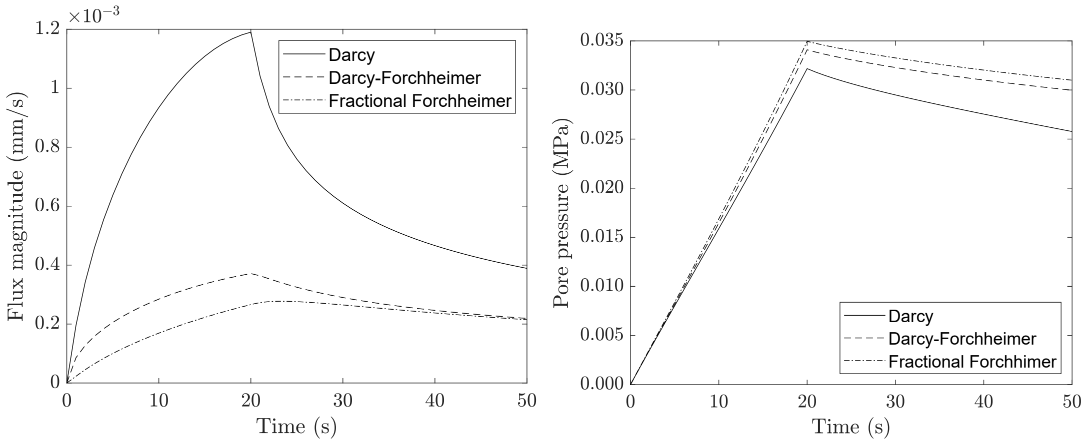


**(a)** Flux magnitude **(b)** Pore pressure

**Figure 3.** Comparison between the Darcy, the Darcy-Forchheimer and the fractional Forchheimer models of the time evolution of the Euclidean norm of the filtration velocity $\|\boldsymbol{q}(X_{\mathrm{L}}, t)\|$ ("Flux magnitude" in Figure 4(a)), evaluated at the node corresponding to the point $X_{\mathrm{L}} = (1.5,\ 0\,, 0.14) \in \Gamma_{\mathrm{L}}$, and of the pore pressure $P(X_{\mathrm{O}}, t)$ ("Pore pressure" in Figure 4(b)), evaluated at the node corresponding to the point $X_{\mathrm{O}} = (0, 0, 0) \in \Gamma_{\mathrm{B}}$, located at center of the bottom surface $\Gamma_{\mathrm{B}}$. For the simulation of the fractional Forchheimer model we selected $\alpha = 0.4$ and $t_{\mathrm{c}} = 50\,\mathrm{s}$.

Forchheimer model, which, in turn, predicts values already higher than in Darcy's model. Depending on the tissue under investigation, this result could be interpreted, for example, either as an accumulation of fluid in some regions of the pore network, which, because of tortuosity or other inhibitors of the hydraulic conductivity, may act as slowly emptying "buffers", or as the manifestation at the tissue scale of inertial or viscous effects and fluid-solid interactions at the pore scale.

Figure 4 displays the magnitude, predicted by the fractional Darcy-Forchheimer model, of the fluid radial filtration velocity evaluated at $X_{\mathrm{O}} \in \Gamma_{\mathrm{B}}$. This magnitude coincides with that of the total filtration velocity since $\Gamma_{\mathrm{B}}$ is in contact with the lower plate, which is impermeable. We notice that, in general, the filtration velocity of the fluid is smaller than the one obtained with the non-fractional Darcy model, i.e., for $c_0 = 0$ and $\alpha = 0$ (see Figure 3). However, during the maintenance phase of the loading history, and in response to the value of $\alpha$, there exist cases in which the fluid filtration velocity is higher than the one computed with the non-fractional Darcy-Forchheimer model (see Figure 4a). It is also interesting to note that, in $X_{\mathrm{O}} \in \Gamma_{\mathrm{B}}$, pore pressure increases monotonically with $\alpha$ (see Figure 4c), in spite of the transition in the fluid dynamic behavior, which, as explained above, passes from being slower to being faster than it would be in the non-fractional Darcy-Forchheimer case, depending on loading phase and on $\alpha$. Under the steady state loading, ($t > t_{\mathrm{ramp}}$), as time goes by, the history effect decreases, and the flux comes closer to the non-fractional model (see Figure 4a). Finally, only a very marginal impact of $\alpha$ on normal stress is observed (see Figure 4d).

If some chemical substances, like salts or drugs, were considered in our models, and if one were interested in studying the situation in which such substances, dissolved in the fluid, are for some reason

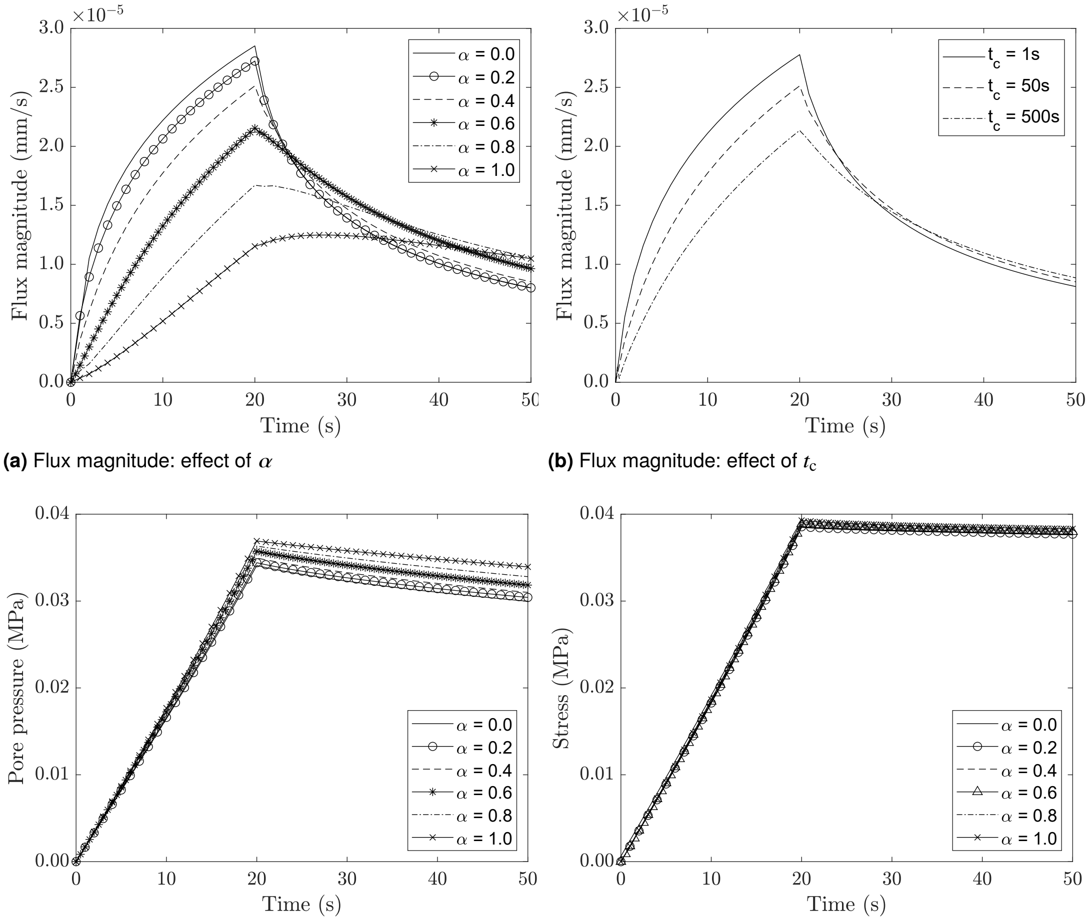


**(a)** Flux magnitude: effect of $\alpha$

**(b)** Flux magnitude: effect of $t_c$

**(c)** Pore pressure

**(d)** Stress

**Figure 4.** Time evolution of the Euclidean norm of the filtration velocity $\|\boldsymbol{q}(X_\mathrm{O}, t)\|$ ("flux magnitude" in Figure 3(a) and 3(b)), pore pressure $P(X_\mathrm{O}, t)$ ("pore pressure" in Figure 3(c)), and absolute value of the axial component of Cauchy stress, $|\sigma_3{}^3(X_\mathrm{O}, t)|$ ("Stress" in Figure 3(d)), evaluated at the node $X_\mathrm{O} = (0, 0, 0) \in \Gamma_\mathrm{B}$, located at center of the bottom surface $\Gamma_\mathrm{B}$ (corresponding to the origin of the given reference frame) for $\alpha = 0$ (non-fractional Darcy-Forchheimer case) and for varying $\alpha \in \{0.2, 0.4, 0.6, 0.8, 1.0\}$, with characteristic time $t_\mathrm{c} = 50\,\mathrm{s}$ (Figures 3(a), 3(c) and 3(d)), and for $t_\mathrm{c} \in \{1\,\mathrm{s}, 50\,\mathrm{s}, 500\,\mathrm{s}\}$, with $\alpha = 0.4$ (Figure 3(b)).

concentrated in the lower region of the specimen, then the radial filtration velocity of the fluid would be responsible for their transport towards the outer region of the specimen itself.

If we look at Figure 4, we notice that, for $\alpha = 0$, the filtration velocity tangential to $\Gamma_\mathrm{B}$ exhibits a much higher variance in values with respect to the case for $\alpha = 1$ that, instead, tends to change slowly.

Finally, a visual comparison between the non-fractional Forchheimer correction (which corresponds to the case $\alpha = 0$) and the fractional Forchheimer correction can be drawn by looking at Figures 5 and 6. At the time $t = t_{\mathrm{ramp}}$, we plot the spatial distributions of pore pressure, magnitude of the filtration velocity, magnitude of the displacement field, and von Mises stress both for the non-fractional Darcy-Forchheimer model and for the fractional Forchheimer's model with $\alpha = 0.4$. The plots for the pore pressure and for the magnitude of filtration velocity confirm that the region of interest for understanding the behavior of the fluid are the lower central region, where the overpressure area is located, and the lower lateral surface. The effect of the fractional order $\alpha$ on the coupling of the fluid with the solid phase is weak, since the spatial distribution of the total deformation and von Mises stress are barely affected (Figure 6) by $\alpha$, and the evolution of the normal stress on the center of the bottom surface is similar (see Figure 4d).

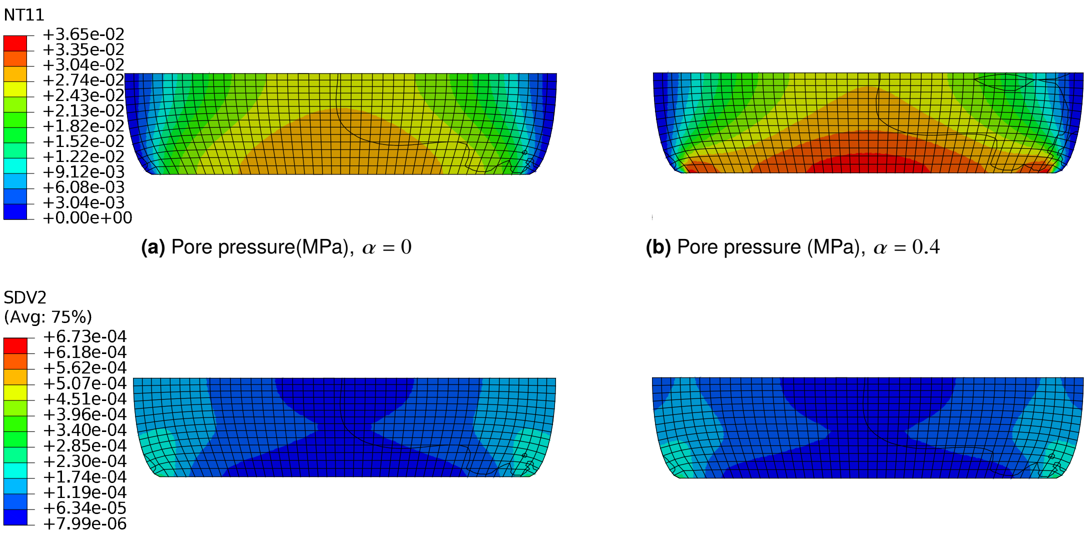


**(a)** Pore pressure(MPa), $\alpha = 0$

**(b)** Pore pressure (MPa), $\alpha = 0.4$

**(c)** Flux magnitude (mm/s), $\alpha = 0$

**(d)** Flux magnitude (mm/s), $\alpha = 0.4$

**Figure 5.** Comparison between the standard Darcy-Forchheimer model and the fractional Forchheimer model, with the choice of parameters $\alpha = 0.4$ and $t_c = 50\,\mathrm{s}$, at time $t = 20\,\mathrm{s}$, of the spatial distributions of the pore pressure (Figures (5a) and (5b)) and flux magnitude (Figures (5c) and (5d)). The black solid lines in the plots represent different layers of elements of the finite element discretization

## 9 Conclusions

In this work, we have described a hypothetical biological tissue, viewed as a saturated and hydrated porous medium, by formulating a mechanical model having the fractionalization of Forchheimer's correction to Darcy's law in finite deformations as target. This amounts to considering the concomitant effect of two deviations from the "classical" Darcian regime, and has been done with the purpose of studying a scenario that may originate in a tissue with a complex microstructure, like articular cartilage, when memory effects have to be combined with flow velocities that do not justify Darcy's approximation. The main motivation

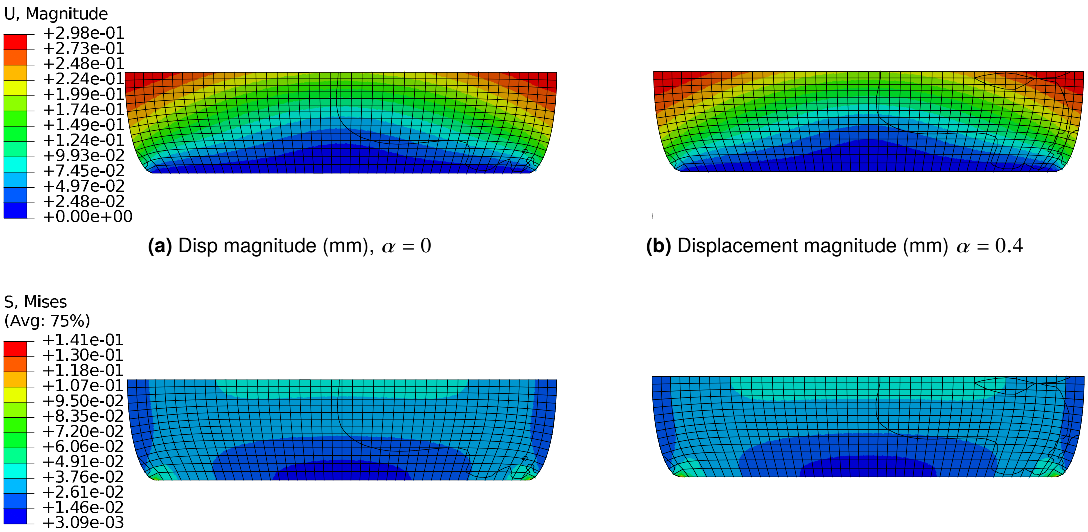


**(a)** Disp magnitude (mm), $\alpha = 0$

**(b)** Displacement magnitude (mm) $\alpha = 0.4$

**(c)** Von Mises Stress (MPa), $\alpha = 0$

**(d)** Von Mises Stress (MPa) $\alpha = 0.4$

**Figure 6.** Comparison between the standard Darcy-Forchheimer model and the fractional Forchheimer model, with the choice of parameters $\alpha = 0.4$ and $t_c = 50\,\mathrm{s}$, at time $t = 20\,\mathrm{s}$, of the spatial distributions of the displacement magnitude (Figures (6a) and (6b)) and of the von Mises stress (Figures (6c) and (6d)). The black solid lines in the plots represent different layers of elements of the finite element discretization

for undertaking this study is the generalization of a class of flow models already existing in the literature, and aiming at describing Darcy's law with memory, to the case in which the interactions of the fluid with the solid matrix require to include inertial effects.

This work sets the modelling framework for understanding the role of the fluid flow in the deformation process of biological media. With the recent development of numerical methods coupled with image analysis (CFD-IA, [123]), image-based simulation from high-resolution x-ray tomography and multiphoton microscopy of native meniscal tissue [124,125] can reveal the fluid flow at the pore scale. Ongoing work on FSI (fluid-structure interaction) - IA, which couples FEM and meshless fluid flow solvers (such SPH), will give rise to running simulation of deforming the solid and fluid phases of native tissue architecture, retaining the complexity of the pores' morphology. These simulations will provide the data to verify the model proposed here and elsewhere [65] as well as contribute to one of the main questions when dealing with fractional models, i.e., what is the relation between the fractional parameters and the architecture of the tissue. In other words, can we give a physical meaning to the fractional parameters?

To assess what our model predicts for a very typical benchmark problem, we have solved an initial and boundary value problem that simulates the uni-axial compression of a cylindrical specimen of the hypothetical tissue under investigation, and, to this end, we have devised a numerical procedure capable of framing fractional and highly nonlinear flow laws within the context of finite deformation poro-elasticity, and we implemented it in ABAQUS®.

In spite of the fact that, by applying the fractional operator only to the filtration velocity, we have particularized the constitutive picture presented in[54], our research encompasses two essential generalizations. The first one pertains to the definition of the fractional operator applied to the filtration velocity, and describes the non-linearity of the flow model related to the passage from the Darcian to the Forchheimer regime. Indeed, in Equation (53) we define a generalized Caputo derivative in which the kernel of the integral operator features the resistivity tensor $\boldsymbol{r}_{\mathrm{F}}(\|\boldsymbol{q}(\tau)\|)$ applied to the Truesdell derivative of $\boldsymbol{q}$ at time $\tau$, $\mathcal{T}_{\mathrm{S}}\boldsymbol{q}(\tau)$. This yields a modified Cattaneo's model for the filtration velocity $\boldsymbol{q}$ that weighs the evolution of $\boldsymbol{q}$ by means of a resistivity coefficient that depends on $\boldsymbol{q}$ itself in a non-linear way.

The second generalization is inherent to the coupling between flow and deformation. Indeed, since our approach is entirely formulated for finite deformations, it requires to employ the *correct* objective derivative for the kinematic parameter chosen to describe the filtration motion of the fluid through the deforming solid matrix. In this respect, since we have chosen the filtration velocity $\boldsymbol{q}$, which is a pseudo-vector, we have reformulated Caputo's classical fractional derivative of $\boldsymbol{q}$ in such a way that the time derivative of $\boldsymbol{q}$, featuring under the integral operator in the classical definition, is replaced by its Truesdell derivative, $\mathcal{T}_{\mathrm{S}}\boldsymbol{q}$. Although the use of the objective rates is well established in Continuum Mechanics, its employment in the present context makes it clear how the deformation affects such reformulation. Indeed, looking at Equation (58), the pull-back of the "modified" Caputo derivative, i.e., with $\mathcal{T}_{\mathrm{S}}\boldsymbol{q}$ in lieu of $\dot{\boldsymbol{q}}$, transforms it into a Caputo-type fractional derivative for $\boldsymbol{Q}$, i.e., expressed in terms of $\dot{\boldsymbol{Q}}(\tau)$, at the price of introducing $J(t)\boldsymbol{F}^{-1}(t)$ and $J^{-1}(\tau)\boldsymbol{F}(\tau)$ in the kernel of the corresponding integral operator: the latter defines the push-forward of $\dot{\boldsymbol{Q}}(\tau)$ to the placement of the medium at time $\tau$, whereas the former defines the pull-back, to the reference placement, of the integral in Equation (58), which captures the whole history of the medium from $t_{\mathrm{in}}$ to $t$.

We point out that the fractional order $\alpha$, by analogy with Cattaneo's model[126], can be interpreted as a measure of how much the history of the process influences the filtration velocity $\boldsymbol{q}$. Depending on the history, such effect can be antagonizing or sympathetic, and, in the latter case, it can lead to an outflow greater than the one obtainable in the standard Darcy-Forchheimer model under the same loading conditions. We have also observed that the introduction of the fractional law leads to a higher value of pressure in the central region with respect to the Darcy and Darcy-Forchheimer models, although we did not observe coupling effects that could alter significantly the stress state of the solid phase. To this end, we remark that different couplings could be studied by considering a different fractional law[54], or by introducing remodeling effects, either structural[121,127] or due to growth (a fractional model of which has been recently presented in[128]) or due to the spatial reorientation of fibers[46,119,127,129–131].

A different kind of nonlinear coupling, that we would be interested to study in the future, is the combined effect of a fractional Forchheimer's law for the flow and a fractional viscoelastic behavior of the solid phase. This approach would aim at a better characterization of the mechanical behaviour of biological tissues for which fractional models have been successful in describing the solid phase, but no fractional law has been proposed to describe the interstitial fluid.

## Conflict of Interests

The Authors declare that they have no conflict of interests.

## Authors' contributions

All authors have equally contributed to this work. This work is part of a joint research project conducted in equal measure by the authors Sachin Gunda and Alessandro Giammarini, and constitutes an intersection of their respective PhD programs.

### Acknowledgements

This work is partially supported by MIUR (Italian Ministry of Education, Universities and Research) through the PRIN project n. 2017KL4EF3 on *"Mathematics of active materials: From mechanobiology to smart devices."* Sachin Gunda would like to acknowledge the financial support of the Prime Minister's Research Fellowship (PMRF ID: 2502381), Ministry of Education, Govt. of India, for his graduate study at the Indian Institute of Technology Madras. Sachin Gunda would like to acknowledge the International Immersion Experience Award, Office of Global Engagement, IIT Madras, for the financial support. Sachin Gunda and Sundararajan Natarajan acknowledge using the computing resources at HPCE, IIT Madras.

## References

1. Ateshian G. On the theory of reactive mixtures for modeling biological growth. *Biomechanics and Modeling in Mechanobiology* 2007; 6(6): 423–445. DOI:10.1007/s10237-006-0070-x.
2. Mansour J. *Biomechanics of cartilage*, chapter 5. 2013. pp. 69–83.
3. Torzilli P and Mow VC. On the fundamental fluid transport mechanisms through normal and pathological articular cartilage during function—i the formulation. *Journal of Biomechanics* 1976; 9(8): 541–552. DOI: 10.1016/0021-9290(76)90071-3.
4. Torzilli P and Mow VC. On the fundamental fluid transport mechanisms through normal and pathological articular cartilage during function—II. the analysis, solution and conclusions. *Journal of Biomechanics* 1976; 9(9): 587–606. DOI:10.1016/0021-9290(76)90100-7.
5. Mow VC, Kuei SC, Lai WM et al. Biphasic creep and stress relaxation of articular cartilage in compression: Theory and experiments. *Journal of Biomechanical Engineering* 1980; 102(1): 73–84. DOI:10.1115/1.3138202.
6. Mow VC, Holmes MH and Lai WM. Fluid transport and mechanical properties of articular cartilage: a review. *J Biomech* 1984; 17(5): 377–394.
7. Holmes M and Mow V. The nonlinear characteristics of soft gels and hydrated connective tissues in ultrafiltration. *Journal of biomechanics* 1990; 23: 1145–1156. DOI:10.1016/0021-9290(90)90007-P.
8. Byrne H and Preziosi L. Modelling solid tumour growth using the theory of mixtures. *Mathematical Medicine and Biology* 2003; 20(4): 341–366. DOI:10.1093/imammb/20.4.341.
9. Klisch SM, Chen SS, Sah RL et al. A growth mixture theory for cartilage with application to growth-related experiments on cartilage explants. *Journal of Biomechanical Engineering* 2003; 125(2): 169–179. DOI: 10.1115/1.1560144.
10. Garikipati K, Arruda E, Grosh K et al. A continuum treatment of growth in biological tissue: the coupling of mass transport and mechanics. *J Mech Phys Solids* 2004; 52: 1595–1625. DOI:10.1016/j.jmps.2004.01.004.
11. Huyghe JM, Loon RV and Baaijens F. Fluid-solid mixtures and electrochemomechanics: the simplicity of lagrangian mixture theory. *Computational & Applied Mathematics* 2004; 23(2-3). DOI:10.1590/s0101-82052004000200008.

12. Loret B and Simões F. A framework for deformation, generalized diffusion, mass transfer and growth in multi-species multi-phase biological tissues. *Eur J Mech A* 2005; 24: 757–781. DOI:10.1016/j.euromechsol.2005.05.005.
13. Grillo A, Federico S and Wittum G. Growth, mass transfer, and remodeling in fiber-reinforced, multi-constituent materials. *Int J Nonlinear Mech* 2012; 47: 388–401. DOI:10.1016/j.ijnonlinmec.2011.09.026.
14. MAROUDAS A and BULLOUGH P. Permeability of articular cartilage. *Nature* 1968; 219(5160): 1260–1261. DOI:10.1038/2191260a0.
15. Guilak F. Compression-induced changes in the shape and volume of the chondrocyte nucleus. *Journal of Biomechanics* 1995; 28(12): 1529–1541. DOI:10.1016/0021-9290(95)00100-x.
16. Qiu G and Pence T. Remarks on the behavior of simple directionally reinforced incompressible non-linearly elastic solids. *Journal of Elasticity* 1997; 49(1): 1–30. DOI:10.1023/a:1007410321319.
17. Holzapfel G, Gasser T and Ogden R. A new constitutive framework for arterial wall mechanics and a comparative study of material models. *J Elast* 2000; 61(1-3): 1–48.
18. Mollenhauer J, Aurich M, Muehleman C et al. X-ray diffraction of the molecular substructure of human articular cartilage. *Connective Tissue Research* 2003; 44(5): 201–207. DOI:10.1080/03008200390244005.
19. Merodio J and Ogden R. Mechanical response of fiber-reinforced incompressible non-linearly elastic solids. *Int J Nonlinear Mech* 2005; 40(2-3): 213–227. DOI:10.1016/j.ijnonlinmec.2004.05.003.
20. Merodio J. On constitutive equations for fiber-reinforced nonlinearly viscoelastic solids. *Mechanics Research Communications* 2006; 33(6): 764–770. DOI:10.1016/j.mechrescom.2006.03.009.
21. Athanasiou KA, Darling EM and Hu JC. *Articular Cartilage Tissue Engineering*. Springer International Publishing, 2010. DOI:10.1007/978-3-031-02578-5.
22. Lanir Y. Constitutive equations for fibrous connective tissues. *J Biomech* 1983; 16: 1–12.
23. Gasser T, Ogden R and Holzapfel G. Hyperelastic modelling of arterial layers with distributed collagen fibre orientations. *J R Soc Interface* 2006; 3: 15–35. DOI:10.1098/rsif.2005.0073.
24. Federico S and Herzog W. Towards an analytical model of soft biological tissues. *J Biomech* 2008; 41: 3309–3313. DOI:https://doi.org/10.1016/j.jbiomech.2008.05.039.
25. Federico S and Herzog W. On the permeability of fibre-reinforced porous materials. *Int J Solids Struct* 2008; 45: 2160–2172. DOI:https://doi.org/10.1016/j.ijsolstr.2007.11.014.
26. Federico S and Gasser T. Non-linear elasticity of biological tissues with statistical fibre orientation. *J R Soc Interface* 2010; 7: 955–966. DOI:10.1098/rsif.2009.0502.
27. Carfagna M and Grillo A. The spherical design algorithm in the numerical simulation of biological tissues with statistical fibre-reinforcement. *Comput Vis Sci* 2017; 18: 157–184. DOI:10.1007/s00791-017-0278-6.
28. Holzapfel G and Ogden R. On fiber dispersion models: Exclusion of compressed fibers and spurious model comparisons. *J Elast* 2017; 129(1-2): 49–68. DOI:10.1007/s10659-016-9605-2.
29. Holzapfel G, Ogden R and Sherifova S. On fibre dispersion modelling of soft biological tissues: a review. *Proc R Soc A* 2019; 475(2224): 1–22. DOI:https://doi.org/10.1098/rspa.2018.0736.
30. Federico S and Grillo A. Elasticity and permeability of porous fibre-reinforced materials under large deformations. *Mech Mater* 2012; 44: 58–71. DOI:10.1016/j.mechmat.2011.07.010.
31. Tomic A, Grillo A and Federico S. Poroelastic materials reinforced by statistically oriented fibres — numerical implementation and application to articular cartilage. *IMA J Appl Math* 2014; 79: 1027–1059. DOI:10.1093/imamat/hxu039.
32. Quinn T, Dierickx P and Grodzinsky A. Glycosaminoglycan network geometry may contribute to anisotropic hydraulic permeability in cartilage under compression. *Journal of Biomechanics* 2001; 34(11): 1483–1490.

DOI:10.1016/s0021-9290(01)00103-8.

33. Ateshian G and Weiss J. Anisotropic hydraulic permeability under finite deformation. *J Biomech Engng* 2010; 132: 111004–1–111004–7. DOI:10.1115/1.4002588.
34. Holzapfel GA and Ogden RW. Constitutive modelling of arteries. *Proceedings of the Royal Society A: Mathematical, Physical and Engineering Sciences* 2010; 466(2118): 1551–1597. DOI:10.1098/rspa.2010.0058.
35. Pierce DM, Ricken T and Holzapfel GA. A hyperelastic biphasic fibre-reinforced model of articular cartilage considering distributed collagen fibre orientations: continuum basis, computational aspects and applications. *Computer Methods in Biomechanics and Biomedical Engineering* 2013; 16(12): 1344–1361. DOI:10.1080/10255842.2012.670854.
36. Holzapfel GA, Niestrawska JA, Ogden RW et al. Modelling non-symmetric collagen fibre dispersion in arterial walls. *Journal of The Royal Society Interface* 2015; 12(106): 20150188. DOI:10.1098/rsif.2015.0188.
37. Holzapfel GA and Ogden RW. On the tension–compression switch in soft fibrous solids. *European Journal of Mechanics - A/Solids* 2015; 49: 561–569. DOI:10.1016/j.euromechsol.2014.09.005.
38. Hashlamoun K, Grillo A and Federico S. Efficient evaluation of the material response of tissues reinforced by statistically oriented fibres. *Z Angew Math Phys* 2016; 67: 113–145. DOI:10.1007/s10237-006-0049-7.
39. Li K, Ogden R and Holzapfel G. Computational method for excluding fibers under compression in modeling soft fibrous solids. *Eur J Mech A/Solids* 2016; 57: 178–193. DOI:10.1016/j.euromechsol.2015.11.003.
40. Gizzi A, Pandolfi A and Vasta M. A generalized statistical approach for modeling fiber-reinforced materials. *Journal of Engineering Mathematics* 2017; 109(1): 211–226. DOI:10.1007/s10665-017-9943-5.
41. Holzapfel GA and Ogden RW. A damage model for collagen fibres with an application to collagenous soft tissues. *Proceedings of the Royal Society A: Mathematical, Physical and Engineering Sciences* 2020; 476(2236). DOI:10.1098/rspa.2019.0821.
42. Federico S and Grillo A. Erratum to: Poroelastic materials reinforced by statistically oriented fibres - numerical implementation and application to articular cartilage. *IMA Journal of Applied Mathematics* 2014; 80(1): 233–234. DOI:10.1093/imamat/hxu059.
43. Mow VC, Ratcliffe A and Poole AR. Cartilage and diarthrodial joints as paradigms for hierarchical materials and structures. *Biomaterials* 1992; 13(2): 67–97. DOI:10.1016/0142-9612(92)90001-5.
44. Han SK, Federico S, Grillo A et al. The mechanical behaviour of chondrocytes predicted with a micro-structural model of articular cartilage. *Biomechanics and Modeling in Mechanobiology* 2006; 6(3): 139–150. DOI:10.1007/s10237-006-0016-3.
45. Grillo A, Carfagna M and Federico S. Non-Darcian flow in fibre-reinforced biological tissues. *Meccanica* 2017; 52: 3299–3320. DOI:10.1007/s11012-017-0679-0.
46. Di Stefano S, Carfagna M, Knodel MM et al. Anelastic reorganisation of fibre-reinforced biological tissues. *Computing and Visualization in Science* 2019; 20(3-6): 95–109. DOI:10.1007/s00791-019-00313-1.
47. Alaimo G, Piccolo V, Cutolo A et al. A fractional order theory of poroelasticity. *Mechanics Research Communications* 2019; 100: 103395. DOI:10.1016/j.mechrescom.2019.103395.
48. Hassanizadeh S. Derivation of basic equations of mass transp. porous med., part 2. generalized Darcy's and Fick's laws. *Adv Water Resour* 1986; 9: 207–222.
49. Bear J and Bachmat Y. *Introduction to Modeling of Transport Phenomena in Porous Media*. Kluwer, Dordrecht, 1990.
50. Bennethum L, Murad M and Cushman J. Macroscale thermodynamics and the chemical potential for swelling porous media. *Transport in Porous Media* 2000; 39(2): 187–225. DOI:10.1023/a:1006661330427.

51. Khaled AR and Vafai K. The role of porous media in modeling flow and heat transfer in biological tissues. *International Journal of Heat and Mass Transfer* 2003; 46(26): 4989–5003. DOI:10.1016/s0017-9310(03)00301-6.
52. Grillo A, Carfagna M and Federico S. The Darcy-Forchheimer law for modelling fluid flow in biological tissues. *Theoretical and Applied Mechanics (TEOPM7)* 2014; 41(4): 283–322.
53. Thauvin F and Mohanty KK. Network modeling of non-darcy flow through porous media. *Transport in Porous Media* 1998; 31(1): 19–37. DOI:10.1023/a:1006558926606.
54. Deseri L and Zingales M. A mechanical picture of fractional-order Darcy equation. *Communications in Nonlinear Science and Numerical Simulation* 2015; 20(3): 940–949. DOI:10.1016/j.cnsns.2014.06.021.
55. Jang J and Chen J. Variable porosity and thermal dispersion effects on vortex instability of a horizontal natural convection flow in a saturated porous medium. *Wärme- und Stoffübertragung* 1994; 29. DOI: doi.org/10.1007/BF01548599.
56. Bulle R, Alotta G, Marchiori G et al. The human meniscus behaves as a functionally graded fractional porous medium under confined compression conditions. *Applied Sciences* 2021; 11(20). DOI:10.3390/app11209405.
57. Abd AEGE and Milczarek JJ. Neutron radiography study of water absorption in porous building materials: anomalous diffusion analysis. *Journal of Physics D, Applied Physics* 2004; 37. DOI:10.1088/0022-3727/37/16/013.
58. Ramos N, Delgado JM and de Freitas V. Anomalous diffusion during water absorption in porous building materials – experimental evidence. In *Diffusion in Solids and Liquids III*, *Defect and Diffusion Forum*, volume 273. Trans Tech Publications Ltd, pp. 156–161. DOI:10.4028/www.scientific.net/DDF.273-276.156.
59. Küntz M and Lavallée P. Experimental evidence and theoretical analysis of anomalous diffusion during water infiltration in porous building materials. *Journal of Physics D: Applied Physics* 2001; 34(16): 2547–2554. DOI:10.1088/0022-3727/34/16/322.
60. de Azevedo EN, da Silva DV, de Souza RE et al. Water ingress in y-type zeolite: Anomalous moisture-dependent transport diffusivity. *Phys Rev E* 2006; 74: 041108. DOI:10.1103/PhysRevE.74.041108.
61. Iaffaldano G, Caputo M and Martino S. Experimental and theoretical memory diffusion of water in sand. *Hydrology and Earth System Sciences* 2005; 10: 93–100. DOI:10.5194/hessd-2-1329-2005.
62. Caputo M. Models of flux in porous media with memory. *Water Resources Research* 2000; 36(3): 693–705. DOI:10.1029/1999wr900299.
63. Meerschaert M, Mortensen J and Wheatcraft S. Fractional vector calculus for fractional advection-diffusion. *Physica A: Statistical Mechanics and its Applications* 2006; 367: 181–190. DOI:10.1016/j.physa.2005.11.015.
64. Sapora A, Cornetti P, Chiaia B et al. Nonlocal diffusion in porous media: A spatial fractional approach. *Journal of Engineering Mechanics* 2016; 143: D4016007. DOI:10.1061/(ASCE)EM.1943-7889.0001105.
65. Gunda S, Natarajan S and Barrera O. On the fractional transversely isotropic functionally graded nature of soft biological tissues: Application to the meniscal tissue. *Journal of the Mechanical Behavior of Biomedical Materials* 2023; 143: 105855.
66. Barrera O. A unified modelling and simulation for coupled anomalous transport in porous media and its finite element implementation. *Computational Mechanics* 2021; 68: 1267–1282.
67. Caputo M and Plastino W. Diffusion in porous layers with memory. *Geophysical Journal International* 2004; 158(1): 385–396. DOI:10.1111/j.1365-246x.2004.02290.x.
68. Uzuner S, Li L, Kucuk S et al. Changes in knee joint mechanics after medial meniscectomy determined with a poromechanical model. *Journal of Biomechanical Engineering* 2020; 142(10). DOI:10.1115/1.4047343.

69. Amiri F, Bologna E, Nuzzo G et al. Fractional-order poromechanics for a fully saturated biological tissue: Biomechanics of meniscus. *International Journal for Numerical Methods in Biomedical Engineering* 2023; DOI:10.1002/cnm.3732.
70. Nutting P. A new general law of deformation. *Journal of the Franklin Institute* 1921; 191(5): 679–685. DOI:10.1016/s0016-0032(21)90171-6.
71. Carpinteri A and Mainardi F (eds.) *Fractals and Fractional Calculus in Continuum Mechanics*. Springer Vienna, 1997. ISBN 321182913X.
72. Paola MD, Pirrotta A and Valenza A. Visco-elastic behavior through fractional calculus: An easier method for best fitting experimental results. *Mechanics of Materials* 2011; 43(12): 799–806. DOI: 10.1016/j.mechmat.2011.08.016.
73. Ionescu C, Lopes A, Copot D et al. The role of fractional calculus in modeling biological phenomena: A review. *Communications in Nonlinear Science and Numerical Simulation* 2017; 51: 141–159. DOI: 10.1016/j.cnsns.2017.04.001.
74. Maes JA and Donahue TH. Time dependent properties of bovine meniscal attachments: Stress relaxation and creep. *Journal of Biomechanics* 2006; 39(16): 3055–3061. DOI:10.1016/j.jbiomech.2005.09.025.
75. Camarda L, Bologna E, Pavan D et al. Posterior meniscal root repair: a biomechanical comparison between human and porcine menisci. *Muscle Ligaments and Tendons Journal* 2019; 09(01): 76. DOI: 10.32098/mltj.01.2019.03.
76. Bologna E, Paola MD, Dayal K et al. Fractional-order nonlinear hereditariness of tendons and ligaments of the human knee. *Philosophical Transactions of the Royal Society A: Mathematical, Physical and Engineering Sciences* 2020; 378(2172): 20190294. DOI:10.1098/rsta.2019.0294.
77. Norberg C, Filippone G, Andreopoulos F et al. Viscoelastic and equilibrium shear properties of human meniscus: Relationships with tissue structure and composition. *Journal of Biomechanics* 2021; 120: 110343. DOI:10.1016/j.jbiomech.2021.110343.
78. Aspden RM and Hukins DW. Collagen organization in articular cartilage, determined by x-ray diffraction, and its relationship to tissue function. *Proceedings of the Royal Society of London Series B Biological Sciences* 1981; 212(1188): 299–304. DOI:10.1098/rspb.1981.0040.
79. Pajerski J. Nonlinear biphasic microstructural numerical analysis of articular cartilage and chondrocytes. *MSc Thesis* 2010; .
80. Magin RL and Royston TJ. Fractional-order elastic models of cartilage: A multi-scale approach. *Communications in Nonlinear Science and Numerical Simulation* 2010; 15(3): 657–664. DOI:10.1016/j.cnsns.2009.05.008.
81. Smyth PA and Green I. Fractional calculus model of articular cartilage based on experimental stress-relaxation. *Mechanics of Time-Dependent Materials* 2015; 19(2): 209–228. DOI:10.1007/s11043-015-9260-1.
82. Quiligotti S. On bulk growth mechanics of solid-fluid mixtures: kinematics and invariance requirements. *Theoret Appl Mech* 2002; 28-29: 277–288.
83. Quiligotti S, Maugin G and F dell'Isola. An eshelbian approach to the nonlinear mechanics of constrained solid-fluid mixtures. *Acta Mech* 2003; 160: 45–60. DOI:10.1007/s00707-002-0968-z.
84. Grillo A, Guaily A, Giverso C et al. Non-linear model for compression tests on articular cartilage. *Journal of Biomechanical Engineering* 2015; 137(7). DOI:10.1115/1.4030310.
85. Holzapfel G and Gasser T. A viscoelastic model for fiber-reinforced composites at finite strains: continuum basis, computational aspects and applications. *Mech Res Commun* 2002; 29: 477–483. DOI:https://doi.org/10.1016/S0045-7825(00)00323-6.

86. Hassanizadeh M and Gray WG. General conservation equations for multi-phase systems: 1. averaging procedure. *Advances in Water Resources* 1979; 2: 131–144. DOI:10.1016/0309-1708(79)90025-3.
87. Hassanizadeh SM. Derivation of basic equations of mass transport in porous media, part 1. macroscopic balance laws. *Advances in Water Resources* 1986; 9(4): 196–206. DOI:10.1016/0309-1708(86)90024-2.
88. Bennethum L and Giorgi T. Generalized Forchheimer equation for two-phase flow based on hybrid mixture theory. *Transport in Porous Media* 1997; 26: 261–275.
89. Köpf M, Corinth C, Haferkamp O et al. Anomalous diffusion of water in biological tissues. *Biophysical Journal* 1996; 70(6): 2950–2958. DOI:10.1016/s0006-3495(96)79865-x.
90. Özarslan E, Basser PJ, Shepherd TM et al. Observation of anomalous diffusion in excised tissue by characterizing the diffusion-time dependence of the MR signal. *Journal of Magnetic Resonance* 2006; 183(2): 315–323. DOI:10.1016/j.jmr.2006.08.009.
91. Magin RL, Abdullah O, Baleanu D et al. Anomalous diffusion expressed through fractional order differential operators in the bloch–torrey equation. *Journal of Magnetic Resonance* 2008; 190(2): 255–270. DOI:10.1016/j.jmr.2007.11.007.
92. Magin RL, Ingo C, Colon-Perez L et al. Characterization of anomalous diffusion in porous biological tissues using fractional order derivatives and entropy. *Microporous and Mesoporous Materials* 2013; 178: 39–43. DOI:10.1016/j.micromeso.2013.02.054.
93. Magin RL, Li W, Velasco MP et al. Anomalous NMR relaxation in cartilage matrix components and native cartilage: Fractional-order models. *Journal of Magnetic Resonance* 2011; 210(2): 184–191. DOI:10.1016/j.jmr.2011.03.006.
94. Federico S and Herzog W. On the anisotropy and inhomogeneity of permeability in articular cartilage. *Biomech Model Mechanobiol* 2008; 7: 367–378. DOI:10.1007/s10237-007-0091-0.
95. Marsden J and Hughes T. *Mathematical Foundations of Elasticity*. Dover Publications, Inc., Mineola, New York, 1983.
96. Federico S, Grillo A and Segev R. Material description of fluxes in terms of differential forms. *Continuum Mechanics and Thermodynamics* 2015; 28(1-2): 379–390. DOI:10.1007/s00161-015-0437-2.
97. Grillo A, Giverso C, Favino M et al. Mass transport in porous media with variable mass. In *Advanced Structured Materials*. Springer Berlin Heidelberg, 2012. pp. 27–61. DOI:10.1007/978-3-642-30532-0_2.
98. Bonet J and Wood R. *Nonlinear Continuum Mechanics for Finite Element Analysis*. Cambridge University Press, New York, 2008.
99. Hassanizadeh SM and Leijnse A. A non-linear theory of high-concentration-gradient dispersion in porous media. *Advances in Water Resources* 1995; 18(4): 203–215. DOI:10.1016/0309-1708(95)00012-8.
100. Liu I. Method of lagrange multipliers for exploitation of the entropy principle. *Archive Rational Mech Anal* 1972; 46: 131–148.
101. Ateshian G and Humphrey J. Continuum mixture models of biological growth and remodeling: Past successes and future opportunities. *Annual Review of Biomedical Engineering* 2012; 14(1): 97–111. DOI:10.1146/annurev-bioeng-071910-124726.
102. Sanchez-Palencia E. Homogenization method for the study of composite media. In *Lecture Notes in Mathematics*. Springer Berlin Heidelberg, 1983. pp. 192–214. DOI:10.1007/bfb0062368.
103. Cioranescu D and Donato P. *An Introduction to Homogenization*, volume 17. Oxford University Press, 1999.
104. Penta R, Ambrosi D and Shipley RJ. Effective governing equations for poroelastic growing media. *The Quarterly Journal of Mechanics and Applied Mathematics* 2014; 67(1): 69–91. DOI:10.1093/qjmam/hbt024.

105. Whitaker S. The forchheimer equation: A theoretical development. *Transport in Porous Media* 1996; 25(1): 27–61. DOI:10.1007/bf00141261.
106. Grillo A, Logashenko D, Stichel S et al. Forchheimer's correction in modelling flow and transport in fractured porous media. *Computing and Visualization in Science* 2012; 15: 169–190.
107. Tek M, Coats K and Katz D. The effect of turbulence on flow of natural gas through porous reservoirs. *Journal of Petroleum Technology* 1962; 14(07): 799–806. DOI:10.2118/147-pa.
108. Geertsma J. Estimating the coefficient of inertial resistance in fluid flow through porous media. *Society of Petroleum Engineers Journal* 1974; 14(05): 445–450. DOI:10.2118/4706-pa.
109. Wang X, Thauvin F and Mohanty K. Non-darcy flow through anisotropic porous media. *Chemical Engineering Science* 1999; 54(12): 1859–1869. DOI:10.1016/s0009-2509(99)00018-4.
110. Federico S. The truesdell rate in continuum mechanics. *Zeitschrift für angewandte Mathematik und Physik* 2022; 73(3). DOI:10.1007/s00033-022-01738-4.
111. Atanacković T, Konjik S, Oparnica L et al. The cattaneo type space-time fractional heat conduction equation. *Continuum Mechanics and Thermodynamics* 2011; 24(4-6): 293–311. DOI:10.1007/s00161-011-0199-4.
112. Želi V and Zorica D. Analytical and numerical treatment of the heat conduction equation obtained via time-fractional distributed-order heat conduction law. *Physica A: Statistical Mechanics and its Applications* 2018; 492: 2316–2335. DOI:10.1016/j.physa.2017.11.150.
113. Eringen A. *Mechanics of continua 2nd edition*. Robert E. Krieger Publishing Company, 1980.
114. Podlubny I. *Fractional Differential Equations: An Introduction to Fractional Derivatives, Fractional Differential Equations, to Methods of Their Solution and Some of Their Applications (ISSN Book 198)*. Academic Press, 1998. ISBN 9780080531984.
115. Grillo A, Prohl R and Wittum G. A poroplastic model of structural reorganisation in porous media of biomechanical interest. *Continuum Mech Therm* 2016; 28: 579–601. DOI:10.1007/s00161-015-0465-y.
116. Grillo A, Prohl R and Wittum G. A generalised algorithm for anelastic processes in elastoplasticity and biomechanics. *Math Mech Solids* 2017; 22(3): 502–527. DOI:10.1177/1081286515598661.
117. Simo J and Hughes T. *Computational Inelasticity*. Springer, New York, 1998.
118. *Abaqus 6.11 Theory Manual*. United States: Dassault Systèmes Simulia Corp, 2011.
119. Knodel M, Di Stefano S, Nägel A et al. An efficient algorithm for biomechanical problems based on a fully implicit nested newton solver. *Theoretical and Applied Mechanics* 2022; 49(2): 183–221. DOI: 10.2298/tam221115012k.
120. Giverso C, Stefano SD, Grillo A et al. A three dimensional model of multicellular aggregate compression. *Soft Matter* 2019; 15(48): 10005–10019. DOI:10.1039/c9sm01628g.
121. Di Stefano S, Giammarini A, Giverso C et al. An elasto-plastic biphasic model of the compression of multicellular aggregates: the influence of fluid on stress and deformation. *Z Angew Math Phys* 2022; 73: 79–118. DOI:https://doi.org/10.1007/s00033-022-01692-1.
122. Holmes MH. Finite deformation of soft tissue: Analysis of a mixture model in uni-axial compression. *Journal of Biomechanical Engineering* 1986; 108(4): 372–381. DOI:10.1115/1.3138633.
123. Waghorne J, Bonomo F, Rabbani A et al. On the characteristics of natural hydraulic dampers: An image-based approach to study the fluid flow behaviour inside the human meniscal tissue. *arXiv preprint arXiv:230713060, Acta Biomaterialia, under review* 2023; .
124. Agustoni G, Maritz J, Kennedy J et al. High resolution micro-computed tomography reveals a network of collagen channels in the body region of the knee meniscus. *Annals of Biomedical Engineering* 2021; 49: 2273–2281.

125. Vetri V, Dragnevski K, Tkaczyk M et al. Advanced microscopy analysis of the micro-nanoscale architecture of human menisci. *Scientific Reports* 2019; 9(1): 18732.
126. Compte A and Metzler R. The generalized cattaneo equation for the description of anomalous transport processes. *Journal of Physics A: Mathematical and General* 1997; 30(21): 7277–7289. DOI:10.1088/0305-4470/30/21/006.
127. Crevacore E, Di Stefano S and Grillo A. Coupling among deformation, fluid flow, structural reorganisation and fibre reorientation in fibre-reinforced, transversely isotropic biological tissues. *International Journal of Nonlinear Mechanics* 2019; 111: 1–13. DOI:https://doi.org/10.1016/j.ijnonlinmec.2018.08.022.
128. Ramírez-Torres A, Di Stefano S and Grillo A. Influence of non-local diffusion in avascular tumour growth. *Mathematics and Mechanics of Solids* 2021; 26(9): 1264–1293. DOI:10.1177/1081286520975086.
129. Driessen N, Peters G, Huyghe J et al. Remodelling of continuously distributed collagen fibres in soft connective tissues. *J Biomech* 2003; 36: 1151–1158. DOI:10.1016/S0021-9290(03)00082-4.
130. Driessen N, Wilson W, Bouten C et al. A computational model for collagen fibre remodelling in the arterial wall. *J Theor Biol* 2004; 226: 53–64. DOI:10.1016/j.jtbi.2003.08.004.
131. Olsson T and Klarbring A. Residual stresses in soft tissue as a consequence of growth and remodeling: application to an arterial geometry. *Eur J Mech A* 2008; 27(6): 959–974. DOI:10.1016/j.euromechsol.2007.12.006.
132. Barrera O, Tarleton E, Tang H et al. Modelling the coupling between hydrogen diffusion and the mechanical behaviour of metals. *Computational Materials Science* 2016; 122: 219–228.
133. Sreejith P, Srikanth K, Kannan K et al. A thermodynamic framework for additive manufacturing of crystallizing polymers, part ii: Simulation of the printing of a stent. *International Journal of Engineering Science* 2023; 184: 103790.
134. Smith M. *Abaqus 6.11 User Subroutines Reference Manual*. United States: Dassault Systèmes Simulia Corp, 2015.

## Appendix

Equations (69a)-(69a) are solved within ABAQUS® by using some formal analogies among thermoelasticity, poroelasticity and mass diffusion and by having recourse to the user subroutines "UMAT" and "UMATHT" in the same fashion as[65,66,132,133]. ABAQUS™ "UMATHT" solves the energy conservation equation (111). This is similar to the weak form of the mass conservation Equation (69b) that can be written as follows. Integration is taken over the reference placement $\mathscr{B}$, here assumed to coincide with medium's initial placement, i.e.,

$$-\int_{\mathscr{B}} \frac{J_m - J_{m-1}}{\Delta t_m} P_{\mathrm{v}} + \int_{\mathscr{B}} \boldsymbol{Q}_m \mathrm{Grad} P_{\mathrm{v}} - \int_{\partial_{\mathrm{N}}^{P}\mathscr{B}} (\boldsymbol{Q}_m \boldsymbol{N}) P_{\mathrm{v}} = 0. \tag{109}$$

By converting the integrals in Equation (109) to the current placement $V$, Equation (109) transforms into

$$-\int_{\mathscr{B}_t} \frac{1}{\Delta t_m} \left[ \left( \frac{J_m - J_{m-1}}{J_m} \right) \circ (\Xi, \mathrm{t}) \right] p_{\mathrm{v}} + \int_{\mathscr{B}_t} \boldsymbol{q}_m \mathrm{grad} p_{\mathrm{v}} - \int_{\partial_{\mathrm{N}}^{P}\mathscr{B}_t} (\boldsymbol{q}_m \boldsymbol{n}) p_{\mathrm{v}} = 0, \tag{110}$$

whereas the weak form of the energy balance equation given in ABAQUS® reference manual[134] reads

$$\underbrace{\frac{1}{\Delta t}\int_V \delta\theta\rho(U_{t+\Delta t}-U_t)dV}_{0} = \int_V \delta g\cdot\underbrace{\mathbf{f}}_{\boldsymbol{q}_m} dV + \int_S \delta\theta \underbrace{q}_{-\boldsymbol{q}_m\boldsymbol{n}} dS + \int_V \delta\theta \underbrace{r}_{-\frac{J_m-J_{m-1}}{J_m\Delta t_m}\circ(\Xi,\mathrm{t})} dV, \tag{111}$$

where $\delta\theta$ is a virtual variation of temperature, and, thus, plays the role of $p_{\mathrm{v}}$, while $\delta g$ stands for the spatial gradient of $\delta\theta$, and corresponds to our grad $p_{\mathrm{v}}$. Further equivalences between the variables featuring in Equations (110) and (111) are made for making "UMATHT" suitable for solving Equation (59b) and (59c). The corresponds are as follows: the temperature $\theta$ of "UMATHT" is pore pressure $p$ (and, thus, to $P\circ(\chi,\mathcal{T})$); rate of heat generation is the rate of volumetric deformation, so that $r$ corresponds to $-\big((J_m-J_{m-1})/(J_m\Delta t_m)\big)\circ(\Xi,\mathrm{t})$; the heat flux $\mathbf{f}$ corresponds to the filtration velocity $\boldsymbol{q}_m$; the density $\rho$ introduced in "UMATHT" is set equal to zero.

The pseudo-code for the implementation of our equations in ABAQUS® is provided in Algorithm 1. Within "UMATHT", the filtration velocity is solved from Equation (59c) by using the methodology explained in subsection 6.2. Variations of flux with respect to the gradient of pore pressure are calculated according to Equation (101). The information of the gradient required for calculating the filtration velocity through Equation (67) is passed to "UMATHT" from "UMAT" by storing it among global variables. The terms that are calculated in "UMATHT" required as output to ABAQUS® are given as

$$FLUX \text{ (see (104))} : \boldsymbol{q}_m^{k-1} = \frac{1}{J_m^{k-1}}\boldsymbol{F}_m^{k-1}\boldsymbol{Q}_m^{k-1}, \tag{112a}$$

$$DFDG \text{ (see (101))} : \mathfrak{B}_m^{k-1} := \frac{1}{J_m^{k-1}}\boldsymbol{F}_m^{k-1}\left[\frac{\partial\mathcal{Z}}{\partial\boldsymbol{Q}_m}(\sharp_m^{k-1})\right]^{-1}\left[\frac{\partial\mathcal{Z}}{\partial\mathrm{Grad}P_m}(\sharp_m^{k-1})\right][\boldsymbol{F}_m^{k-1}]^{\mathrm{T}}. \tag{112b}$$

The subroutine "UMAT" is used to solve the balance of linear momentum, and to define the coupling terms. The Neo-Hookean potential energy density is stated in Equation (82), and the *consistent Jacobian matrix* given in Equation (89) can be written for the problem solved in Section 7 as follows (see (89)):

$$DDSDDE : \mathbb{a}_m^{k-1} = \Phi_s\frac{\mu_s}{2J}\left(\boldsymbol{I}\underline{\otimes}\boldsymbol{B}_m^{k-1} + \boldsymbol{I}\overline{\otimes}\boldsymbol{B}_m^{k-1} + \boldsymbol{B}_m^{k-1}\underline{\otimes}\boldsymbol{I} + \boldsymbol{B}_m^{k-1}\overline{\otimes}\boldsymbol{I}\right) + \left(\Phi_s\frac{\lambda_s}{J} - P\right)\boldsymbol{I}\otimes\boldsymbol{I}. \tag{113}$$

Here, $\boldsymbol{B}$ is the left Cauchy-Green tensor defined as $\boldsymbol{B} := \boldsymbol{F}\boldsymbol{F}^{\mathrm{T}}$. Other terms that are calculated in "UMAT" required as output to ABAQUS® are given as

$$STRESS : \boldsymbol{\sigma} = \frac{1}{J_m^{k-1}}\boldsymbol{T}_{\mathrm{I}m}^{k-1}[\boldsymbol{F}_m^{k-1}]^{\mathrm{T}} \qquad \text{(see (83))}, \tag{114a}$$

$$DDSDDT : -\boldsymbol{\eta}^{-1} \qquad \text{(see (91))}, \tag{114b}$$

$$RPL := -\frac{J_m^{k-1}-J_{m-1}}{J_m^{k-1}\Delta t}, \tag{114c}$$

$$DRPLDE := -\frac{1}{\Delta t}\boldsymbol{\eta}^{-1} \qquad \text{(see (98))}, \tag{114d}$$

$$DRPLDT = 0. \tag{114e}$$

**Algorithm 1** Pseudo Code of "UMAT" and "UMATHT" for ABAQUS®

**Common Module**
Define global variables to store the deformation gradient in "UMAT" to be used by "UMATHT", and to store the history terms for the calculation of fractional integral.
**UMATHT**:
*Inputs*: Pore pressure, Increment of pore pressure, Current gradient of pore pressure and other terms.
Calculate permeability $\kappa_{\text{iso}}$ from (43)
Calculate Forchheimer's coefficient $\mathcal{A}_{\text{iso}}$ from (40)
Compute $\mathcal{R}_{\text{F}}$ from (57)
Calculate $\mathcal{F}_{\alpha}$ from (65)
Compute filtration velocity $\boldsymbol{Q}$ using the Newton Raphson method using the method given in section 6.2
Compute flux rate $\dot{\boldsymbol{Q}}_{\text{app}}$ using (64b)
Compute the contribution from the current time step to the History variable $\mathcal{F}_{\alpha}(t_m)$ using (65) and store it in global variables.
Compute flux (112a), Variation of flux with respect to pore pressure gradient using (112b).
*Output*: Flux at the end of the increment (FLUX), Variation of the flux vector with respect to the spatial gradients of pore pressure (DFDG).
**UMAT**:
*Input*: Deformation gradient at the increment's start and end, Stress, Pore pressure at the start of the increment, increment of pore pressure and other terms.
Compute Stress (114a), Consistent Jacobian matrix (113), Variation of stress with pore pressure(114b), rate of volumetric deformation (114c) and its variation with strain increment (114d) and temperature increment (114e)
Store deformation gradient in the global variable.
*Output*: Stress at the end of the increment(STRESS), Consistent Jacobian matrix (DDSDDE), Volumetric heat generation per unit time (RPL), Variation of stress with respect to pore pressure(DDSDDT), Variation of RPL with Pore pressure(DRPLDT), Variation of RPL with strain increments(DRPLDE).